The influence of winter time boreal forest tree transmissivity on tree emission and passive microwave snow observations

by

Qinghuan Li

A thesis

presented to the University of Waterloo

in fulfillment of the

thesis requirement for the degree of

Doctor of Philosophy

in

Geography

Waterloo, Ontario, Canada, 2019

©Qinghuan Li 2019

Examining Committee Membership

The following served on the Examining Committee for this thesis. The decision of the Examining Committee is by majority vote.

External Examiner	Roger De Roo Lecturer IV and Associate Research Scientist, Climate and Space Sciences and Engineering, University of Michigan.
Supervisor(s)	Richard Kelly Professor, Geography Environmental Management, University of Waterloo
Internal Member	Ellsworth LeDrew Professor, Geography Environmental Management, University of Waterloo.
	Chris Derksen Adjunct Professor, Geography Environmental Management, University of Waterloo. Research Scientist, Cryosphere and Climate Interaction, Environment and Climate Change Canada.
Internal-external Member	Michael Drescher Associate Professor, School of Planning, University of Waterloo.

AUTHOR'S DECLARATION

This thesis consists of material all of which I authored or co-authored: see Statement of Contributions included in the thesis. This is a true copy of the thesis, including any required final revisions, as accepted by my examiners.

I understand that my thesis may be made electronically available to the public.

Statement of Contributions

In this manuscript-style thesis, Chapters 4, 5 and 6 represent three manuscripts. Qinghuan Li is the first author of the three manuscripts. The manuscript in Chapter 4, the influence of thermal properties and canopy-intercepted snow on passive microwave transmissivity of a Scots Pine, has been accepted by IEEE Transactions on Geoscience and Remote Sensing as a, 2019, DOI: 10.1109/TGRS.2019.2899345. Richard Kelly co-developed the framework of this study and made a significant revision. Juha Lemmetyinen contributed very important thoughts and inputs. The other co-authors include Leena Leppänen, Juho Vehviläinen, Anna Kontu, and Jouni Pulliainen. They made great contributions in the data collection and instrument management. The manuscript in Chapter 5, simulating the influence of temperature on microwave transmissivity of trees during winter observed by spaceborne microwave radiometery, has been submitted to IEEE Geoscience and Remote Sensing Letters. Richard Kelly co-developed the framework of this study and made a significant revision. Juha Lemmetyinen contributed very important thoughts and inputs. Jinmei Pan provided good suggestions in the model simulation. The manuscript in Chapter 5, modelling influence of tree transmissivity variation on frequency difference passive microwave snow retrieval algorithms under sub-zero temperature conditions. Richard Kelly co-developed the framework of this study and made a significant revision. Juha Lemmetyinen contributed very important thoughts and inputs. Jinmei Pan provided good suggestions in the model simulation.

Abstract

Forest cover significantly attenuates natural upwelling ground microwave emission from seasonal terrestrial snow. This presents a major challenge for the accurate retrieval of snow from airborne or spaceborne passive microwave (PM) observations. Forest transmissivity is a key parameter describing tree emission because not only does it influence the proportion of sub-canopy upwelling microwave emission penetrating through the forest canopy, it also controls the forest thermal emission. Hence, it is a very important parameter for correcting the influence of forests on spaceborne or airborne observations of the Earth's land surface. Under sub-zero temperatures, vegetation water content can be frozen influencing the microwave transmissivity of trees. Yet this phenomenon has not been verified through experimentation leaving significant uncertainty in tree emission modelling and spaceborne microwave observations. Therefore, a season-long experiment was designed to study this phenomenon. Ground-based radiometer observations of tree emission, spaceborne observations of forest emission, and model simulations of canopy emission were conducted during this experiment. Based on this experiment, the influence of physical temperature on tree transmissivity was verified, and a model developed to quantitatively describe this temperature-transmissivity relationship. An evaluation of this temperature-transmissivity relationship was conducted showing that both ground-based and spaceborne observations of tree emission are significantly influenced by this phenomenon. Furthermore, passive microwave spaceborne snow retrievals in forested regions are influenced by this phenomenon. Finally, an approach to reduce the influence of the temperature-transmissivity relationship on passive microwave spaceborne snow retrievals is demonstrated.

Acknowledgements

First and foremost, I would like to express my most sincere gratitude to my supervisor Dr. Richard Kelly. This thesis would not have been possible without his support. Thank you very much for your guidance and encourage during the whole of my graduate study period. With your help, I could overcome the difficulties, and learn to become a researcher. I also would like to thank my committee members, Drs. Ellsworth LeDrew, Michael Drescher, Chris Derksen, and my external examiner (not decided yet). Thanks for providing me great suggestions.

I also would like to acknowledge my collaborators, Drs. Juha Lemmetyinen, Leena Leppänen, Juho Vehviläinen, Anna Kontu, and Jouni Pulliainen. I deeply appreciate for your valuable inputs and assistances. Thank you also to my amazing colleagues: Nastaran Saberi, Aaron Thompson, Vicky Vanthof, Paul Donchenko, and Margot Flemming. Thanks for all your support and encouragements during my PhD program.

I really appreciate the help from my friend Jinmei Pan in my study and research. Thank you also to my friend Jun Luo, who always gives me good suggestions about how to manage my life better in Canada. Last but most important, I give my deepest gratitude to my parents. The courage and unquestioning love you give to me is the biggest inspirations during my graduate study.

Table of Contents

List of Figures

List of Tables

List of abbreviations, acronyms and nomenclature

γ	Transmissivity
r	Reflectivity
τ	Optical depth
ω	Single scattering albedo
D_{max}	The greatest diameter of the snow grain
D_o	Optical grain size
f	Forest fraction
SC	Snow cover condition of the forest canopy
T	Temperature
Tb	Brightness temperature
ΔTb	Tb difference
r_0	Reflectivity of the ground
r_{forest}	Reflectivity of the forest
r_{ground}	Reflectivity of the ground
γ_M	Tree transmissivity estimated by Mätzler's approach
γ_0	Tree transmissivity when air temperature higher than 0 °C
Tb_1	Tb of the target tree
Tb_2	Tb of the sky
Tb_0	Tb of the ground
Tb_{ground}	Tb of the ground
$Tb_{\downarrow tree}$	The down-welling Tb of the tree
Tb_{sky}	The down-welling Tb of the sky
$\downarrow Tb_{forest}$	The down-welling Tb of the forest
$\uparrow Tb_{forest}$	The up-welling Tb of the forest
$\Delta Tb_{fground}$	The ΔTb of the ground emission beneath the forest
ΔTb_{forest}	The ΔTb of the up-welling emission observed above the canopy
ΔTb_{sb}	The ΔTb of the AMSR2 observation
$\Delta Tb_{oground}$	The ΔTb of the ground emission in the forest openings

$\Delta Tb_{sbground}$	The ΔTb of ground emission underneath forests from the spaceborne AMSR2 observation footprint
$\Delta Tb_{isground}$	The ΔTb of the ground emission at the *in-situ* observation scale
ΔTb_{AMSR}	Tb difference of the Tb_{AMSR}
Tb_{AMSR}	AMSE2 observed ground emission
T_{tree}	Tree skin temperature
T_{air}	Air temperature
T_{soil}	Soil temperature
T_{snow}	Snow temperature
$Tb_{isground}$	Radiometer observed Tb of the ground
$\downarrow Tb_{istree}$	Radiometer observed down-welling Tb of the tree
Tb_{issky}	Radiometer observed down-welling Tb of the sky
SD_{forest}	AWS measured snow depth in the forest
SD_{open}	AWS measured snow depth in the forest opening
SD_{is}	The *in-situ* estimated snow depth of the AMSR2 footprint
T_{isair}	Air temperature of the study site
$T_{isground}$	Soil temperature
T_{istree}	Tree skin temperature
$\Delta Tb_{RTforest}$	The ΔTb_{forest} estimated by the tree RT model
$\Delta Tb_{APPforest}$	The ΔTb_{forest} estimated by the approximation
ΔTb_{APPsb}	The ΔTb_{sb} estimated by the approximation approach
$\Delta Tb_{APPsbground}$	The $\Delta Tb_{sbground}$ estimated by the approximation
AMSR-E	Advanced Microwave Scanning Radiometer - EOS
AMSR2	Advanced Microwave Scanning Radiometer 2
AWS	Automatic weather station
DMSP	Defense Meteorological Satellite Program
GCOM-W1	Global Change Observation Mission 1st-Water
HPBW	Half-Power Beam Width
IDP	Permittivity (imaginary part)
IOA	Intensive Observation Area

PM	Passive microwave
RDP	Permittivity (real part)
RMSE	Root mean square errors
RT	Radiative transfer
SD	Snow depth
SDP	Soil dielectric permittivity
SMMR	Scanning Multi-channel Microwave Radiometer
SodRad	Sodankylä Radiometer
SSA	Specific Surface Area
SSM/I	Special Sensor Microwave Imager
SSMIS	Special Sensor Microwave Imager/Sounder
SWE	Snow water equivalent
VIS/IR	Visible-infrared

Chapter 1

Introduction

1.1. Motivation

Satellite observation technologies are one of the most effective tools for studying and monitoring the snow distribution and variation at global and regional scales. The brightness temperatures (Tb) observed by spaceborne passive microwave (PM) instruments are sensitive to snow water equivalent (SWE) and snow depth (SD), which makes the SWE and SD retrievals with PM observations possible. While spaceborne PM sensor observations usually have coarser spatial resolutions than visible-infrared (VIS/IR) sensors, they are barely influenced by cloud cover and solar illumination. Thus, observations under overcast conditions during both day and night are possible. Furthermore, the daily temporal resolution of most spaceborne PM instruments is relatively high. Therefore, these characteristics make spaceborne PM instrument an ideal tool for regional to global-scale snow observations.

Spaceborne and airborne PM snow retrievals are challenging in forested areas because sub-canopy snow is masked by the tree canopy in forested regions. Forests not only strongly attenuate the ground emission, but also contribute their own thermal emission. Therefore, forests significantly influence the spaceborne PM ground observations through attenuation of the upwelling ground Tb. Accordingly, PM SD and SWE retrievals are significantly influenced by this effect with the sensitivity of above-canopy Tb observations to SD and SWE decreased [12]. The study shows that at 37 GHz as little as 20% forest spatial coverage can modify the observed

ground Tb by up to 10 K, and if the forest fraction is greater than 60%, the signal contributed by the snowpack on the observed ground Tb could be completely masked out [9]. Since forests are one of the prevailing land cover types in mid-high latitude regions, coarse-spatial resolution passive microwave footprint are usually partially or fully covered by forests. A pressing question, therefore, is how to reduce the influence of forests in spaceborne PM snow retrievals?

Characterizing the radiative transfer (RT) of forests effectively is the key to correcting the influence of forests on PM snow retrievals. Once the RT of forests is modelled, the influence of forests on the upward ground Tb can be described by RT models. Accordingly, the influence of forests can be corrected by these models. Forest transmissivity is the key parameter in forest RT models. It controls both tree thermal emission and the proportion of sub-canopy upwelling microwave emission penetrating through the tree canopy. Hence transmissivity is a very important parameter in correcting the influence of forest on PM SD and SWE or other geophysics parameters retrievals in forested regions.

Vegetation transmissivity is strongly influenced by vegetation permittivity, and the vegetation permittivity is controlled by vegetation water content [19, 20, 24, 59]. Because ice has a much lower permittivity than liquid water, the vegetation permittivity decreases after its water content freezes. This phenomenon was observed in the experiment on a small piece of corn leaf [20]. Accordingly, the vegetation transmissivity increases as the vegetation permittivity decreases. However, for trees in a natural environment, the anti-freeze mechanism of trees can mitigate the freezing process [35, 60]. Moreover, because trees have a large biomass and complex structure, the thermal characters of trees are heterogeneous indicating that the tree water content freezing and thawing is a complex and uneven process in a natural environment. As Mayr [61] observed, the freezing and thawing rate at the top of the tree is greater than at the

trunk base. Therefore, the relationship between the overall tree transmissivity and physical temperature under freezing conditions in a natural environment is relatively unknown.

Most studies consider transmissivity as a constant value in tree emission modelling (e.g. [14, 27, 32]). To ignore the influence of temperature on transmissivity might cause a bias in tree emission modelling and might introduce uncertainties in PM snow retrievals. Since tree transmissivity is a very important parameter in tree emission modelling, the relationship between tree transmissivity and temperature under freezing conditions in a natural environment required to be studied. How this transmissivity and temperature relationship influences tree emission, and how this relationship influences PM SD and SWE retrievals in forested regions should be further evaluated.

1.2. Objectives

Since the variation of vegetation permittivity caused by the vegetation water content freezing has been observed by Ulaby's experiment, the first objective of this paper is to study the relationship between physical temperature and tree transmissivity in a natural environment under sub-zero temperatures. Having established and verified the relationship between physical temperature and tree transmissivity through the observation, the second objective of this paper is to develop a model to describe the relationship between physical temperature and tree transmissivity in a natural environment. And then, with the developed model, to evaluate how this temperature-transmissivity relationship could influence the spaceborne PM Tb observation and snow observation in forested region is the third objective of this paper. The fourth objective of this paper is to develop a feasible solution to reduce the influence of this temperature-transmissivity relationship on spaceborne PM SD and SWE retrievals.

In this thesis, chapters 3, 4 and 5 represent three manuscripts. The manuscript in chapter 3 explains how physical temperature influences tree transmissivity under sub-zero temperatures (Accepted by IEEE TGRS, 2019, DOI: 10.1109/TGRS.2019.2899345). The model to describe the temperature-transmissivity relationship is developed in the chapter 4 manuscript. Based on the developed model, the influence of this temperature-transmissivity relationship on the spaceborne PM observation and on the frequency difference algorithms of PM snow retrievals are then evaluated. The chapter 5 manuscript presents a feasible solution to reduce the influence of temperature-transmissivity relationship on the frequency difference algorithms of spaceborne PM SD and SWE retrieval has been developed.

Chapter 2

Background: observations of snow in forested regions

2.1. The general characteristics of snow

2.1.1. The importance of snow

As one of the most important elements in the Cryosphere, snow has a major influence on climate. Snow not only effectively reflects the incoming solar radiation back into space due to its high reflectivity, but also increases the ground energy loss through long-wave radiation. Therefore, the decrease of the global snow extent tends to increase the total energy budget of the Earth's surface. The increased energy tends to enhance the global warming. which in turn leads to a decreasing extent of the global snow cover. This feedback mechanism is called the "snow-albedo" feedback and plays an important role in global warming [62].

Snow also has a significant influence on atmospheric dynamics. The cooling effect of snow can enhance or maintain a trough of cold air in the troposphere. In turn, the cold trough will favor the persistence of snow. Based on the study of Garcia-Herrera and Barriopedro [63], snow cover and atmospheric blocking are related at both the local and subcontinental scales. This feedback can further influence the distribution of atmospheric pressure systems and the pattern of air flux.

In addition to these large scale effects, snow also has a great influence on planetary water cycling [64], surface gas exchanges [65], ecosystem function [66], and human activities. Therefore, snow observation in global scale is very important.

2.1.2. The key factors to control evolution of snowpack

The physical characters of the snow influence the RT of the snowpack thereby influencing the microwave response of snow, and consequently, PM snow retrievals. In general, the physical characters of the snowpack are largely controlled by the weather, especially precipitation, air temperature, and wind speed. The air temperature controls snow melting and snow metamorphism. The melting causes the development of melt forms inside snowpack, such as clustered rounded grains, rounded polycrystals, slush, and melt-freeze crusts. Snow metamorphism, which is caused by the mass exchange between ice, air and liquid inside snowpack, controls the transformation of snow grains. The thermal condition of the snowpack is the key factor controlling the types of snow metamorphism. Because snow is a thermally insulating medium, a vertical temperature gradient exists through the pack between ground and above snow air. If the air temperature is low, a stronger vertical temperature gradient is created since the ground temperatures are typically less cold. In this situation, constructive metamorphism is likely to occur. The vertical vapor pressure gradient created by the vertical temperature gradient pushes water molecules to move upward, and molecules sink at the colder area. This process decreases the total number of snow grains and creates larger size snow grains (e.g. depth hoar). Conversely, when the vertical temperature gradient is weak, destructive metamorphism likely happens whereby the local vapor pressure gradients between snow grains control the movement of water molecules because the vertical vapor pressure gradient created by the vertical temperature gradient is not strong enough. The convex surfaces of the snow grains

have a higher vapor pressure than the concave surfaces. Hence, the water molecules in convex surfaces of the snow grains tend to move into the concave surfaces [67]. Destructive metamorphism usually leads to the rounding and sintering of snow grains, and the grain growth rate under this type of metamorphism is relatively slow [1].

Precipitation and wind effects determine the snow depth and sets up the stratigraphy when multiple events accumulate. Because a deeper snowpack tends to have a weaker vertical temperature gradient, the depth of snowpack can further influence the metamorphism of snow through influence the vertical temperature gradients. Wind redistribution of snow affects surface grain size and density. Wind can break snow crystal into smaller pieces, and these smaller grains are easy to sinter into cohesive wind slabs. The wind pressure compresses the snowpack. Pomeroy suggested that, at wind speeds greater than 7m/s, the rate of the density increase of the exposed non-melting snowpack in the open area is 9 kg/m^3h during the wind event [68].

2.1.3. The difference between taiga snow and tundra snow

Based on the concept that long-term weather patterns ultimately determine the physical character of the snowpack, climatologically, Sturm proposed a physically-based classification system to relate the snow class to climate (Fig. 2.1) [69]. The study site of this paper is in the Northern boreal forest belt. According to the classification system proposed by Sturm, in this region, the dominant snow class in forested areas is called taiga snow. While, the snowpack in the open areas which surround the forests is called tundra snow. Therefore, these two snow classes of are introduced in this section.

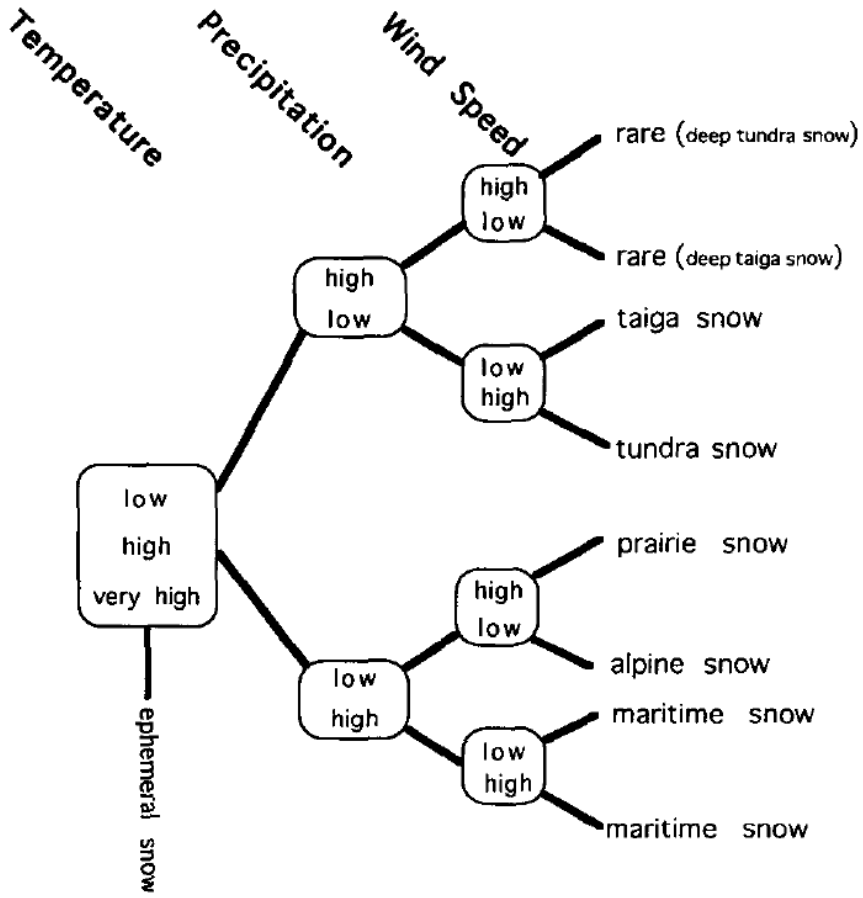

Fig. 2.1 A dichotomous key for snow class identification [69]

Wind speed and the vegetation are the major factors that shape the difference between taiga snow and tundra snow. In open areas, the wind speed is greater than in forested areas. Hence, surface wind slabs typically develop in open (tundra) areas. Usually, if the precipitation happened more than once during the wintertime, multiple wind slabs can be found inside tundra snowpack. While, inside forested areas, the wind speed is decreased, and so wind slab does not develop. Therefore, in taiga snow, wind slab is unlikely to be found, and the percentage of depth hoar is higher than tundra snow because direct thermal conductivity between vegetation and snowpack creates a strong temperature gradient, which is favorable for the development of depth hoar.

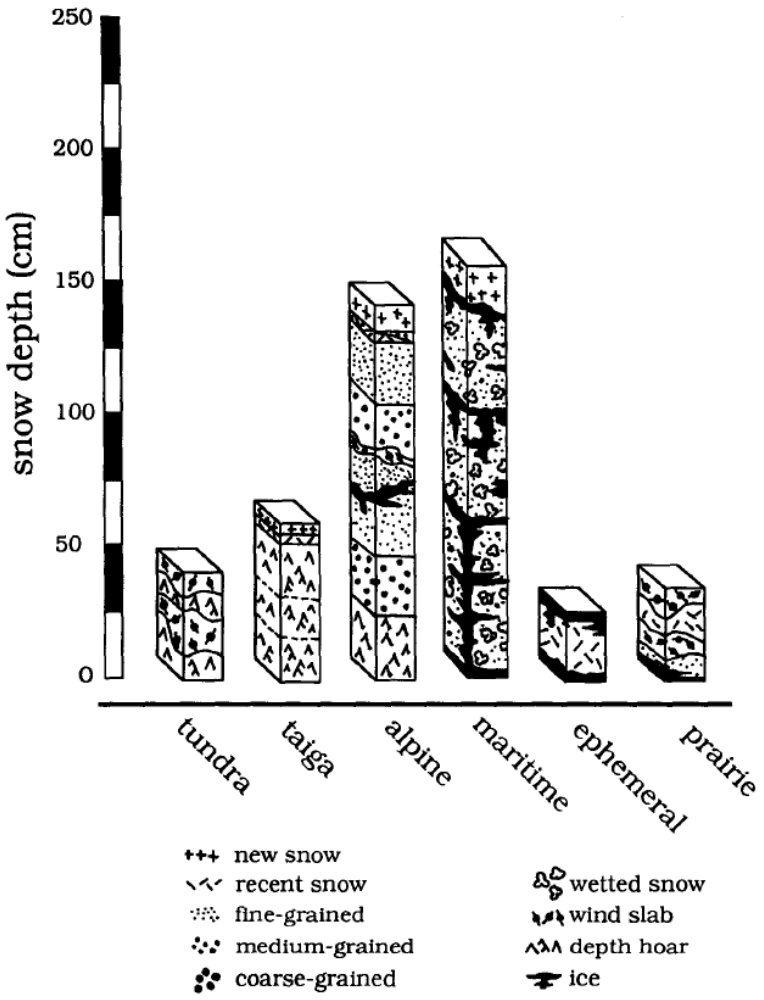

Fig. 2.2 The basic stratigraphic and textural attributes of each class of snow cover as they would appear in middle to the late winter [69]

From the perspective of microwave propagation, depth hoar has strong electromagnetic scattering properties and can effectively attenuate the microwave emission from the ground beneath the snowpack. Conversely, the scattering properties of wind slab and new snow are relatively low. More details about how the snowpack properties interact with the snow emission will be discussed after.

2.2. Characteristics of spaceborne passive microwave observations of snow

2.2.1. Spaceborne sensors and approaches to PM snow retrievals

The primary PM sensors used for spaceborne snow monitoring include the Scanning Multi-channel Microwave Radiometer (SMMR), Special Sensor Microwave Imager (SSM/I), Advanced Microwave Scanning Radiometer - EOS (AMSR-E), and Advanced Microwave Scanning Radiometer 2 (AMSR2). SMMR was launched with the Nimbus-5 in 1978. The primary objective of this sensor was to obtain sea surface temperature, wind stress, sea ice coverage and terrain variables. The SSM/I on the Defense Meteorological Satellite Program (DMSP) launched in 1987 has wider swath and improved Tb sensitivity compared with SMMR. The Special Sensor Microwave Imager/Sounder (SSMIS), the upgraded model of SSM/I, started to operate from 2003. The AMSR-E was lunched onboard the Aqua in 2002. AMSR-E has 12 channels with 6 frequencies and 2 polarizations. The JAXA's AMSR2 on board the Global Change Observation Mission-Water (GCOM-W1) mission is a follow on from the AMSR-E and has similar characteristics. Comparing SMMR and SSM/I, AMSR-E and AMSR2 have higher spectral and spatial resolution, better sensitivity, and wider swath coverage. The details of PM sensors are represented in Table 2.1.

Table 2.1 Parameters of the PM sensors were used as primary sensors in snow observation [71, 72]

		SMMR	SSM/I	AMSR-E	AMSR2
Operational period		1978-1987	1987-present*	2002-2011	2012-now
Platform		Nimbus-7	DMSP	Aqua	GCOM-W1
Frequencies and IFOV (km x km)	6.6 GHz	156 x 156	N/A	75 x 43	62 x 35
	10.7 GHz	97 x 97	N/A	51 x 29	62 x 35
	18.0 GHz	60 x 60	69 x 43	27 x 16	42 x 24
	21.0GHz	60 x 60	60 x 40	32 x 18	22 x 14
	37.0 GHz	30 x 30	37 x 29	14 x 8	19 x 11
	85.5 GHz	N/A	15 x 13	6 x 4	12 x 7
Polarizations		H/V	H/V	H/V	H/V
Incidence angle (degree)		49	53	53	55
Data acquisition		Every other day	Daily	Daily	Daily
Swath width		780 km	1400 km	1450 km	1450 km
Radiometric resolution (K)		0.9–1.5	0.8–1.1	0.3–1.1	0.3–1.2

2.2.2. The snowpack physical properties controlling the RT of seasonal snow

The successful RT of snow is key to successful PM SD and SWE retrievals. Therefore, the snowpack physical properties control the RT of snowpack are the important parameters in PM snow retrievals. The relative permittivity, grain properties (e.g. grain type, size), density, and stratigraphic structure of snow have significant influences on the RT of the snowpack. The relative permittivity influences both absorption and scattering capacities of the snowpack. Hence, it is one of the key parameters in RT models. In each snow layer, ice, air, and liquid water are the major components of a snowpack and so the snowpack's permittivity is controlled by the

proportions of these three elements. The permittivity of air and ice are relatively low, while the permittivity of the water is much higher. Hence, the percentage content of free liquid water significantly influences the permittivity of snowpack. In dry snow, the content of liquid water is generally considered as 0. In this case, the proportion of ice inside the snowpack is the key controlling factor because ice has a higher permittivity than air. The permittivity of dry snow increases with the density because the increase of ice mass. The permittivity of snow could be estimated by the dielectric mixing models. For example, using the weighted average of each component (ice, water, and air) is a simplified approach to estimate snowpack permittivity [77]. More sophisticated models include the Polder-Van Santen mixing formula [78], Tinga model [79], and Debye like semi-empirical model [80].

The shape of snow grains can also have a significant influence on microwave propagation. Usually, the snowpack is composed of larger snow grains (e.g. depth hoar) which have a higher attenuation capacity than smaller snow grains (e.g. small rounded grains or wind broken particles). Snow grains can be largely classified into 7 groups: needle, columnar, plane, combination of column and plane, rimed, and irregular crystals [81]. The wind blow, metamorphism, compression and melting are the major factors that influence the evolution of the snow grains. Descriptors have therefore been developed to describe the geometric structures of snow grains in RT models. The maximum length (diameter) of the dominant particles is known as D_{max}. This is a descriptor that can be conveniently measured although it is a highly subjective measurement based on the experience of the observer with a potentially strong uncertainty. The D_{max} descriptor largely ignores the influence of the snow grain types on the RT of snowpack. Therefore, the descriptors such as the optical grain size (D_o) [82], correlation length [83], and

specific surface area (SSA) [84, 85] have been introduced into RT models to provide a more robust representation.

The density of the snowpack influences snowpack permittivity and snow density and the grain size together can represent the amount of snow grains in a certain volume of snowpack. Therefore, the density influences snowpack emission. The density of the snowpack is largely influenced by the weather factors, which include precipitation, air temperature, wind and season duration. Sturm *et al.* [86] developed a statistical model for density estimation of seasonal snowpacks.

A snowpack usually has stratigraphic structure. The factors which influence the stratigraphic structure of the snowpack has been discussed in section 2.1.2 and 2.1.3. The properties like snow grain, density, and permittivity are different in each snow layer. Therefore, the snow layers with different snowpack properties have a different influence on microwave propagation. Furthermore, the boundaries of these snow layers could cause reflection and transmission of propagated microwaves. Hence, most of the snowpack RT models (e.g. The Microwave Emission Model of Layered Snowpacks (MEMLS) [73], The Dense Media Radiative Transfer - Multi Layers model (DMRT_ML) [74], and Helsinki University of Technology (HUT) snow microwave emission model [11]) describe snowpack as a multi-layer structure medium.

As mentioned above, the successful RT representation of snow is key to effective PM SD and SWE retrievals. Numerical models of snow have been developed to quantitatively describe the RT of snow-covered ground. For example, HUT [29], MEMLS [73], and DMRT-ML [74]. In spaceborne global SD and SWE retrievals, the frequency difference algorithms are usually applied for tractability (e.g. [1, 2, 3, 28]). This type of simplified algorithm developed based on

RT theory requires fewer inputs and parameters than the traditional snowpack RT models. Hence, it is easily applied in global and regional scale study. The Tb difference between a low frequency channel and a high frequency channel (ΔTb) is the key element in frequency difference algorithms (usually is the combination of 18-37 GHz). The Tbs of the ground underneath the snowpack in high frequency channels are attenuated by the snowpack. The attenuation of the snowpack on Tb of high frequency channel is related to SD and SWE while the low frequency Tbs from the sub-nivean ground surface are minimally attenuated by the snowpack. Therefore, low frequency channels function as a reference channel to reduce the influences of the factors which are not related to SD and SWE on ΔTb, specifically, physical temperature variation, soil dielectric permittivity change, and atmosphere attenuation [1]. This ΔTb approach has been adopted by several spaceborne PM snow retrieval algorithms, for example, the algorithm of the GlobSnow SWE product [75] and the forthcoming AMSR2 satellite-based microwave snow algorithm (SMSA) [76].

2.3. The influence of the forest on PM snow retrievals

2.3.1. An overview of the boreal forest belt

The boreal forest belt crosses the territory of Canada, Siberia, and Scandinavia. It covers vast areas in the mid-high latitude region. Due to the cold climate conditions, the species diversity of boreal forests is relatively low compared with temperate or tropical forests. Despite the low species diversity, there are regional differences in forest types in Canada, Siberia, and Scandinavia. In Siberia, a deciduous conifer (*larix*) dominates [87] and these forests have experienced heavy logging in the past [88]. The boreal forests of Scandinavian are also strongly influenced by human activities and as a consequence, original primary-growth forests are very

rare. In Scandinavia, conifer trees dominate with pine (*Pinus sylvestris*), spruce (*Picea abies*) and brich (*Betula pendula*) the most important tree types [89]. In Canada, the forests have been less disturbed by humans in general. Evergreen conifers (*Picea mariana*, *P.glauca*, and *Pinus banksiana*) are the major types of forests in this region [90].

2.3.2. The influence of boreal forests on PM snow retrievals

The major elements of the spaceborne observed Tb above the forest canopy include are shown in Fig. 2.3 and include: (1) upward emission from the atmosphere; (2) downward emitted reflected atmospheric radiation; (3) downward forest canopy emission reflected by the ground; (4) downward snowpack emission reflected by ground; (5) upward soil emission; (6) upward snowpack emission; (7) upward forest canopy emission [11].

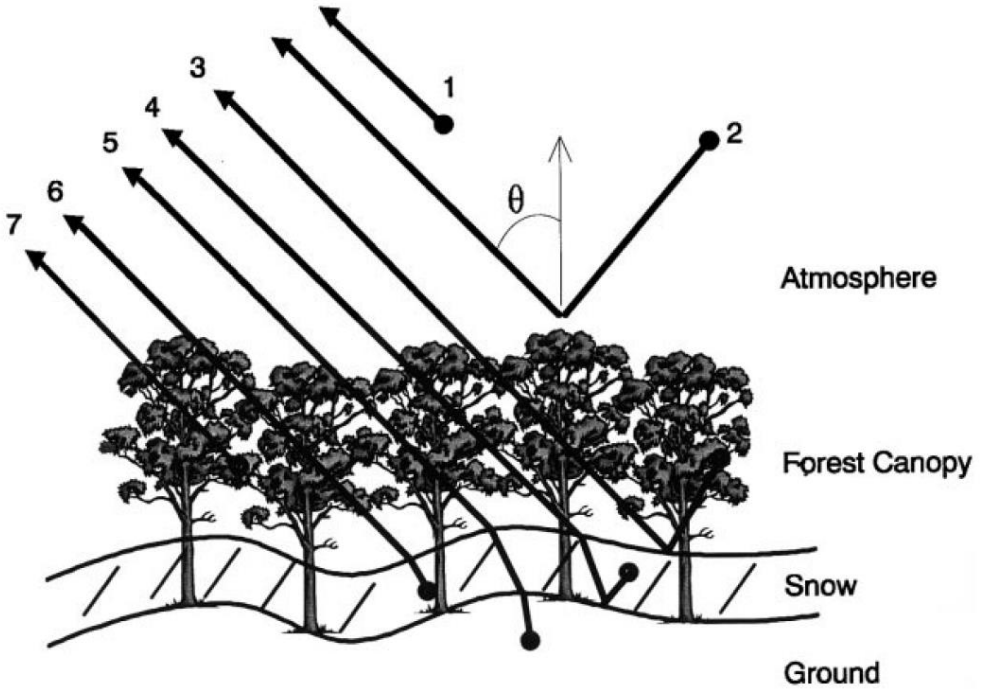

Fig. 2.3 Major contributions for space-borne observed scene brightness temperature in the forested region [11]

As Fig. 2.3 shows, forests attenuate the upward radiation from the ground, and emit its own emission. The forest attenuation and emission increase with the increase of forest density. The contribution from the trees will gradually overwhelm the emission from the ground as the forest density increases [8]. The retrieval approaches designed for spaceborne PM SWE and SD retrievals in open areas, therefore, are limited in the forested regions. For the frequency difference algorithms, the ΔTb of the tree thermal emission is much lower than the ΔTb of the snow-covered ground. Moreover, the ΔTb of the tree thermal emission is insensitive to the ground SWE and SD. Therefore, forests tend to decrease the sensitivities of ΔTb to SD and SWE, and to decrease the value of the spaceborne observed ΔTb. As discussed, the sensitivities of the spaceborne observed Tb and ΔTb to SD and SWE are the foundation of spaceborne PM SD and SWE retrievals. The decreased sensitivities of the Tb and ΔTb to SD and SWE tend to cause underestimations of SD a nd SWE retrievals in forested areas.

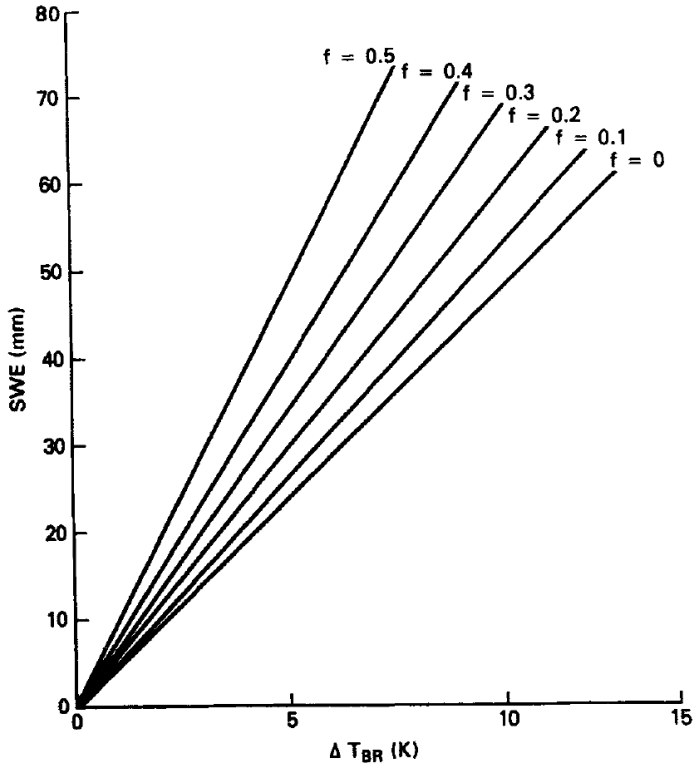

Fig. 2.4 Calculated brightness temperature versus SWE for different fractional forest cover [12]

2.3.3. The major factors influencing the RT of trees

The RT of forest biomass is the key to correcting the influence of forests on PM snow retrievals. Hence, the factors that influence the RT of trees are very important in PM snow retrievals in forested areas. In general, the RT of trees is influenced by the permittivity of the vegetation and the geometrical properties of the tree.

Similar to snow, the permittivity of the vegetation influences both absorption and scattering properties of the tree. The permittivity of the vegetation is influenced by the four major components of vegetation tissue: the free water (saline water), bound water, dried vegetation material, and air. The permittivity of dried vegetation material is relatively low and insensitive to

the frequency and temperature. Thus, it is typically considered negligible in the dielectric mixing models. The bound water can remain unfrozen at low temperature (usually 20°C or -25°C), and its dielectric behavior is similar to ice if the water is tightly bound to the host material. The free water in vegetation is the saline liquid which contains the free ions (including organic or non-organic). The permittivity of the free water is much higher than the dried vegetation material and ice. Therefore, the content of free water in vegetation is the key factor to influence the permittivity of the vegetation [19, 20]. El-Rayes and Ulaby [20] estimated the permittivity of free water and bound water by solving the Debye equation. According to Ulaby's work from 1984 to 1987 [19, 20, 23], the moisture and temperature can influence vegetation permittivity which is frequency dependent.

Trees have a complex structure. The geometrical properties of leaves, branches, and the trunk can all influence the microwave propagation. The geometric structures of the tree are often approximately represented by simpler geometries in tree RT models. For example, coniferous leaves can be represented by needles, deciduous leaves can be represented by discs, and twigs, branches, and trunks can be represented by cylinders. And then, according to the shape and the size of the geometries, the scattering approximations can be applied to estimate the RT of trees. For example [29], the Rayleigh-Gans approximation can be applied in coniferous leaves and small deciduous leaves [91], the physical optics approximation can be applied in larger deciduous leaves [92], and the Infinite Length approximation can be applied in twigs, branches, and trunks [80].

2.3.4. The challenges in correcting the influence of forests on PM snow retrievals

To reduce the influence of forests on PM snow retrievals, empirical approaches have been developed (e.g. [12, 93]). Foster [12] suggests that because the sensitivities of the ground Tb to SD and SWE are decreased by forests, a correction coefficient could be introduced into the PM SD and SWE retrieval algorithms to correct the influence of forest attenuation. However, forests have very complex structures and biophysical processes. And, the characters of forests have a high spatial variability in at the global scale. Hence, a single correction coefficient with a constant value is insufficient to describe the influence of forests on PM snow retrievals; the complexity of forests decreases the reliability of such an approach.

The ground-based tree emission observations (e.g. [19, 20, 21, 22]) and modelling studies (e.g. [23, 24, 25, 59]) have helped to develop a better understanding of forest and tree RT processes. Typically, the ground-based tree RT models require many parameters and inputs which make their implementation problematic at the satellite observation scale. Hence, these models are impracticable to be applied in the global or regional scale studies.

The simplified forest RT models, such as the HUT [11] and tau-omega models [14], require fewer parameters and inputs than ground-based tree RT models, and therefore, have been developed and applied to large scale spaceborne microwave applications (e.g. [14, 15, 26, 28, 29, 30, 32]). However, despite their simplicity, the parameters of the simplified forest RT models are still difficult to obtain for regional and global scale studies. For example, although forest transmissivity can be estimated through the vegetation water content [54], the tree stem volume [14, 27, 32], or the leaf area index [94], the estimation approaches only have been tested and

calibrated at one or two locations due to lack of ground observations. In addition, some inputs required by these parameter estimation approaches are not globally available, for example, tree stem volume. Therefore, the simplified forest RT models still have challenges in their implementation at the regional to global scales.

In summary, although the approaches to reduce the influence of forests on spaceborne PM SD and SWE retrievals have been developed (e.g. [11, 12, 13, 14, 15, 18]), the influence of forest remains a big challenge for regional to global scale spaceborne PM SD and SWE or other geophysical parameter retrievals. This thesis addresses this issue directly through a combination of field experimentation and the numerical modelling to correct for the influence of forest transmissivity on PM Observations of snow.

Chapter 3

The general information about the study site and the overview about the research

The study site selected for this research is the Arctic Space Centre, Sodankylä, Finland. This observatory is located 120 km north of the Arctic Circle in the northern Finland (67° 22' N, 26° 38' E). The study site is included in the boreal region, but with regard to stratospheric meteorology, it can be classified as an Arctic site. This unique location makes this study site an excellent place for studying various themes of global change in a northern context.

The FMI Sodankylä field station is a satellite calivation / validation field state that supports programs exploring upper-air chemistry and physics, atmospheric column measurements, snow and soil hydrology, biosphere-atmosphere interaction and satellite calibration-validation studies. The extensive *in-situ* and ground-based remote sensing instrumentation enables reliable satellite calibration and validation activities as well as related scientific research and technological development. The main infrastructure of FMI for Earth Observation satellite data reception, storage and distribution are also hosted in this site. The figure below shows the location of the study site.

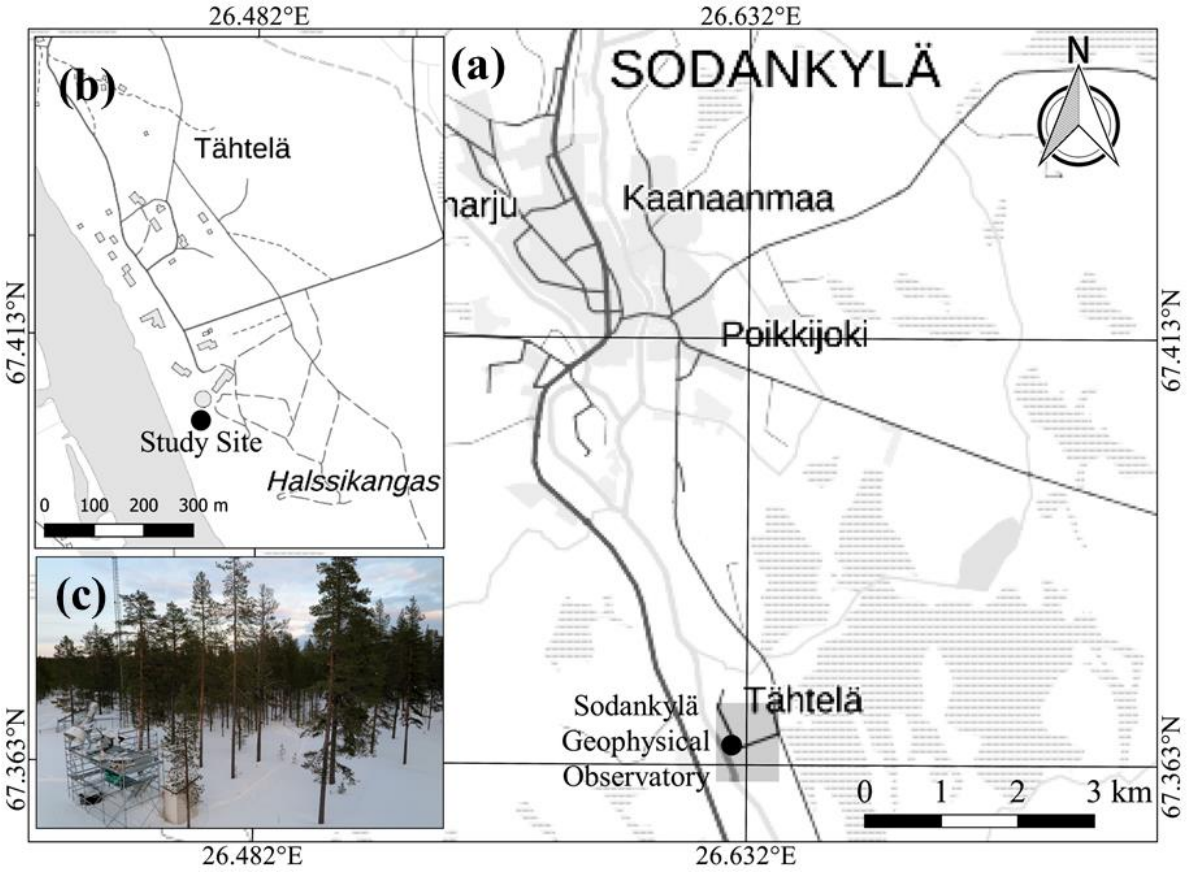

Fig. 3.1 The location of the Finnish Meteorological Institute (FMI) Arctic Research Center shown in (a) and (b), (c) is the image of the Intensive Observation Area in Arctic Research Center. The dot in (a) and (b) represent the location of the ground observation study site (c)

According to the climate statistics provided by FMI, from 1981 to 2010 in Sodankylä the annual average temperature is -5 °C. The coldest month is in January, the average temperature is -13.6 °C. The warmest month is in July with an average temperature of 14.4 °C. The annual average precipitation is 520.5 mm. The maximum snow depth is usually found in March, with about 60-80 cm accumulation on the ground. Sodankylä typifies the landscape in the boreal forest belt. The forest dominates about 54.7% of the land cover in this region, and is mixed with about 75.4 % pine, 14.7% spruce, and 9.8% birch [46]. The Fig. 3.2 (left) shows the landscape of

the forest in Sodankylä, and the Fig. 3.2 (right) shows the image of the Intensive Observation Area (IOA) in Arctic research Center.

Fig. 3.2 The forest around the FMI Arctic Research Center (left), and the image of the Intensive Observation Area in Arctic Research Center (right)

The tree experimentation conducted in this thesis was instigated in the IOA during the fall, winter, and spring of 2016-17. The operation includes the radiometer observation, automatic weather station observation, *in-situ* observation, and the spaceborne observation. I visited this study site for the month of March 2017. With the cooperation of the FMI staff, experiments regarding snowpack characteristics, radiometer observations and calibration, and forest tree biophysical properties were conducted during the visit.

Chapter 4

The influence of thermal properties and canopy-intercepted snow on passive microwave transmissivity of a Scots pine

Overview

While many microwave studies related to tree emission have been undertaken, few have considered the effect of phenological change on the emission from coniferous trees. Permittivity of vegetation tissue is known to be influenced by water content, while the water content and phase is sensitive to temperature in particular at temperatures below freezing. In addition to temperature, canopy-intercepted snow might also modify the tree emission and transmissivity in the microwave range. In this study, a season-long experiment was designed to quantify the effect of snow accumulation and temperature on the observed microwave transmissivity from a Scots pine tree. A ground-based, upward-pointing multi-frequency radiometer was used to monitor the microwave emissivity of a single coniferous tree at a site in Northern Finland. Radiometer measurements were combined with measurements of the canopy-intercepted snow cover and tree skin temperature. This paper presents two important findings. First, the tree transmissivity was strongly correlated with tree skin temperature under sub-zero temperature conditions, but uncorrelated with skin temperature changes above freezing. Second, although the tree

transmissivity was slightly affected by the snow accumulation on the tree canopy, the overall influence on tree emission was statistically insignificant in this study.

4.1. Introduction

Spaceborne passive microwave (PM) systems have been used for retrieval of snow cover parameters for almost 40 years. Global snow water equivalent (SWE) and snow depth (SD) retrievals have been developed by several groups (e.g. [1-7]). The influence of forest cover on the accuracy of these retrievals was acknowledged in early studies with the mitigation for forest cover typically performed by means of a fractional forest cover algorithm (e.g. [8-10]). Although progress has been made to reduce the influence of forest with the empirical or semi empirical approaches (e.g. [10-17]), forest cover still poses a major challenge that reduces the accuracy of PM snow retrievals in forested landscapes (e.g. [18]). An improved understanding of the physical mechanisms of the tree microwave transmissivity is crucial for the further improvement of spaceborne PM snow parameters and other geophysical parameters (e.g. soil moisture) retrievals in forested regions.

Spaceborne PM sensors have a coarse spatial resolution. Therefore, the observed brightness temperature (Tb) over heterogeneous areas such as typical land surfaces is a mixed signal from multiple emission sources. Trees effectively attenuate the below-canopy microwave emission through absorption and scattering, and also contribute to the total emission. Since forested landscapes are prevalent in snow affected regions, especially at mid-latitudes, it is an unavoidable challenge that must be accounted for in PM snow parameter retrievals at the global scale. However, because of the complexity of forest microwave scattering and absorption processes, modeling of the transmissivity of forests (i.e. fraction of emission which is visible

through the forest canopy) with a robust and generally applicable model at the global scale is very challenging.

Studies of microwave transmissivity of individual trees and forest vegetation have been conducted from an observation perspective (e.g. [19-22], [57-58]) and modelling perspective (e.g. [23-25]). Zeroth order τ - ω models (e.g. [14-15], [26-32]) tend to simplify the complex microwave interactions with trees into robust, tractable equations which require few parameters, making them suitable for large scale applications, especially when sufficient ancillary data, e.g. the canopy structure, are unavailable to support higher order models.

Several challenges and uncertainties related to modeling of forest microwave interactions persist. For example, although the effect of defoliation on the microwave emission from deciduous trees has been characterized in some studies (e.g. [21], [24], [33]), few have reported on the long-term temporal variations of microwave emission from coniferous trees, in particular during winter. The water state and free water content in vegetation tissue is affected by sub-zero temperatures. The variation of the water content, in turn, has a notable influence on the dielectric properties of the vegetation tissue, thus affecting also microwave emission from the tree. Rayes and Ulaby [20] found that under laboratory conditions, the permittivity of chopped vegetation tissue measured at 1, 4, and 8 GHz experienced a significant decrease from unfrozen to frozen state at around -7 °C. Mavrovic et al. [53] measured the permittivity of the tree trunk tissue underneath the bark by L-band open-ended coaxial probe measurements. The measurments also shows that a frozen vegetation tissue has a lower permittivity than the unfrozen one. This was due to the lower permittivity of ice compared to free water in the lower microwave range. Under natural conditions, the freezing process is more complicated. Some plants have the capacity to retain free water inside cells in a super cooled state, with water in a liquid phase even at –40 °C

[34]. On the other hand, the adaptation of some plants means that ice can form in extracellular cavities, with some species surviving at -70 °C by means of "extracellular equilibrium freezing" or "extra-organ freezing" [35]. In both cases the dormancy and hardiness of the plant during the winter time leads to physiological and structural changes which can affect the water content of the vegetation [36]. Roy [56] observed the tree permittivity to be sensitive to the physical temperature in sub-zero conditions with the in tree hydro probe measurements. Studies characterizing how these temperature-driven phenological changes influence the tree microwave emission are still limited. However, notable changes can be expected due to the contrast in permittivity between water and ice over parts of the microwave spectrum.

In addition to plant physiological changes, canopy-intercepted snow can also influence the microwave emission from forests. Various studies have examined the mass and energy interactions with taiga and tundra snow (e.g. [37-41]), the energetics of snow interception (e.g. [39]), canopy-intercepted snow accumulation and unload (e.g. [42-43]), and the energy flux of the snow-covered canopy (e.g. [44-45]). However, few studies have examined the impact of canopy-intercepted snow on microwave emission.

This study aims to develop a deeper understanding of the multi-frequency transmissivity of a natural coniferous tree in winter. Specifically, this paper addresses how tree skin temperature and canopy-intercepted snow influences transmissivity and Tb at different frequencies. We apply twice-daily measurements of the microwave response of a single coniferous tree throughout a winter season, combined with measurements of environmental conditions, temperature of the tree and properties of snow accumulated on the tree canopy.

4.2. Materials and Methods

Observations of the microwave emission of a single coniferous tree specimen were made from Sep 5, 2016 to Mar 24, 2017 by an upward-looking radiometer. Observations were supported by *in-situ* measurements of physical temperatures and snow properties. The details are presented in the following sub-sections. The workflow of the methodology is presented in the figure below:

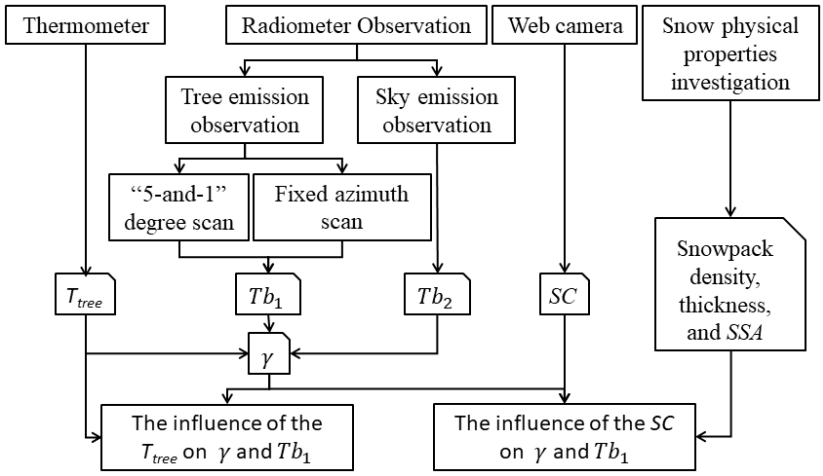

Fig. 4.1 The workflow of the methodology

As the figure shows, the instruments have been applied in this study includes: the thermometer installed in the tree trunk, the radiometer, and the web camera. The tree skin temperature (T_{tree}) collected by thermometer, the microwave brightness temperature (Tb) of the target tree (Tb_1) and the Tb of the sky (Tb_2) collected by the radiometer, the snow cover condition of the tree canopy (*SC*) collected by the web camera, and the snowpack properties of the ground snowpack and the snowpack accumulated on tree canopy obtained by snowpack investigation. With the approach developed by Mätzler [21], the tree transmissivity (γ) is calculated. Accordingly, the influence of the T_{tree} on γ is evaluated. Besides, the influence of the snowpack accumulated on tree canopy on tree transmissivity and tree emission are also evaluated.

4.2.1. The Study Site

The experiment was conducted at the FMI Arctic Research Centre, Sodankylä, Finland located 120 km north of the Arctic Circle (67° 22' N, 26° 38' E). The location is representative of the Northern boreal forest belt with forest cover being the dominant land cover type. Scots pine (*Pinus sylvestris L.*) account for about 76% of the trees while birch represent about 7% [46]. Because the Scots pine dominates the boreal forest belt in this region, a Scots pine specimen was selected as a target for this study.

4.2.2. The Configuration and the Observation Method

Fig. 4.2 illustrates the configuration of the experiment, the description of the measured Tb. Photographs of the instrumentation as well as the observed tree specimen are shown. Details about Fig. 4.2 (a) are explained below.

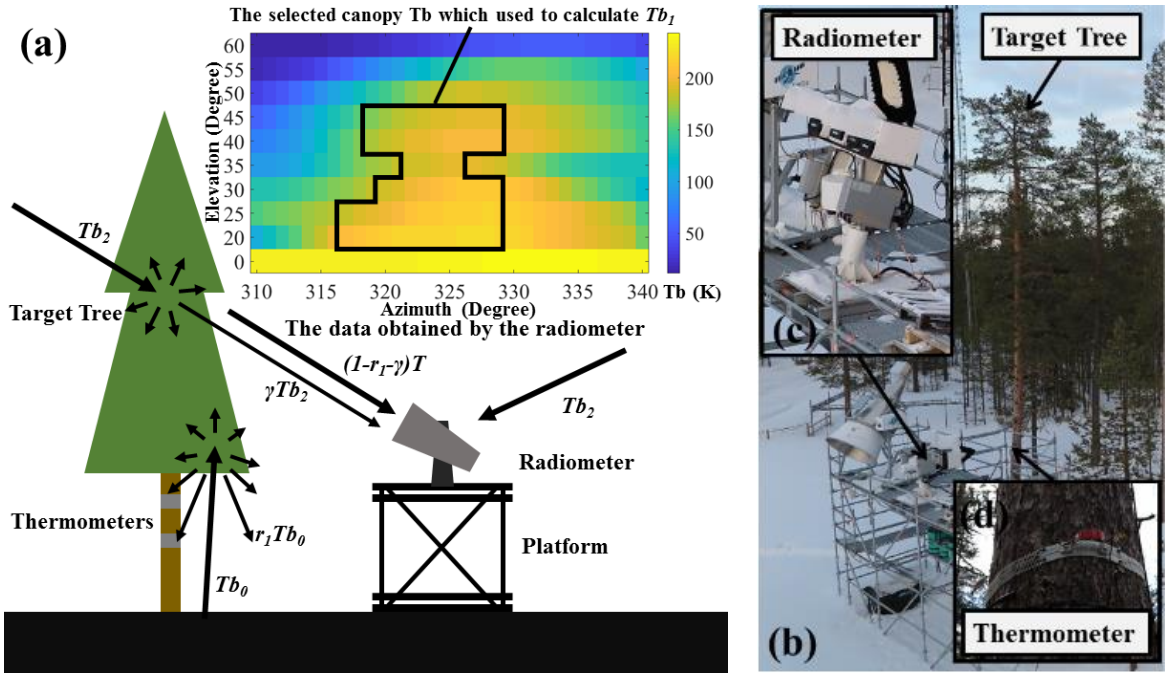

Fig. 4.2 The configuration of the experiment and the description of the measured Tb. (a) shows a schematic of the observation configuration. The setup is depicted in (b), with insets (c) and (d) showing the used SodRad multi-frequency radiometer system and the thermometer installation on the tree, respectively.

i. Tree and the sky microwave emission observations

The SodRad (Sodankylä Radiometer) system (in Fig. 4.2 (c)) was mounted on a 4.1 m high platform (as Fig. 4.2 (b) shows) to record the microwave brightness temperature (Tb) of the target tree (Tb_1) and the Tb of the sky (Tb_2) during the fall, winter, and spring of 2016-17. The distance between target tree and radiometer was about 3 m. The measurement frequencies included 10.65, 18.7, 21 and 36.5 GHz in horizontal (H) and vertical (V) polarizations. The bandwidth for all channels was 400 MHz, the absolute system stability 1.0 K, the Half-Power Beam Width (HPBW) 6.0°, and the sidelobe level is less than -30dB [47]. Because the radiometer was mounted the platform, and was placed close to the target tree, the sidelobe was

almost certainly not influenced by ground emission. Furthermore, the sidelobe power is relatively low. rendering its influence negligible on the observation.

Two scan configurations for tree observation were devised. The first configuration was made during Sep 5, 2016 to Mar 12, 2017 when the radiometer performed a twice daily scan of the target tree with steps of 5° elevation and 1° azimuth. This scan, called the "5-and-1" degree scan, was executed at every 11 am (daylight) and 11 pm (night) UTC. A comparison of day- and night-time observations showed that the solar radiation had little or no significant influence on the measured microwave Tbs. The tree was scanned from 20° to 45° elevation. To better represent the general microwave emission behavior of the entire tree, a representative section of the azimuth-elevation scan including the trunk, branches and the canopy was selected based on the width of the tree at each elevation. Fig. 4.2(a) shows the radiometer-observed tree Tb, with the black contour line enclosing the selected representative section of the tree. The average value of the Tb inside the black contour line was calculated to represent overall the down-welling radiation of the tree Tb_1. Tb data at 36.5 GHz in both V and H polarization were not collected from September 5 to November 1 due to a sensor malfunctioning issue.

A second configuration consisted of an hourly scan to observe the diurnal variation of the tree emission from Mar 13 to Mar 24, 2017. The radiometer scanned the tree hourly at a fixed azimuth facing the direction of the tree trunk, with a step of 5° from 20° to 45° in elevation. The average value of the measured Tb was calculated to represent the down-welling radiation. This scan is called the "fixed azimuth scan".

Tb_2 (sky down-welling emission) was scanned at corresponding 25° to 45° elevations in an azimuth direction free of forest vegetation. This was used as the background sky Tb which considered isotropic in all azimuth directions.

ii. Tree skin temperature and air temperature recordings

Thermometers (in Fig. 4.2 (d)) were installed beneath the tree bark, at the bark-cambium interface, facing to the north at a height of 2.2 m and 4.5 m. The temperature was recorded every 10 minutes for the entire duration of the experiment. The averaged value of the temperatures measured at the height of 2.2 m and 4.5 m was used as the tree skin temperature (T_{tree}).

iii. Canopy-intercepted snow cover condition observations

Web cameras were installed both above and below the target tree to observe the accumulation of snow on the canopy. An image from both cameras was recorded every 10 minutes. An estimate of snow cover conditions (*SC*) at the representative section of the target tree (the area enclosed by the black line in Fig. 4.2 (a)) was estimated from the web camera image based on a visual interpretation. *SC* was classified into two classes: snow-free (label=0) or snow-covered (label=1). Fig. 4.3 shows examples in snow covered and snow free conditions.

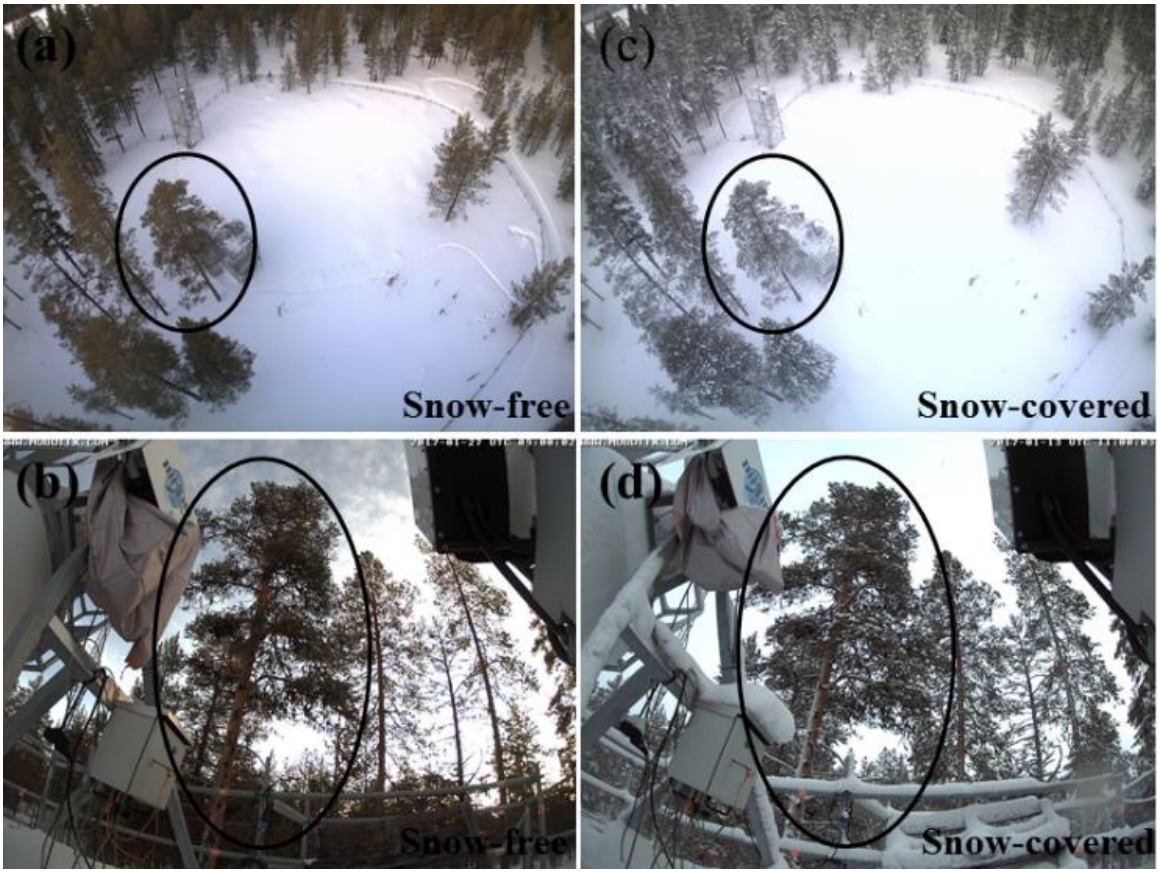

Fig. 4.3 Photographs of the target tree (indicated by circles). (a) and (b) show the target tree under snow-free conditions, and (c) and (d) under snow-covered conditions.

iv. Measurements of snow physical properties

Additional measurements for quantifying snow intercepted by the tree canopy and snow on the ground were conducted. The 15 minute thermometric snow property was recorded from March 20 to March 21 to give diurnal temperatures.

The properties of the canopy-intercepted snow and the nearby ground were measured on March 11, 2017, 5 days after a precipitation event. For the canopy-intercepted snow, 9 samples on different branches each with a different orientation were measured. The branches are about 1.2 m high. Measurements included the snow grain class, snowpack density, snowpack thickness, the greatest diameter of the snow grain (D_{max}), and the Specific Surface Area (*SSA*).

Three thermometers were placed in canopy-intercepted snow on mid-level branches oriented in different directions. Three thermometers were also buried in the ground snowpack at heights of 55 cm (top), 30 cm (middle), and 5 cm (ground) above ground. Two further thermometers were used to record the air temperature. For comparing with the canopy-intercepted snow, a snow profile on the nearby ground snowpack was investigated, the measurements were made at the height of 10 cm, 30 cm, and 60 cm (top layer) from the ground. At each height, 3 measurements were made including grain class, density, $D_{\max}$, and *SSA*. *SSA* measured using an Icecube device [48-49].

4.2.3. Estimation of tree transmissivity

As shown in Fig 4.3 (a), the observed down-welling radiation from the tree Tb_1 can be expressed by the first order radiative transfer equation [21]

$$Tb_1 = \gamma Tb_2 + r_1 Tb_0 + (1 - r_1 - \gamma)T_{tree} \tag{4.1}$$

where the γ and r_1 are the transmissivity and reflectivity of the tree respectively, and T_{tree} is the tree physical temperature, estimated here by the measured tree skin temperature. The first term in the equation (4.1) (γTb_2) is the downward sky Tb emission that passes through the tree, the second term ($r_1 Tb_0$) is the ground emission reflected from the bottom of the tree, and the third term $[\,(1 - r_1 - \gamma)T_{tree}\,]$ is the thermal emission of the tree. Accordingly, the up-welling emission from the tree (Tb_4) can be expressed by:

$$Tb_4 = \gamma Tb_0 + (1 - r_1 - \gamma)T_{tree} + (1 - r_1 - \gamma)r_0\gamma T_{tree} + r_1 Tb_2 + r_0\gamma^2 Tb_2 \tag{4.2}$$

where r_0 is the reflectivity of the ground. The first term in equation (4.2) (γTb_0) is the upward ground emission that passes through the tree. The second term $[(1 - r_1 - \gamma)T_{tree}]$ is the thermal emission of the tree, the third term $[(1 - r_1 - \gamma)r_0\gamma T_{tree}]$ is the downward thermal emission of

the tree that it is reflected by the ground and propagates through the tree; the fourth term ($r_1 Tb_2$) is the downward sky Tb emission which is reflected by the tree, and the fifth term ($r_0 \gamma^2 Tb_2$) is the downward sky Tb that is reflected by the ground, attenuated by the two-way transmissivity of the tree. Assuming thermal equilibrium r_0 can be estimated by:

$$r_0 \approx 1 - \frac{Tb_0}{T_0} \tag{4.3}$$

where T_0 is the physical temperature of the ground which underneath the snowpack. By following the simplified approach of Mätzler [21], γ can be calculated from:

$$\gamma = \frac{T_{tree} - Tb_1}{T_{tree} - Tb_2} \tag{4.4}$$

4.2.4. The influence of tree skin temperature and canopy-intercepted snow on tree emission

To evaluate how tree transmissivity was affected by tree skin temperature and canopy-intercepted snow, simple multiple linear regression models that connected γ (response variables) with T_{tree} and *SC* (explanatory variables) were evaluated. T-tests on the regression coefficients of the regression models were applied to determine if T_{tree} and *SC* have a significant influence on γ by determining if the regression coefficients can be considered as zero (not significantly different). The null hypothesis of the t-test is that the regression coefficient is equal to zero (the influence is not significant).

To evaluate how *SC* might influence the overall observed tree Tb, the Tb_1 observations were divided into two groups by *SC*. The Wilcoxon rank sum test was then applied to evaluate whether the two groups of observed tree Tbs were significantly different. The Tb differences

between snow-covered/snow-free groups is ΔTb, and the null hypothesis of the Wilcoxon rank sum test is that the ΔTb equal to zero (the difference of the Tb between snow-covered and snow-free group is not significant).

To evaluate how variations of transmissivity (γ) with tree temperature (T_{tree}) might influence the overall observed tree Tbs, the tree Tb with T_{tree} under snow-free conditions (*SC* = 0) were simulated in two scenarios. One scenario considers the relationship between γ and T_{tree} under sub-zero temperature conditions (Scenario 2), and for comparison, another scenario only considers the γ as a constant value (Scenario 1). When T_{tree} was above 0 °C, the values of the γ in both Scenario 1 and Scenario 2 were considered equal to the value of *Intercept* (see Table 4.2). When T_{tree} fell below 0 °C, γ in Scenario 1 remained set equal to the *Intercept* values while for Scenario 2, the multiple linear regression models (see Table 4.2) were applied to determine the values of the γ with variable T_{tree}. According to previous studies (e.g. [14], [21], [32], [50]), reflectivity of the tree (r_1) is relatively small, approaching 0 which is why to ignore the reflectivity is one of the common simplified approximations (e.g. [21], [32], [54], [55]). We follow this approach so r_1 is considered equal to 0. Because of the thermal isolation effect of snow, the temperature of the ground underneath the snow is very stable and around 0 to -5 °C, hence, we regard T_0 equal to 0 °C.

In both scenarios, equation (4.1) was applied to estimate the Tb_1at the range of the T_{tree} from -25 °C to 15 °C. Tb_1 calculated in Scenario 1 and Scenario 2 is defined as $Tb_1(Scenario_1)$ and $Tb_1(Scenario_2)$. Equation (3.2) was applied to estimate Tb_4 in both scenarios at the range of the T_{tree} from -30 °C to 0 °C. Tb_4 was calculated at three different Tb_0 values: 150 K, 200 K, and 250 K, representing a range of typical winter-scene ground Tbs. The calculated Tb_4 was defined as $Tb_4(Scenario_1)$ and $Tb_4(Scenario_2)$.

4.3. Results

4.3.1. The temporal variation of the observed canopy Tb

Fig. 4.4 (a) and (b) show the Tbs for the "5-and-1" scans at H and V polarizations, respectively, for September 5 to March 12. Fig. 4.4 (c) shows the tree skin temperature synchronized with the tree Tbs in Fig. 4.4 (a) and (b); the presence of snow cover on the canopy is indicated. Fig. 4.4 (d) and (e) show the Tbs collected by the hourly "fixed-azimuth" scans at H and V polarization for the period March 13-24. Fig. 4.4 (f) represents the tree skin temperature and the snow-covered state synchronized with the tree Tbs in the Fig. 4.4 (d) and (e)

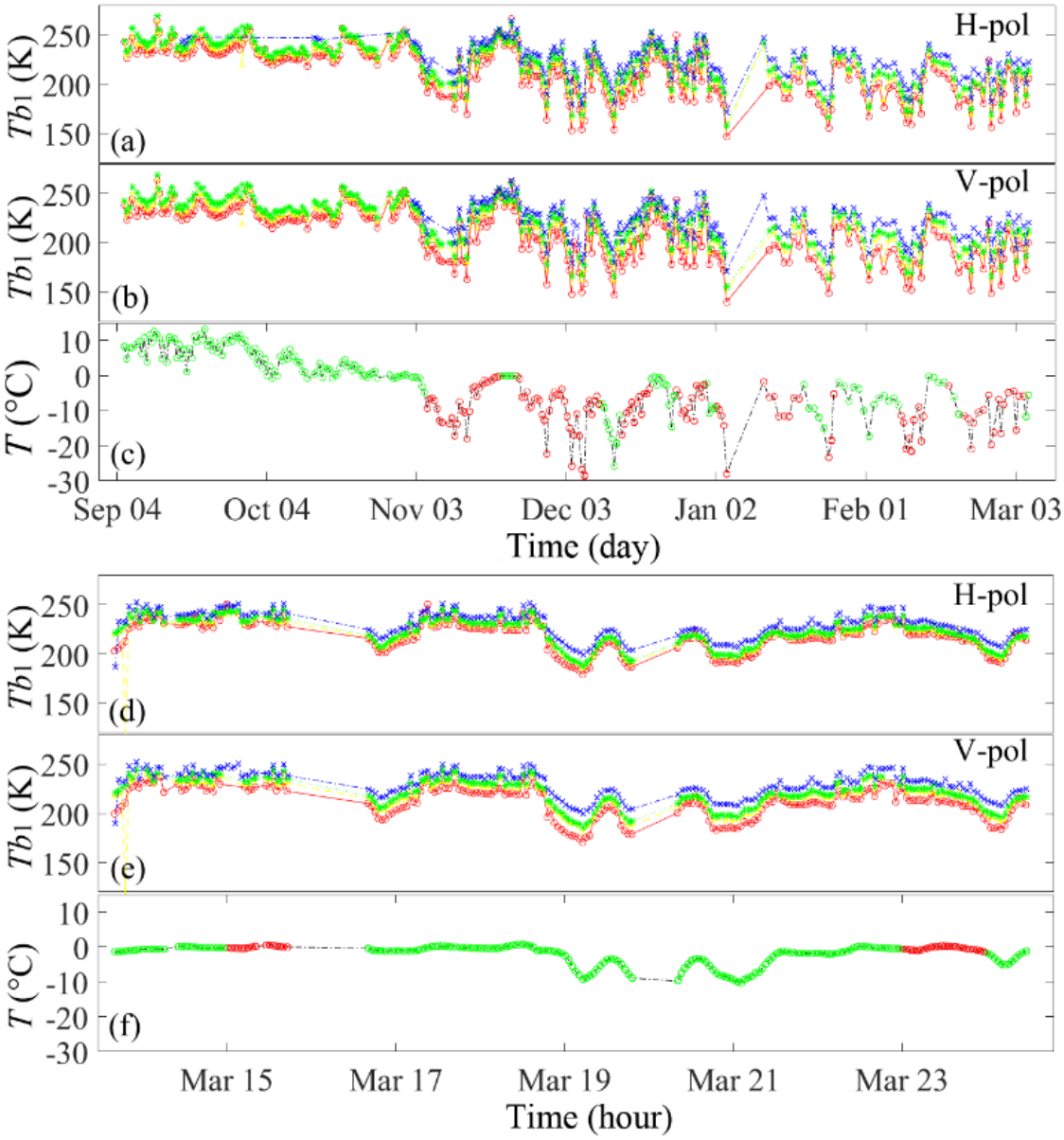

Fig. 4.4 The temporal variation of the observed canopy Tb from September 2016 to March 2017. Red, yellow, green, blue line in in sub-figure a, b, d, e, represent 10.65, 18.70, 21.00, 36.50 GHz radiometer observed Tb. In sub-figures c and f, green marker represents snow free, and red marker represents snow covered.

Fig. 4.4 shows that the Tbs from both data sets ("5-and-1" degree and "fixed azimuth" scan) have similar characteristics. The Tbs variations closely match the tree skin temperature

variations, with the Tbs of higher frequency channels greater than those at lower frequency. The tree skin temperature dropped below 0 °C on November 16, while several snow precipitation events were observed from November to March.

4.3.2. Snowpack properties and the snow cover condition

From September 1, 2016 to March 28, 2017 the target canopy was estimated to be snow covered for 41% of the days. The average snow cover duration was 7 days, with the longest snow cover period of 17 days occurring in November. According to measurements on March 11, 2017 the average thickness of the canopy-intercepted snowpack was 3.5 cm, and the standard deviation was 1.4 cm. From qualitative observations, canopy-intercepted snow cover during the winter of 2016-2017 was typically patchy and did not cover the whole surface of the canopy for prolonged periods.

Table 4.1 shows the grain and density properties of the canopy-intercepted and below-canopy ground snowpack on March 11, 2017. The snow grain classification follows the classification for seasonal snow [51].

Table 4.1 Observed physical properties of snow on the canopy and on the below-canopy ground in march 11, 2017

	Height (cm)	Grain Class	D_{max} (mm)	*SSA* (m^2/kg)		Density (kg/m3)	
			Mean	Mean	Std	Mean	Std
Snowpack on the canopy		PPir/RGsr/ MFcl/ MFpc/MFcr	1	42.4	2.5	131	36
Snowpack on the ground	60	PPir/RGsr	1	48.8	0.8	126	10
	30	FCxr	2	13.0	1.0	240	25
	10	DHxr	6	9.6	0.5	279	21

The left side second column “Height” in Table 4.1 represents the height of the measurements above the ground. According to the Table 3.1, D_{max}, *SSA*, and density of the canopy-intercepted snow were similar to the top layer of fresh snowpack on the ground with the exception of the snow grain types. The snow grains in the canopy snow did not tend to undergo similar metamorphism as snow on the ground in terms of grain growth. Also, the snow grains with the melt forms (e.g. the clustered rounded grains, the rounded polycrystals particles, and the melt-freeze crusts) were more common in the canopy-intercepted snowpack, especially at locations adjacent to the vegetation tissue.

Fig. 4.5 shows diurnal temperature variations of air, canopy-intercepted snow, and ground snowpack (at the height of 55 cm, 30 cm, and 5 cm from the ground) on March 20 to 21, 2017. It shows that the temperature of the canopy-intercepted snowpack was sensitive to the air temperature having a more marked diurnal variation compared with the ground snowpack temperatures. During the daytime, the temperature of the canopy-intercepted snowpack closely matched air temperature, while at night it was slightly higher than the air temperature. As a result, the canopy-intercepted snowpack underwent several melt-refreeze processes during the season.

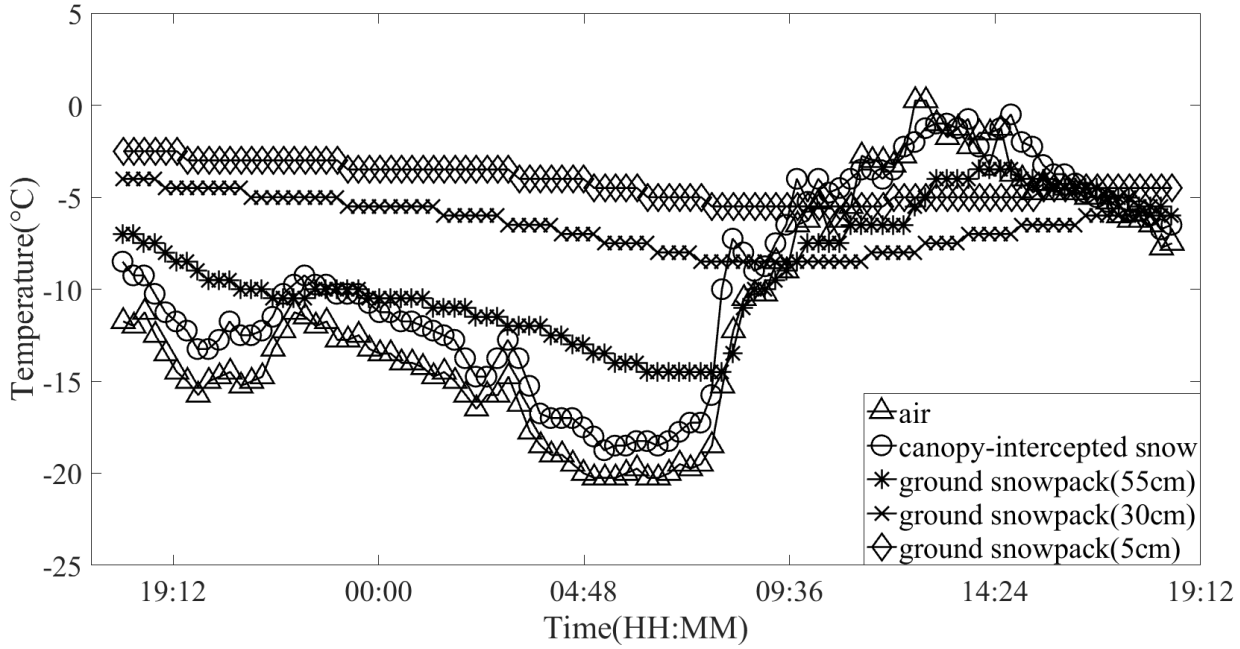

Fig. 4.5 Diurnal temperature variations of the canopy-intercepted snowpack and the ground snowpack on March 20 to 21, 2017.

The D_{max}, *SSA*, and density of canopy-intercepted snow were roughly similar to the fresh snow. However, during measurements on March 11, 2017, the thickness was only about 3.5 cm, and hence, its attenuation and emission properties were considered small for frequencies up to 37 GHz. Furthermore, the duration of the canopy-intercepted snow was shorter than the below-canopy snow.

4.3.3. Influence of tree skin temperature and snow cover on tree canopy emission

Fig. 4.6 shows the relationship between tree transmissivity, snow cover, and tree skin temperature. It shows transmissivity strongly correlated with temperature at sub-zero temperatures. For tree skin temperatures above 0 °C, the correlation between transmissivity and the tree skin temperature was weak. Furthermore, the separation between the transmissivity in

snow covered and snow free conditions was not obvious.

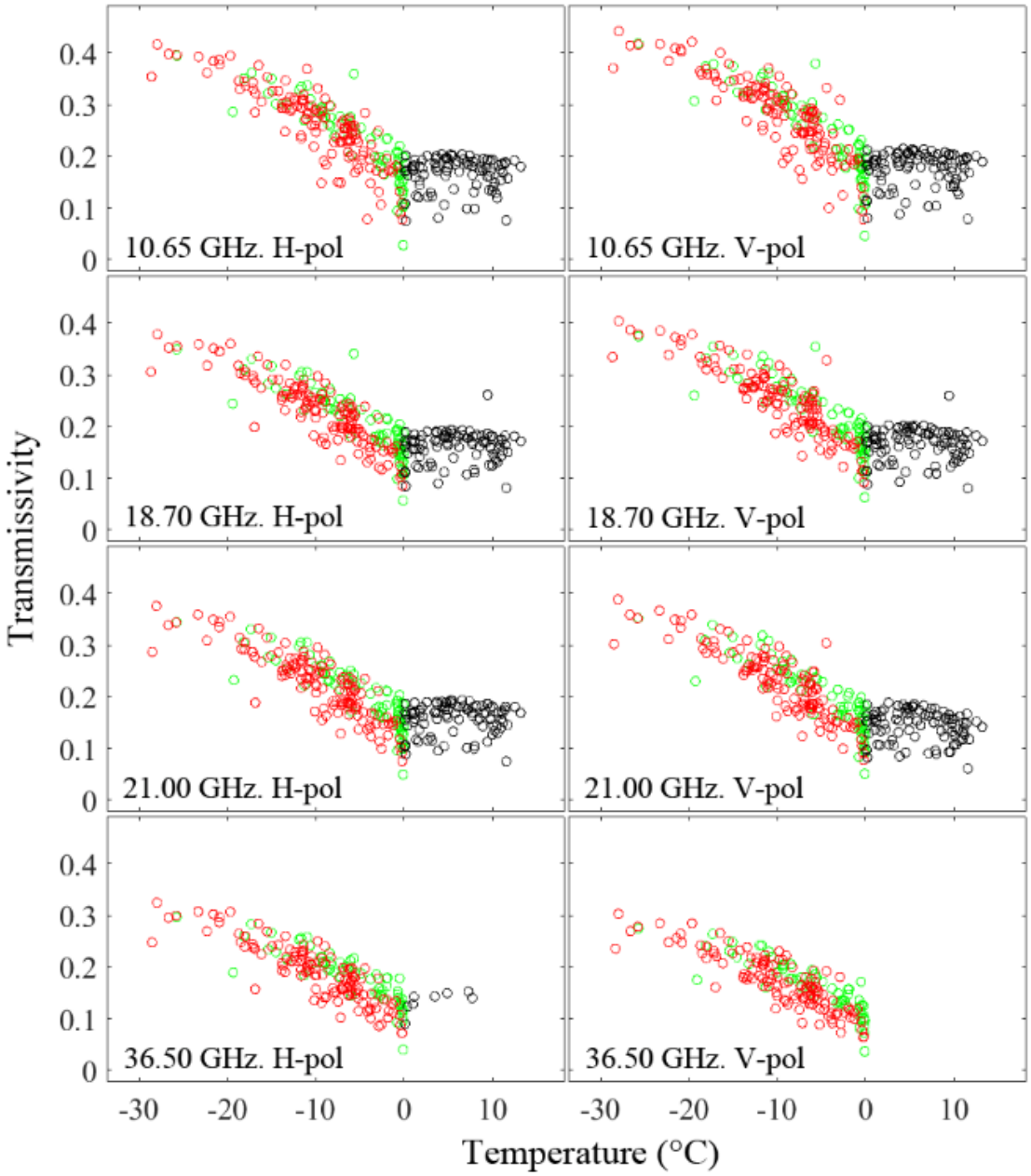

Fig. 4.6 The relationship between trasmissivity, snow cover, and temperature. Red-dots represent the transmissivity for snow-covered canopy conditions, while green-dots represent the transmissivity for the snow-free canopy. Black-dots represent transmissivity of the tree skin temperature above 0 ℃.

Table 4.2 shows linear regression model coefficients of the tree transmissivity against snow cover conditions, and the tree skin temperature in sub-zero conditions. For each channel frequency, the regression model intercept, the snow cover condition ($Coef(SC)$) and tree skin temperature ($Coef(T)$) regression coefficients, and the significance level of the regression coefficients are shown. Also shown is the regression model root mean square errors (RMSE), coefficient of determination (R^2) and observation sample size (Obs). In Table 3.2 and Table 3.3, the significance levels (In Table 4.2 is the significance level of the coefficients, in Table 3.3 is the significant level of the Wilcoxon test) are indicated as 'o' (p-value > 0.05) against the null hypothesis (the null hypothesis cannot be rejected), '*' as a strong rejection of the null hypothesis (p-value ≤ 0.05), and '**' as a very strong rejection of the null hypothesis (p-value ≤ 0.01).

The R^2 values in Table 4.2 indicate that the regression models can explain the variation of the tree transmissivity effectively. The t-test shows that the null hypothesis, for which the $Coef(SC)$ or $Coef(T)$ equaled to 0, was rejected at 0.05 significance level, indicating that the influence of the tree skin temperature and the snow cover condition on the tree transmissivity were statistically significant. The $Coef(T)$ is the rate of the transmissivity change with the temperature.

Table 4.2 The linear regression of the transmissivity, snow cover, and temperature at sub-zero condition

Channel	*Intercept*	$Coef(SC)$	$Coef(T)$	RMSE	R^2	Obs
H10	0.170	-0.014*	-0.011**	0.038	0.740	202
V10	0.187	-0.014*	-0.011**	0.042	0.724	201
H18	0.171	-0.018**	-0.009**	0.033	0.744	203
V18	0.177	-0.019**	-0.010**	0.034	0.748	196
H21	0.143	-0.016**	-0.009**	0.031	0.754	203
V21	0.145	-0.018**	-0.009**	0.031	0.778	196
H37	0.129	-0.019**	-0.008**	0.027	0.753	185
V37	0.134	-0.021**	-0.008**	0.028	0.733	184

The absolute value of $Coef(T)$ decreased with increasing frequency, which indicated that the lower frequency channels were more sensitive to the tree skin temperature. Conversely, the absolute value of $Coef(SC)$ increased with increasing frequency, indicating that the higher frequency channels were more sensitive to canopy-intercepted snow conditions. Although the t-tests in the regression models indicated that the influence of canopy-intercepted snow cover on tree transmissivity was significant, the influence of canopy-intercepted snow on the overall observed tree Tb was unknown. Therefore, Tbs collected under snow-covered and snow-free conditions were divided into two groups and the Wilcoxon rank sum test applied to evaluate whether these groups had a statistically significant difference.

Table 4.3 shows the frequency-dependent mean values of Tb (snow-free), Tb (snow-covered) and ΔTb along with their 95% confidence intervals. The significance level symbols are the same as Table 4.2. Although ΔTb values indicate that the Tbs of the snow-covered group may be slightly greater than the Tbs of the snow-free group, the Wilcoxon rank sum test shows that differences in Tbs between snow-covered and snow-free groups were statistically insignificant.

Table 4.3 The difference of Tbs in the snow-covered/snow-free condition and the 95% confidence intervals

	Tb snow-free (K)	Tb snow-covered (K)	ΔTb (K)	Wilcoxon Significance Levels	Obs
H10	188.6±4.6	192.4±3.5	3.8±5.8	o	74/128
V10	182.9±4.7	187.2±3.6	4.3±6.0	o	74/127
H18	196.2±4.3	200.2±3.2	3.9±5.4	o	74/129
V18	194.3±4.5	198.0±3.4	3.7±5.6	o	73/123
H21	200.8±4.4	204.7±3.3	3.9±5.4	o	73/123
V21	199.6±4.5	203.2±3.4	3.6±5.7	o	74/129
H37	210.9±4.0	214.1±3.1	3.2±5.0	o	73/123
V37	210.4±4.0	214.1±3.1	3.6±5.1	o	60/125

Fig. 4.7 shows that in sub-zero conditions, ignoring the influence of the physical temperature on tree transmissivity likely will cause a bias in tree emission modelling. Also, based on Fig. 4.6 and 4.7, and Table 4.2, the influence of the physical temperature on tree transmissivity may be frequency dependent with the transmissivity at lower frequency channels influenced more by the physical temperature. Furthermore, Fig. 4.7 shows that the influence of the snow cover conditions on tree Tb is not obvious in this experiment.

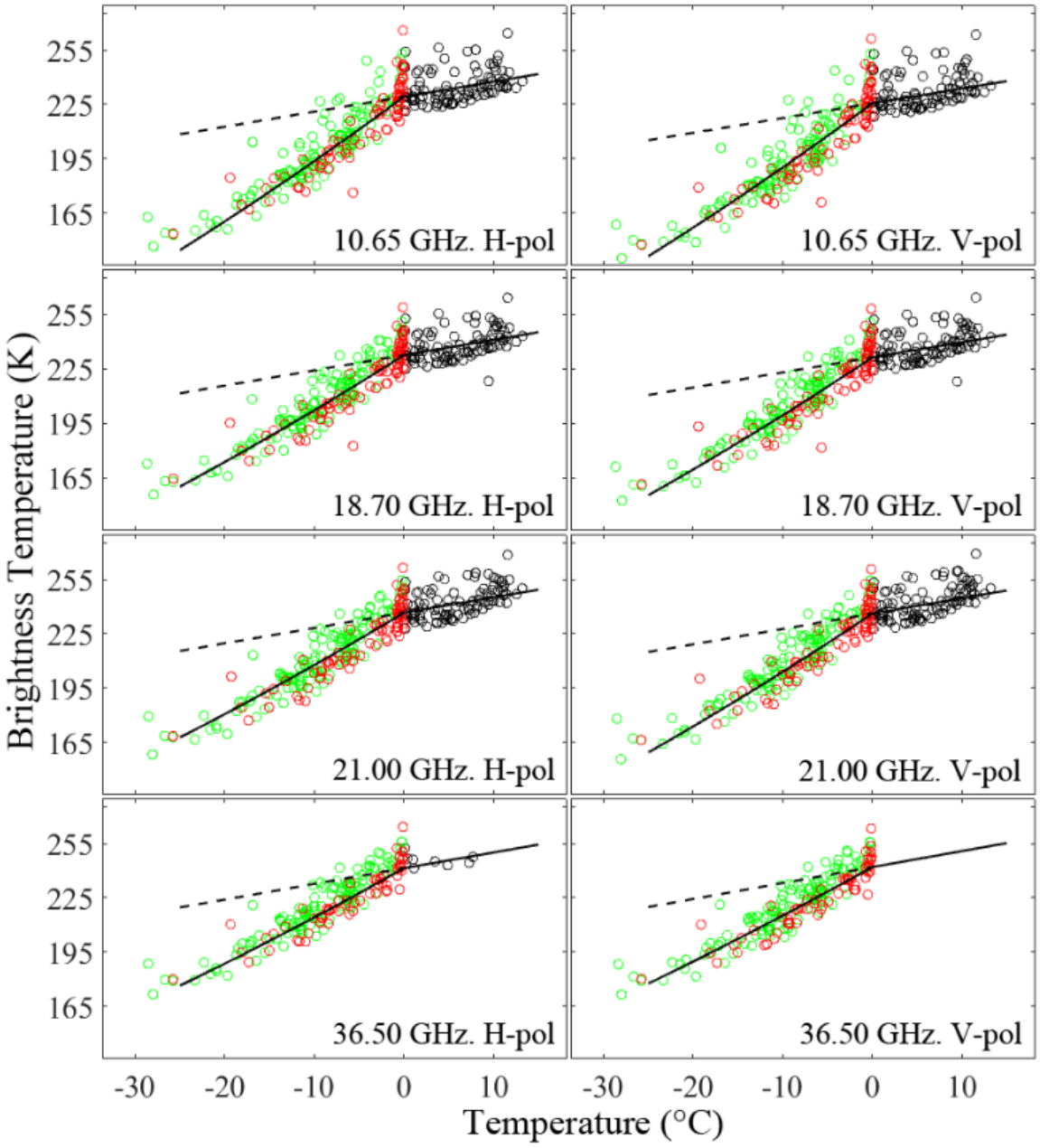

Fig. 4.7 The observed down-welling tree Tb and the Tb simulation. The $Tb_1(Scenario_1)$ (dashed line) and $Tb_2(Scenario_2)$ (solid line) were simulated based on equation (4.1). Red-dots represent observed tree Tbs under snow-covered tree conditions, green-dots represent observed tree Tbs at the snow-free tree condition and black-dots represent observed tree Tbs at the tree skin temperatures greater than 0 °C.

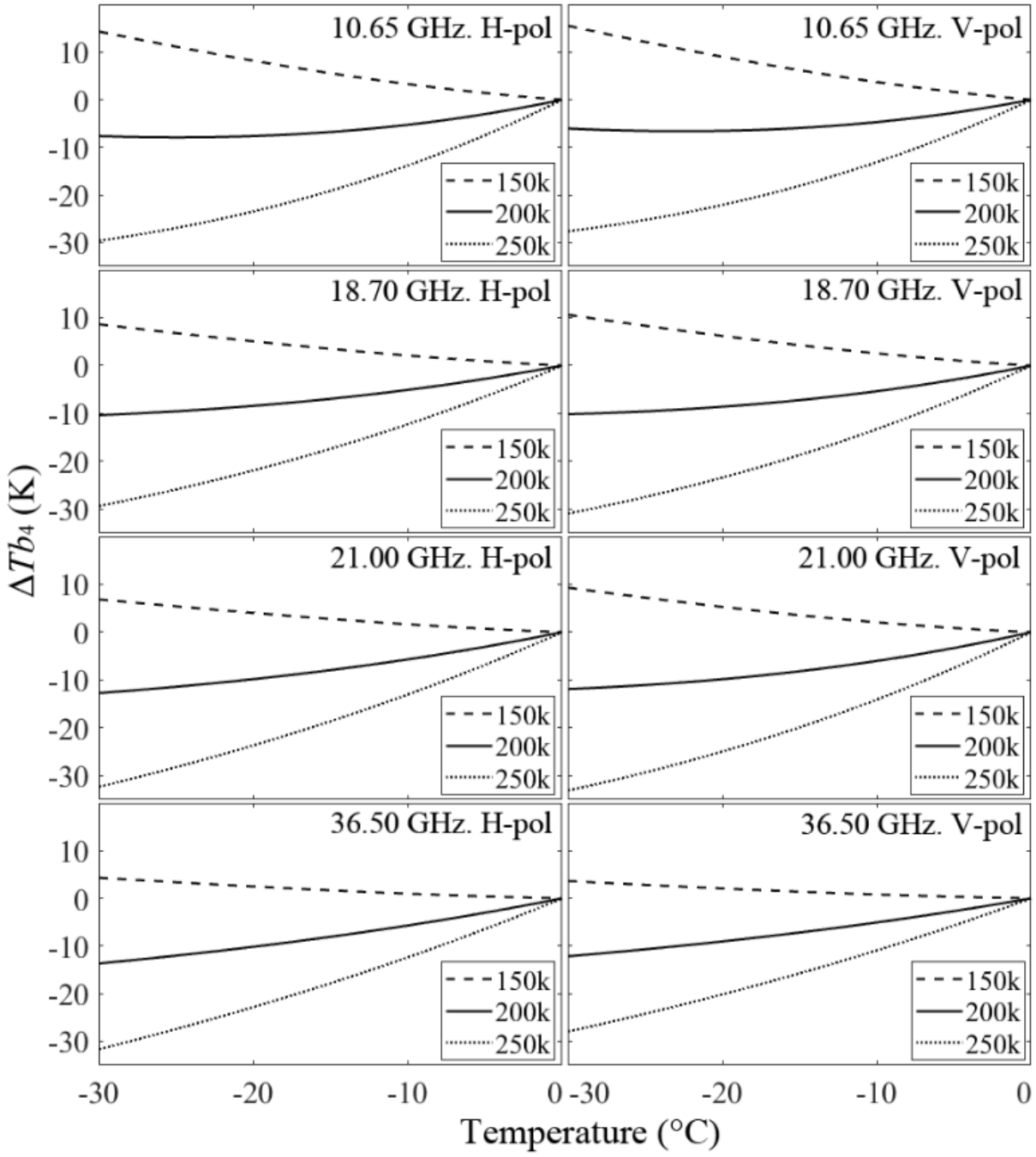

Fig. 4.8 The ΔTb_4 under different ground Tbs (150 K, 200 K, 250 K).

While Scenario 2 considered the relationship between transmissivity and the physical temperature, and Scenario 1 only considered the transmissivity as a constant, the linear difference between $Tb_4(Scenario_1)$ and $Tb_4(Scenario_2)$ (ΔTb_4) represents the estimated error introduced by ignoring the relationship between the transmissivity and the physical temperature

in the up-welling tree emission modelling.

Fig. 4.8 shows the difference in Tbs between model scenarios 1 and 2 when the ground Tb (Tb_0) equals 150 K, 200 K, and 250 K. Tb_0 influences Tb_4. While the emission from the tree mass $[(1-r_1-\gamma)T_{tree}]$ decreases with temperature (T_{tree}), the tree transmissivity increases, therefore the ground emission propagating through the tree (γTb_0) will increase. When Tb_0 is small (e.g. ground covered by deep snow), Tb_4 will decrease because $[(1-r_1-\gamma)T_{tree}]$ decreases. But when Tb_0 is high (e.g. bare frozen ground), the increased (γTb_0) can offset the decrease of the $[(1-r_1-\gamma)T_{tree}]$.

The relationship between transmissivity (γ) and tree temperature (T_{tree}) makes the influence of Tb_0 on Tb_4 sensitive to T_{tree} at sub-zero temperatures. Tb_0 was considered as a constant in Fig. 4.8. Therefore, when considering γ as a constant value, the first term of equation (4.2) (γTb_0) is also a constant value (Scenario 1). In Scenario 2, however, the (γTb_0) increases with the decrease of the T_{tree} because γ increases as T_{tree} decreases. On the other hand, the second term of the equation (4.2) $[(1-r_1-\gamma)T_{tree}]$ decreases faster in scenario 2 than scenario 1 with the decrease of T_{tree} (as shown in Fig. 4.7). This is also because γ increases with T_{tree} decreasing in scenario 2. In scenario 2, the increasing of the γTb_0 could compensate the decreasing of $(1-r_1-\gamma)T_{tree}$. If the Tb_0 is high enough, the Tb_4 could even increase with the decreasing of the T_{tree} in Scenario 2. Therefore, when Tb_0 is high, $Tb_4(Scenario_2)$ is larger than $Tb_4(Scenario_1)$, and vice versa. The Tb difference between $Tb_4(Scenario_1)$ and $Tb_4(Scenario_2)$ could be greater than 30 K.

4.4. Discussion

4.4.1. Influence of canopy-intercepted snowpack

Canopy-intercepted snow is exposed to different energy flux and mechanical stress conditions compared with snow on the ground. First, unlike snow on the ground, snow in the canopy is exposed to air temperature from above and below, thus producing a very weak thermal gradient through the snow. This weak thermal gradient likely promoted destructive metamorphism in the canopy-intercepted snowpack, producing a slow snow grain growth rate [1]. Moreover, being isolated from the ground, the canopy-intercepted snowpack can be more uniformly warmed up and/or melted by the direct and diffuse solar heating. Plus vegetation can act as an effective solar radiation absorber [52] inducing further melt effects through the warming of tree branches. Re-freezing is a likely nighttime outcome in sub-zero temperatures. Second, canopy-intercepted snow typically is subject to a high sublimation rate [39], which reduces the snow duration and thickness. Third, the tree canopy can intercept and hold only a limited amount of snow, depending on the branch mechanical strength and spatial density of branches and needles. Therefore, the load and the interception capacity of the tree canopy limits the thickness of the canopy-intercepted snow [42-43]. For these reasons, the canopy-intercepted snowpack had the following characteristics: small grain size with a melt form shape, limited snow thickness, and a limited duration - usually shorter than the ground snowpack.

These characteristics of the canopy-intercepted snow suggest that its attenuation capacity of microwaves is weak. The radiometer observation results confirmed that, compared with the influence of the forest canopy itself, the canopy-intercepted snow only had limited influence on the canopy microwave emission. However, qualitative assessment of camera imagery suggests that during the year of this experiment, canopy snow interception was limited compared with

preceding years. This experiment was also limited to a single tree specimen; factors such as tree species, age and canopy structure will affect snow catchment on other specimens resulting in variable amounts of canopy-intercepted snow storage and thus variable attenuation from canopy-intercepted snow. Further evaluation of other specimens and different tree species, and under different climate conditions is suggested.

4.4.2. Influence of conifer skin temperature

Microwave transmissivity of the tree specimen in this experiment was shown to have a strong correlation with physical skin temperature in sub-zero temperatures. According to Figs. 6 and 7, and Table 4.2, this correlation has an obvious impact on radiometer observations of forested regions from above the tree canopy at sub-zero temperatures. Furthermore, this impact may be frequency dependent, as can be expected from the differing penetration depths in the vegetation medium and different sensitivities to changes in water phase. We suggest that this relation should be accounted for in future retrieval schemes for snow and other geophysical parameters based on passive microwave sensors in winter.

The geometrical properties of the observed target conifer tree were relatively stable during the winter. With increasing tree skin temperature, the tree transmissivity decreased until the tree skin temperature reached 0 °C. This pattern indicated that the water content of the vegetation tissue was partially frozen in the sub-zero temperature state, reducing the vegetation permittivity. The trunk may experience slower thawing than branches and needles after being frozen, therefore, it may be less sensitive to diurnal temperature variations. However, the leaves can easily be frozen and thawed with diurnal/synoptic scale temperature fluctuations because the leaf of the tree is an effective solar radiation absorber [52], and its surface area to volume ratio is much larger than the trunk and branches making needleleaf tissue more exposed to air and

sunlight. Because the HPBW of the radiometer is 6.0°, even the scan directed towards the trunk will receive a large proportion of the signal from the leaves. This is the reason that the transmissivity is highly sensitive to tree skin temperature.

The steep permittivity decline reported by El-Rayes and Ulaby [20] was not observed in this experiment. Most vegetation species in cold regions have developed an anti-freezing mechanism to prevent cellular ice build-up. For example, super-cooling, extracellular equilibrium freezing, extra-organ freezing are adaptation strategies adopted by several species [34]. The anti-freezing mechanism mitigate the freezing processing, enabling water and ice to coexist inside the vegetation tissue after the air temperature drops below the freezing point. Also, the thermal condition of a tree is heterogenous with some parts having a higher temperature than others (e.g. the location under the wind and toward the sunlight). Therefore, vegetation tissue is unlikely to be frozen or thawed homogeneously which may mitigate the response of the overall tree transmissivity to the measured tree skin temperature. The destructive process in the experiments of El-Rayes and Ulaby (to cut leaf tissue with small piece) [20] and Mavrovic et al. (to remove the bark of the tree trunk with drill) [54] damaged the vegetation tissue. Therefore, as a result the anti-freezing mechanisms of the vegetation likely failed. This explains the steep permittivity decline observed in the experiment of El-Rayes and Ulaby. In its natural state, undamaged vegetation tissue could still be completely frozen in extreme cold conditions, although the ability to withstand sub-zero temperatures is species-dependent.

The relationship between air temperature and tree transmissivity could be included in radiative transfer models of forest vegetation, to help improve the accuracy of spaceborne or airborne retrievals of snow and soil parameters over the forested regions. Considering the complexity of the forest environment, more observations of different types of forest under

different kinds of natural environment will help to establish a more generally applicable approach to describe the influence of temperature on the transmissivity of forest vegetation. Furthermore, more observational data of different tree species and snow conditions would be required to establish the effect of canopy-intercepted snow on the microwave emission from boreal forests. Further experiments should also directly measure the tree dielectric properties e.g. for different depths in the trunk and branches, to associate variations in the microwave response directly to quantified permittivity.

4.5. Conclusion

Using an upward-looking ground-based radiometer, this experiment studied the influence of canopy-intercepted snow and tree skin temperature on the multi-frequency microwave response from a single Scots pine tree specimen. The results indicate that in sub-zero conditions, tree skin temperature had a significant influence on the transmissivity at all observed frequencies, with lower frequencies showing a stronger response. Tree transmissivity increased monotonously with decreasing tree skin temperature up to the coldest reported temperatures of about -30 °C, indicating a gradual change in tree dielectric properties. However, canopy-intercepted snow only had a limited influence on the tree microwave response, possibly due to the relatively limited amount of canopy snow accumulation during the observation season, but also due to the differing characteristics of snow on the canopy, compared to snow on the ground.

The strong relationship between skin temperature and tree transmissivity could be introduced into future active and passive microwave retrievals of geophysical parameters in winter conditions, which typically use a static estimate of forest transmissivity in frozen conditions to estimate the attenuation of microwaves in the forest medium.

Chapter 5

Simulating the influence of temperature on microwave transmissivity of trees during winter observed by spaceborne microwave radiometery

Overview

Forest transmissivity is a key parameter for spaceborne or airborne observations of the Earth's land surface because not only does it influence the proportion of sub-canopy upwelling microwave emission penetrating through the forest canopy, it also controls the forest thermal emission. In frozen winter conditions, observed microwave transmissivity of trees is also strongly influenced by temperature. However, few studies have evaluated this phenomenon with respect to how it could influence spaceborne microwave observations in snow-covered forested landscapes. This study uses ground-based radiometer observations, Advanced Microwave Scanning Radiometer 2 (AMSR2) observations, and model simulation to evaluate how this temperature-transmissivity relationship affects spaceborne passive microwave snow observations. A model is developed to simulate the relationship between tree transmissivity and air temperature. The R^2 of the model is 0.85 (0.81) with a RMSE of 0.03 (0.03) at the 18(37) GHz channels respectively. We find that this temperature-transmissivity relationship has a significant influence on the tree emission, which influences both ground-based radiometer and spaceborne AMSR2 observations. The influence of the temperature-transmissivity relationship on upwelling

ground emission is frequency dependent, demonstrating that the findings have implications for frequency difference based approaches for passive microwave snow depth and snow water equivalent retrievals which observe snow-covered landscapes at air temperatures below freezing. This effect should therefore be accounted for in frequency difference or ratio approaches to snow accumulation retrievals.

5.1. Introduction

Forest cover is a key land cover type in snow affected regions, especially at mid-latitudes. Trees have a strong microwave attenuation and emission capacity. Their complex structures and biophysical processes mean that the presence of forests present a major challenge to the accuracy of airborne and spaceborne passive microwave (PM) geophysical parameter observation retrievals of snow water equivalent (SWE), snow depth (SD) [8, 9, 10, 13], and soil moisture [54].

Tree transmissivity is strongly influenced by tree vegetation permittivity [24, 59]. While dry vegetation mass has a low permittivity, vegetation water content is a key factor controlling its permittivity [19]. Under sub-zero temperatures (°C), the water stored in vegetation freezes as temperatures drop. Hence, the water content decreases due to the water phase change. Accordingly, the permittivity of tree vegetation decreases. This phenomenon was observed by experiment on a small piece of corn leaf [20]. But for natural trees in cold regions, anti-freeze mechanisms can mitigate the freezing process [35, 60]. Furthermore, because trees have a large biomass and complex structure, their thermal character is heterogeneous. For example, Mayr found that the freezing and thawing rate at the top of the tree is greater than at the trunk base [61]. Therefore, tree water content freezing is a complex and uneven process in a natural environment.

Li et al. observed a season-long temperature-transmissivity relationship in a Scots pine tree, and found that the transmissivity changed gradually with temperature at below-freezing conditions [95].

Tree transmissivity variations caused by below-freezing temperatures have a significant influence on the tree emission [95], but typical transmissivity models for forest vegetation ignore this effect (e.g. [14, 27, 32]). Therefore, for observations of cold season snow accumulation, especially SWE, a significant bias is likely introduced if this temperature-transmissivity relationship is ignored. Because the influence of the temperature-transmissivity relationship on upward ground Tb is likely frequency dependent, the brightness temperature (Tb) difference approaches between a low frequency Tb and a high frequency Tb for SD and SWE retrivals (e.g. 18.70 GHz and 36.5 GHz) [1, 2, 75] may also be influenced. A major advantage of the Tb difference approach is that the low frequency channel (e.g. 18 GHz) can be regarded as a reference channel to mitigate the influence of temperature [1]. However, how the temperature-transmissivity correlation could influence the Tb difference is unknown.

In this study, a model to describe the tree temperature-transmissivity relationship is developed using *in-situ* field observations and measurements. Then, application of this model to tree emission observed by the Advanced Microwave Scanning Radiometer 2 (AMSR2) [96] observation is evaluated.

5.2. Methodology

5.2.1. The study site and the configuration of the experiment

This study was conducted using ground-based and satellite data collected over a site near Sodankylä, Finland (67.36 N, 26.63 E). Sodankylä typifies the landscape in the boreal forest belt. The forest dominates about 54.7% of the land cover in this region, and is mixed with about 75.4 % pine, 14.7% spruce, and 9.8% birch [46]. Ground based instruments were located in a forest opening, called the Intensive Observation Area (IOA). The IOA is surrounded by sparse pine forest with trees about 15 m high. The measurement setup allowed ground based instruments to observe both the soil in the forest opening, as well as a single tree specimen from beneath the canopy [95].

The Scots pine (*Pinus sylvestris L.*) is the dominant species in this region. A mature Scots pine tree was selected as a specimen (target tree) for the radiometer tree observation. The up-welling microwave Tb of the ground (Tb_{ground}), the down-welling Tb of the specimen tree ($Tb_{\downarrow tree}$), and the down-welling Tb of the sky (Tb_{sky}) were observed by the Sodankylä Radiometer (SodRad) system located at the edge of the forest opening. Ancillary data were collected from adjacent automatic weather stations (AWS) located inside the forest and inside the forest opening. Fig. 5.1 is the workflow of the methodology:

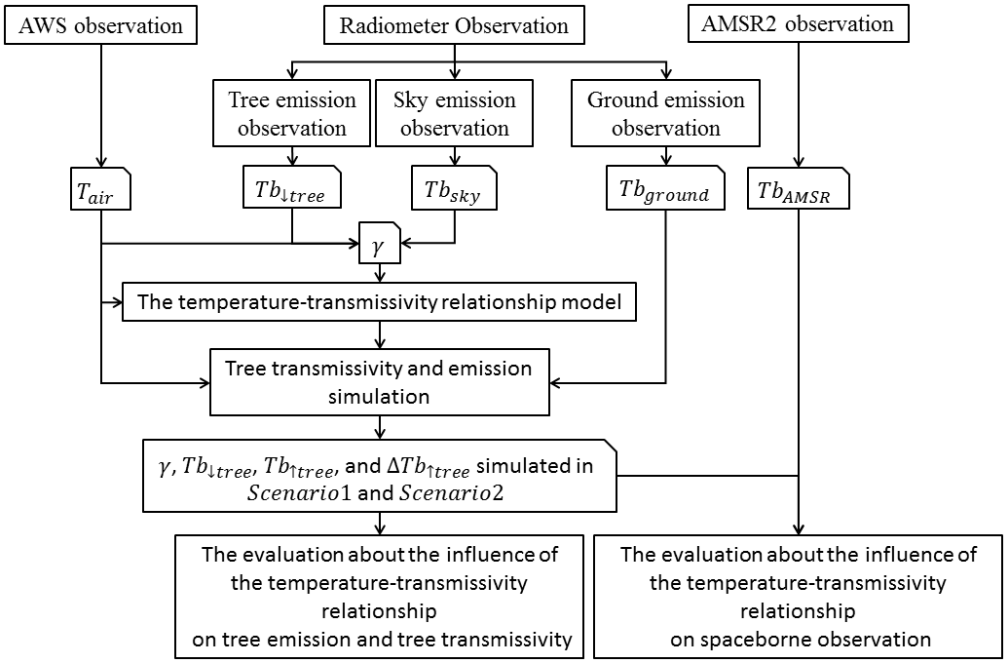

Fig. 5.1 The workflow of the methodology

As the figure shows, the instruments used in ground observation include the automatic weather stations (AWS) and radiometer, the spaceborne Tb observation was obtained by AMSR2 sensor. The air temperature (T_{air}) was collected by AWS. The ground Tb (Tb_{ground}), downwelling radiation from the trees ($Tb_{\downarrow tree}$), and the sky (Tb_{sky}) were collected by radiometer. The satellite observed ground emission (Tb_{AMSR}) was obtained by the AMSR2 sensor. With the approach developed by Mätzler [21], the tree transmissivity (γ) is calculated. Accordingly, the temperature-transmissivity relationship model has been developed. For evaluating the influence of the temperature-transmissivity relationship on tree emission, the model simulation has been made, and the model simulated result has been compared with the spaceborne observation. Fig. 5.2 illustrates the configuration of the study site, and the details of this experiment will be explained in following sub-sections.

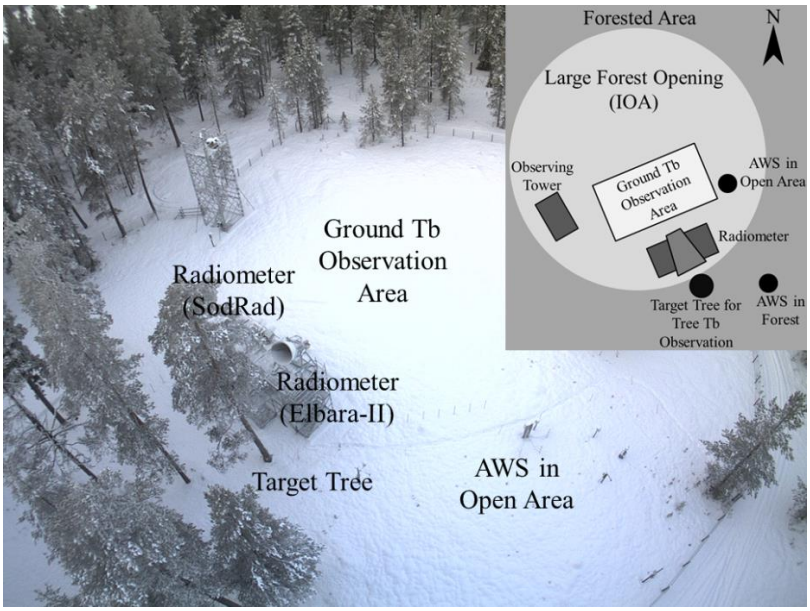

Fig. 5.2. The study site in the IOA, and the configuration of the experiment

5.2.2. Data sources

i. Radiometer observations

The SodRad radiometer system was mounted on a 4.1 m high platform located at the edge of the forest opening. It is a four-frequency dual-polarization system operating at 10.65, 18.7, 21 and 36.5 GHz channels in both horizontal (H) and vertical (V) polarizations. The bandwidths for all frequencies are 400 MHz, the absolute system stability is 1.0 K, the Half-Power Beam Width (HPBW) is 6.0°, and the sidelobe level is less than -30 dB [47].

Tb observations of the ground (Tb_{ground}), the downwelling radiation from the trees ($Tb_{\downarrow tree}$), and the sky (Tb_{sky}) were made at 45° elevation each day from Sep 5, 2016 to Apr 17, 2017. The Tb observations were conducted daily during 11:00 to 3:00 am and 11:00 to 3:00 pm UTC. The horizontal distance between the target tree and the radiometer was about 3 meters, and the ground and the sky were scanned in the opposite direction of the tree scan (Fig. 5.2).

ii. Ancillary data sets

The ancillary data used in the study include the air temperature (T_{air}), snow temperature (T_{snow}), snow depth (SD), soil temperature (T_{soil}), and soil dielectric permittivity (SDP) (in 50MHz) including both the real (RDP) and imaginary (IDP) part. Measurements were acquired every ten minutes by two automatic weather stations (AWS), one in the forest and another in the forest opening. T_{air} and SD were measured in both forest and forest opening by the AWS. T_{air} was measured at 2 meters high by Vaisala PT100 sensor, and SD was measured by Campbell Scientific SR50. T_{snow} and T_{soil} were measured by Campbell Scientific 107-L in the IOA forest opening. T_{snow} was measured from 0 to 120 cm at 10 cm intervals, and T_{soil} was measured at a depth of 5 cm. The RDP and IDP were measured by Stevens Hydra Probe II at a depth of 5 cm.

iii. Satellite observation

The satellite observed ground emission (Tb_{AMSR}) from Sept 1, 2016 to Apr. 30, 2017 was obtained by the AMSR2 onboard Global Change Observation Mission 1st-Water (GCOM-W1) satellite. The descending passes were chosen with an 11:00 pm to 2:30 am crossing time; usually one or two descending passes crossed the IOA each day. Tb_{AMSR} was extract from the Level 1 Resampling product (L1R) [97]. This study used the Tb at 10.65, 18.7, 21 and 36.5 GHz frequency in both H and V polarization. The footprints of the Tbs in all the frequencies were resampled to 24 × 42 km ellipse (along scan × along track). AMSR2 footprints closest to the coordinates of the IOA in the were selected. The forest fraction (percent fraction of forest vegetation) inside the footprint was extracted from the MODIS MOD44b Version 6 Vegetation Continuous Field product [98] in 2016; the forest fraction is 28% for this study area. Since ground is unlikely completely covered by trees even in a forested area, the percentage of forest fraction is likely lower than the percentage of forest cover.

5.2.3. Model description

i. The tree emission modelling

According to Mätzler [21], the down-welling emission from a tree ($Tb_{\downarrow tree}$) can be approximated by the equation (5.1):

$$Tb_{\downarrow tree} = (1 - \gamma - r_{forest})T + \gamma Tb_{sky} + r_{forest} Tb_{ground} \quad (5.1)$$

where γ and r_{forest} are the transmissivity and the reflectivity of the tree respectively and T is the temperature of the tree. Because the skin temperature of the tree is very close to the air temperature [13], we regard T equals to air temperature. The first term in (5.1), $(1 - \gamma - r_{forest})T$, represents the thermal emission from the tree, the second term (γTb_{sky}) represents the sky Tb penetrated through the tree, and the third term ($r_{forest} Tb_{ground}$) represents the up-welling Tb from the ground which is reflected back down by the tree. The up-welling Tb of the tree ($Tb_{\uparrow tree}$) can be written as:

$$Tb_{\uparrow tree} = (1 - \gamma - r_{forest})T + \gamma Tb_{ground} + \gamma r_{forest}(1 - \gamma - r_{forest})T + r_{forest} Tb_{sky} + r_{ground}\gamma^2 Tb_{sky} \quad (5.2)$$

where $(1 - \gamma - r_{forest})T$ is the thermal emission from the tree, γTb_{ground} is the upward ground Tb penetrated through the tree, $\gamma r_{forest}(1 - \gamma - r_{forest})T$ is the downward thermal emission from the tree which is reflected up by the ground and then pass through the tree, $r_{forest} Tb_{sky}$ is the downward sky Tb which is reflected up by the tree, and $r_{ground}\gamma^2 Tb_{sky}$ is the downward sky Tb that is reflected by the ground, attenuated by the two-way transmissivity of the tree. In equation (5.1) and (5.2), Tb_{ground} and Tb_{sky} are obtained by the radiometer, T is the AWS-obtained air temperature. The mean value of the air temperature obtained in the forest and

in the forest opening by the AWS is denoted as T. Since r_{forest} is typicall small, considering the vegetation thus as a simple attenuating layer is a common approach in emission models [3, 28, 32, 54, 55]. Therefore, we follow this approach and assume r_{forest} is 0. Following the approach developed by Mätzler, the transmissivity can be estimated by equation (5.3) [21]. The γ calculated by Mätzler's approach is named henceforth as γ_M.

$$\gamma_M = \frac{T - Tb_{\downarrow tree}}{T - Tb_{sky}} \tag{5.3}$$

In this study, γ_M calculated by equation (5.3) is used to calibrate equation (5.5). Considering T_{ground} equals T_{soil}, the thermal equilibrium r_{ground} is estimated by

$$r_{ground} \approx 1 - \frac{Tb_{ground}}{T_{ground}} \tag{5.4}$$

ii. The temperature-transmissivity relationship

We found that a rational function can describe the relationship between tree transmissivity and air temperature under sub-zero temperatures. This relation is described so that:

$$\gamma = 1 - \frac{(1-\gamma_0)}{1-a_\gamma * T} \qquad T \leq 0$$

$$\gamma = \gamma_0 \qquad T > 0 \tag{5.5}$$

where a_γ is an empirical parameter, T is the air temperature (°C), and γ_0 is the tree transmissivity when T_{air} > 0 °C.

In this model, the rational function $\frac{1}{1-a_\gamma * T}$ in the second term of equation (5.5) is called curve function because this function is used to control the curve line shape of equation (5.5) by adjusting the value of $1 - \gamma_0$. This function is a monotonic increasing function which the value

at the interval of (0,1] when T at the interval of (-∞,0]. Hence, equation (5.5) is a monotonic decreasing function which the value at the interval of (1, γ_0] when T at the interval of (-∞,0].

In this study, for estimating the parameters of equation (5.5), the average γ_M calculated for T_{air} > 0 °C is regarded as γ_0. a_γ is estimated by the least squares fitting method according to the calculated γ_M assuming that the value of γ_0 is determined.

5.2.4. The influence of temperature- transmissivity relathioship on forested snow scene for AMSR2 Tb observations

To evaluate the temperature-transmissivity relationship for tree emission its effect on PM snow observations, the tree transmissivity γ, $Tb_{\downarrow tree}$, $Tb_{\uparrow tree}$, and the Tb difference of the $Tb_{\uparrow tree}$ between 18.7 GHz and 36.5 GHz channel in V polarization ($\Delta Tb_{\uparrow tree}$) were simulated for two scenarios using equations (5.1) and (5.2). In $Scenario1$, the transmissivity was calculated based on the temperature-transmissivity relationship model in equation (5.5). Accordingly, the simulated results are written as: γ_{S1}, $Tb_{\downarrow tree\_S1}$, $Tb_{\uparrow tree\_S1}$, and $\Delta Tb_{\uparrow tree\_S1}$. For $Scenario2$, the temperature-transmissivity relationship is ignored, so transmissivity is considered as $\gamma = \gamma_0$ in all the temperature. Accordingly, the simulated results are written as: γ_{S2}, $Tb_{\downarrow tree\_S2}$, $Tb_{\uparrow tree\_S2}$, and $\Delta Tb_{\uparrow tree\_S2}$. The difference of the simulated results between $Scenario1$ and $Scenario2$ reveals how the temperature-transmissivity relationship can influence tree emission and the ΔTb.

To evaluate the influence of the temperature-transmissivity relationship on spaceborne PM Tb observations, Tb_{AMSR} is compared with the model-simulated $Tb_{\downarrow tree\_S1}$ and $Tb_{\downarrow tree\_S2}$. And the Tb difference of the Tb_{AMSR} (ΔTb_{AMSR}) is compared with $\Delta Tb_{\uparrow tree\_S1}$ and $\Delta Tb_{\uparrow tree\_S2}$. Because the frequency difference algorithm for global SWE and SD estimation is developed

based on the sensitivity of ΔTb to SWE and SD (e.g. [1, 2, 75]), this comparison reveals how the temperature-transmissivity relationship can influence the PM spaceborne SWE and SD retrieval.

5.3. Results

5.3.1. The AWS ancillary data and the spaceborne and ground based radiometer observed Tb

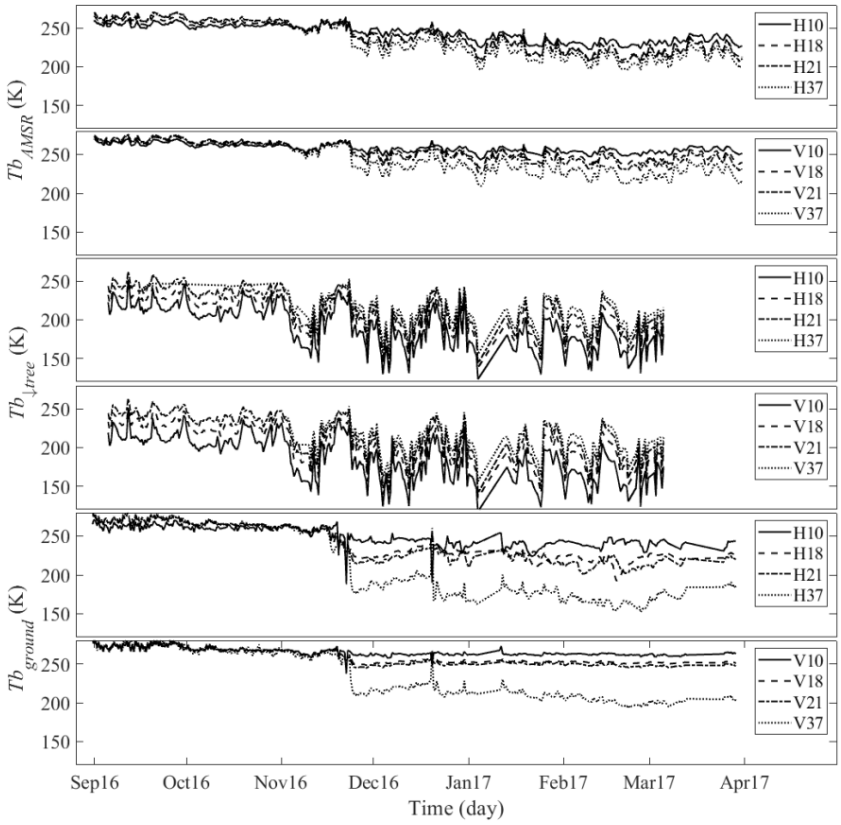

Fig. 5.3 The ground-based radiometer-observed Tb ($Tb_{\downarrow tree}$ represents down welling tree emission, and Tb_{ground} represents ground emission), and the AMSR2 observed Tb (Tb_{AMSR}).

Fig. 5.3 shows the Tb_{AMSR}, $Tb_{\downarrow tree}$, and Tb_{ground} from Sep 5, 2016 to Apr 17. Since the thermal emission of the tree is the major component of $Tb_{\downarrow tree}$, the behavior of $Tb_{\downarrow tree}$ is very

similar as the thermal emission of the tree. $Tb_{\downarrow tree}$ is sensitive to the air temperature. For Tb_{ground}, after the ground is covered by snow, the thermal isolation effect of snow makes the soil temperature underneath the snowpack relatively stable (see Fig. 4.3), so the attenuation of the snowpack is the major factor to influence Tb_{ground}. Hence, Tb_{ground} is sensitive to the snow depth, and the high frequency channels are attenuated more by the snowpack than the low frequency channels. The soil temperature is usually higher than the air temperature (Fig. 4.3). Therefore, Tb_{ground} in a low frequency channel is usually higher than $Tb_{\downarrow tree}$ under sub-zero temperature. Finally, because the forest and the snow-covered ground are the major components inside the AMSR2 observation footprint, Tb_{AMSR} is influenced by both air temperature and snow depth.

Fig. 5.4 shows the environmental ancillary data collected by the AWS from Sep 5, 2016 to Apr 17. In Fig. 5.4 (a), SD_{open} and SD_{forest} represent the AWS measured snow depth inside the forest opening and inside the forest respectively. In Fig. 5.4 (c), 0 cm, 30 cm, 60 cm represents the snow temperature at a height of 0, 30 and 60 cm above the subnivean soil. The ground was covered by snow from Nov. 4, 2016 to Apr. 17, 2017. The ratio of the snow depth in the forest opening to that in the forest is about 1.5:1. During the snow-covered period, the air temperature fluctuated, but the soil temperature remained relatively stable. The soil dielectric permittivity changed significantly at the point when it froze, but it was relatively stable before and after the soil freezing.

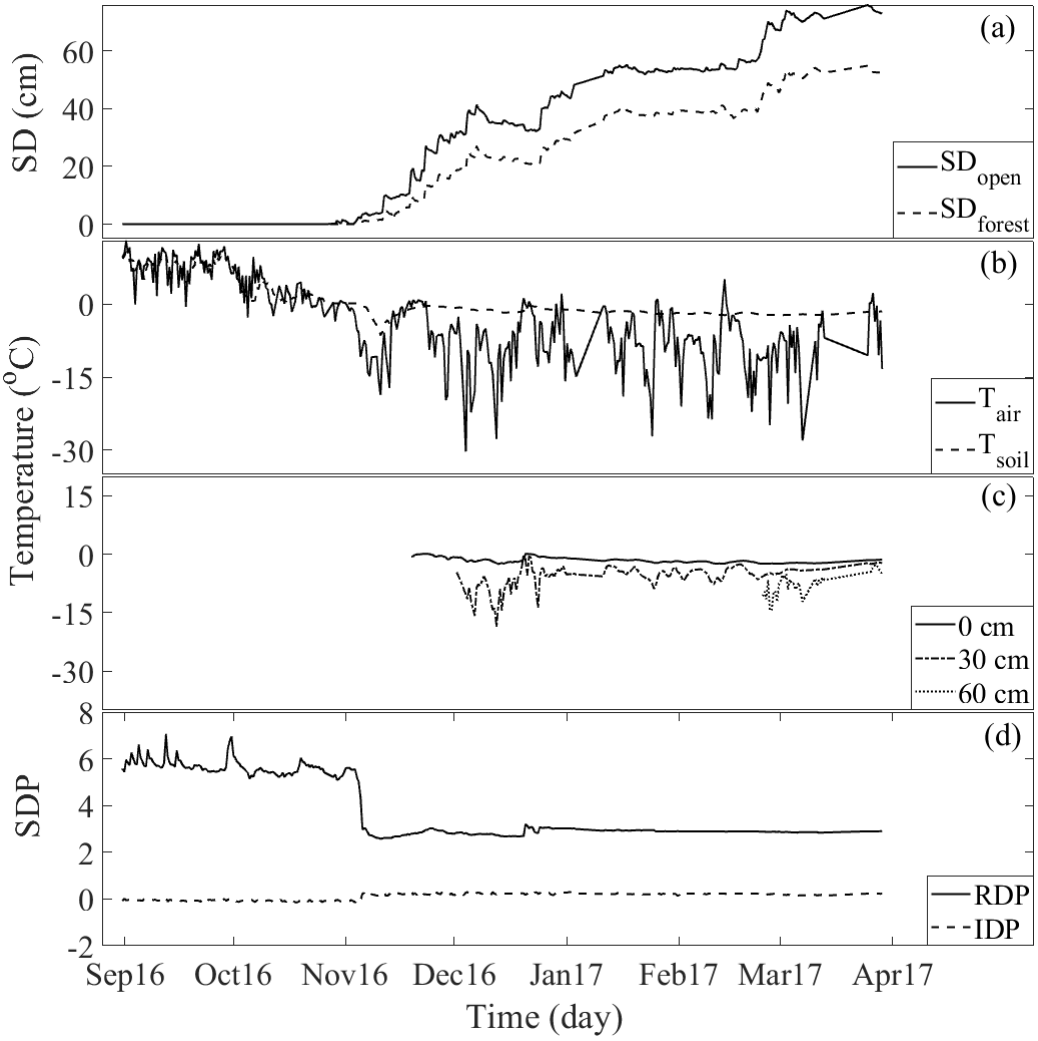

Fig. 5.4 Environmental ancillary data collected by AWS. (a) demonstrates the snow depth in forest opening and forested region, (b) demonstrates the air temperature and soil temperature, (c) demonstrates snowpack temperature profile, and (d) demonstrates the soil dielectric permittivity

5.3.2. The relationship between tree transmissivity and air temperature

To test the temperature-transmissivity model from equation (5.5), and to evaluate the influence of the air temperature on the tree transmissivity, γ_M, γ_{S1} and γ_{S2} are compared in Fig. 5.5. γ_{S1} is the transmissivity calculated from $Scenario1$, which considers the temperature-

transmissivity relationship. While γ_{S2} is the transmissivity calculated from $Scenario2$, which regards transmissivity as a constant.

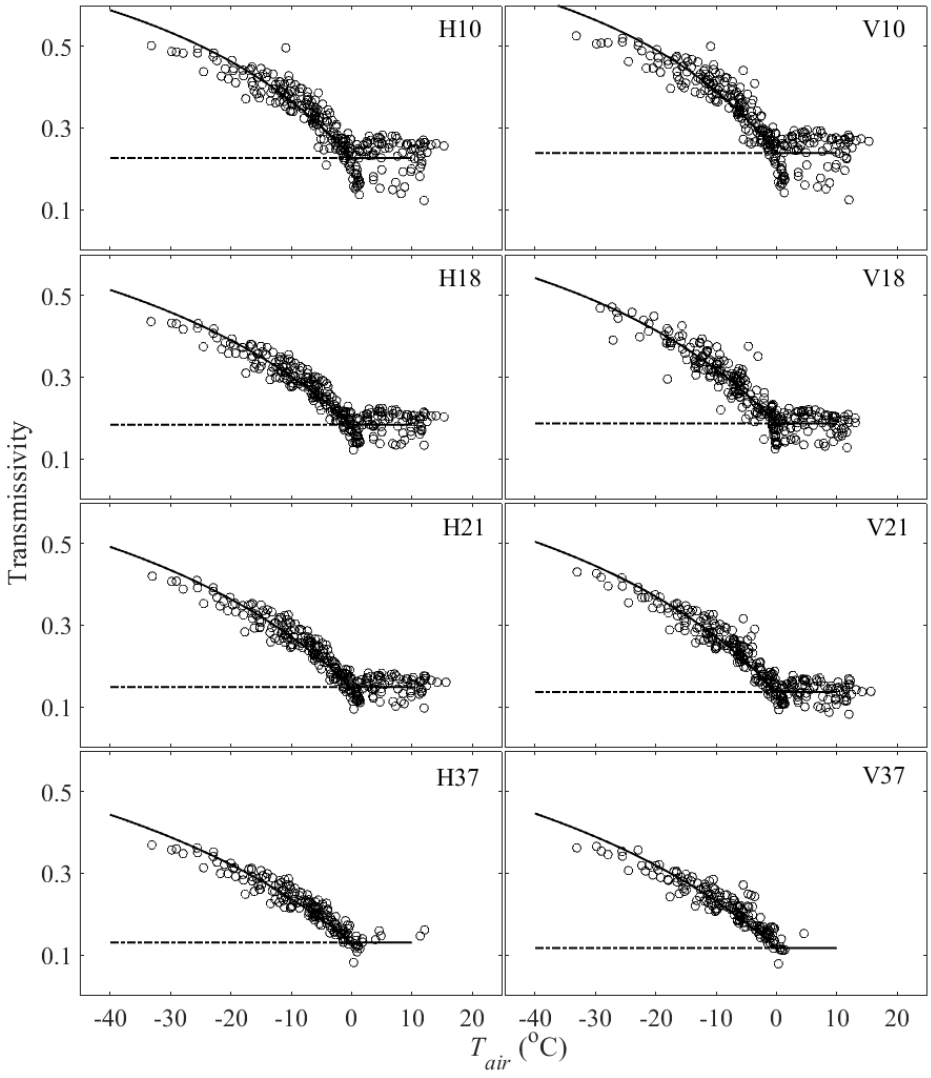

Fig. 5.5 The comparison between γ_M (circle markers), γ_{S1} (solid line), and γ_{S2} (dashed line)

According to Fig. 5.5, the transmissivity of the tree increases as air temperature decreases, while the transmissivity is insensitive to air temperatures higher than 0 °C. The comparison between the estimates from the two model scenarios indicates that the model that uses the air

temperature adjustment (γ_{S1}) fits well with the observed results (γ_M). Table 5.1 below shows the estimated parameters, R^2 and the Root Mean Square Error (RMSE) of equation (5.5).The comparison between γ_{S1} and γ_{S2} indicates that the temperature is a major factor causing the tree transmissivity variations of up to 0.3 under sub-zero temperatures.

Table 5.1 The estimated parameters (γ_0 and a_γ), R^2 and the RMSE of equation (5.5)

	H10	**V10**	**H18**	**V18**	**H21**	**V21**	**H37**	**V37**
γ_0	0.23	0.24	0.18	0.19	0.15	0.14	0.13	0.12
a_γ	0.02	0.03	0.02	0.02	0.02	0.02	0.01	0.02
R^2	0.84	0.83	0.89	0.85	0.90	0.87	0.87	0.81
RMSE	0.03	0.03	0.02	0.03	0.02	0.03	0.02	0.03

5.3.3. Evaluation of temperature influences on transmissivity affecting Tb emissions: implications for PM snow retrievals

Having determined that tree transmissivity is strongly controlled by air temperature, it is possible to estimate $Tb_{\downarrow tree}$ using equations (5.1), (5.2) and (5.5). Fig. 5.6 shows the radiometer observed $Tb_{\downarrow tree}$ and the simulated $Tb_{\downarrow tree}$ of the two model scenarios. When corrected for air temperature, $Tb_{\downarrow tree\_S1}$, and when temperature-transmissivity relationship is ignored, $Tb_{\downarrow tree\_S2}$.

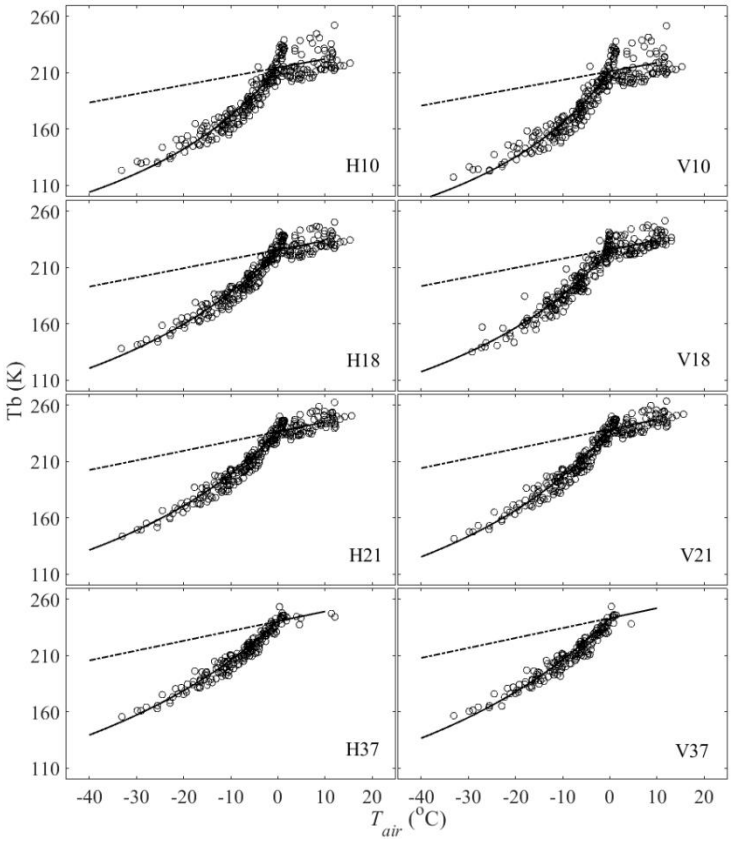

Fig. 5.6 $Tb_{\downarrow tree}$ observed by the radiometer (circle markers), and simulated Tb in $Tb_{\downarrow tree\_S1}$ (solid lines) and $Tb_{\downarrow tree\_S2}$ (dashed lines)

$Tb_{\downarrow tree\_S1}$ has a good agreement with the $Tb_{\downarrow tree}$ observed by the radiometer, which indicated that the tree emission models (equations (5.1) and (5.2)) and the temperature-transmissivity relationship model (equation (5.5)) explains the variation of the radiometer-observed tree emission in this experiment. In a similar manner for the temperature-transmissivity relationship model, $Tb_{\downarrow tree}$ emission responds to the air temperature as temperatures fall below 0 °C. Without the temperature-transmissivity correction ($Scenario2$), estimated $Tb_{\downarrow tree\_S2}$ decreases monotnically with air temperature. The difference between the two scenario models increases as temperature drops to more than 30 K at -30 °C inidicating a significant bias.

With respect to spaceborne Tb observations, Tb_{AMSR} (star makers with Blue-Green-Yellow colors) is compared with estimated Tbs from $Tb_{\uparrow tree\_S1}$ (red circle markers) and $Tb_{\uparrow tree\_S2}$ (black cross markers) in Fig. 5.7. $Tb_{\uparrow tree\_S1}$ is the Tb calculated from $Scenario1$, which considers the temperature-transmissivity relationship. While $Tb_{\uparrow tree\_S2}$ is the Tb calculated from $Scenario2$, which ignores this temperature-transmissivity relationship. The Blue-Green-Yellow scale bar and the colors of the star markers represent the snow depth in the forest opening (warmer color represents higher snow depth). The Tbs in both $Tb_{\uparrow tree\_S1}$ and $Tb_{\uparrow tree\_S2}$ decrease with decreasing air temperature. However, the relationship between $Tb_{\uparrow tree\_S2}$ and air temperature maintains a relatively consistent gradient from low frequency to high frequency estimates, while for $Tb_{\uparrow tree\_S1}$ the gradients of these relationships decreases from high frequency (37 GHz) to low frequency (10 GHz) indicating an decreased sensitivity to air temperature at the lower frequency Tb observations. The differences between Tb estimates in $Tb_{\uparrow tree\_S1}$ and $Tb_{\uparrow tree\_S2}$ are not as large as the differences between $Tb_{\downarrow tree\_S1}$ and $Tb_{\downarrow tree\_S2}$, but the difference between $Tb_{\uparrow tree\_S1}$ and $Tb_{\uparrow tree\_S2}$ also tends to increase as air temperature decreases.

According to the MOD44b product, the forest fraction is 28% in the AMSR2 observation footprint. Outside the forest, most of the land inside the AMSR2 observation footprint is snow-covered ground during wintertime. Hence, Tb_{AMSR} has a higher sensitivity to the snow depth compared with $Tb_{\uparrow tree\_S1}$ and $Tb_{\uparrow tree\_S2}$. Similar as $Tb_{\uparrow tree\_S1}$, the gradient of Tb_{AMSR} variation with the air temperature decreases from high frequency (36 GHz) to low frequency (10 GHz) under sub-zero temperature, especially at V polarization. This similarity between Tb_{AMSR} and $Tb_{\uparrow tree\_S1}$ indicates that Tb_{AMSR} is also influenced by the temperature-transmissivity relationship under sub-zero temperature.

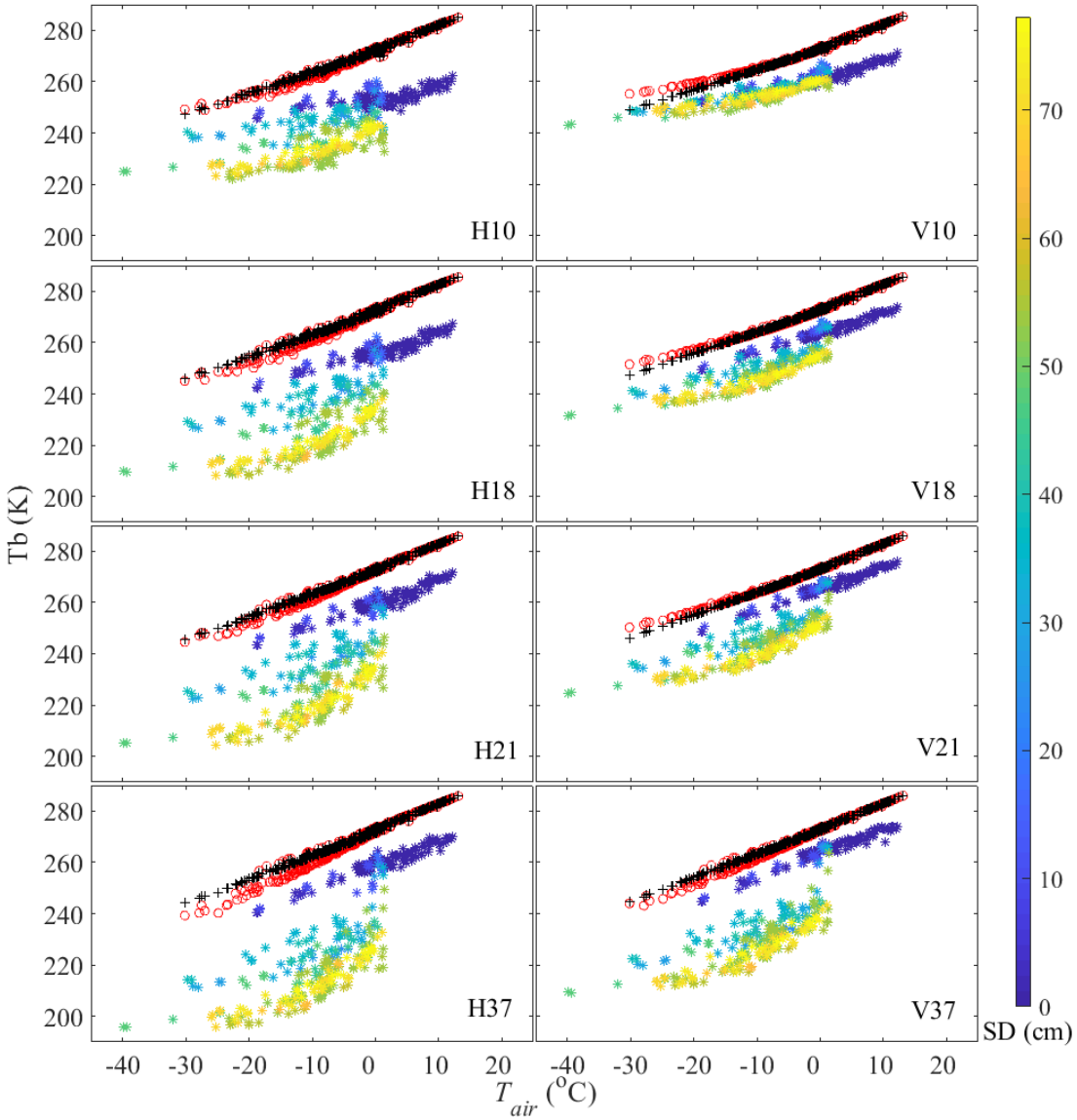

Fig. 5.7 $Tb_{\uparrow tree\_S1}$ (red circle marker), $Tb_{\uparrow tree\_S2}$ (black cross marker), and Tb_{AMSR} (star marker with Blue-green-yellow colors). Blue-green-yellow star markers represent AMSR2 Tbs for different snow depths (Blue-Green-Yellow scale) in the forest opening.

$\Delta Tb_{\uparrow tree\_S1}$, $\Delta Tb_{\uparrow tree\_S2}$, and ΔTb_{AMSR} are compared in Fig. 4.7 to evaluate how the temperature-transmissivity relationship could influence PM snow retrievals that use a Tb difference approach. $\Delta Tb_{\uparrow tree\_S1}$ is the Tb difference calculated from $Scenario1$, which

considers the temperature-transmissivity relationship. While $Tb_{\uparrow tree\_S2}$ is the Tb difference calculated from $Scenario2$, which ignores this temperauture-transmissivity relationship. The sensitivity of $\Delta Tb_{\uparrow tree\_S1}$ to the snow depth increases as air temperature decreases, and $\Delta Tb_{\uparrow tree\_S1}$ has a negative correlation with the snow depth; the sensitivity of $\Delta Tb_{\uparrow tree\_S2}$ to the snow depth is not influenced by the air temperature.

Similar as $\Delta Tb_{\uparrow tree\_S1}$, the sensitivity of ΔTb_{AMSR} to the snow depth also increases with the decrease of the air temperature, and ΔTb_{AMSR} has a negative correlation with the snow depth. The agreement between $\Delta Tb_{\uparrow tree\_S1}$ and ΔTb_{AMSR} indicates that the temperature-transmissivity relationship has a similar influence on ΔTb_{AMSR} and $\Delta Tb_{\uparrow tree\_S1}$. However, because only 28% land cover type is forest in the AMSR2 observation footprint, the influence of the temperature-transmissivity relationship on ΔTb_{AMSR} is weaker than $\Delta Tb_{\uparrow tree\_S1}$, and ΔTb_{AMSR} has a higher sensitivity to the snow depth than $\Delta Tb_{\uparrow tree\_S1}$.

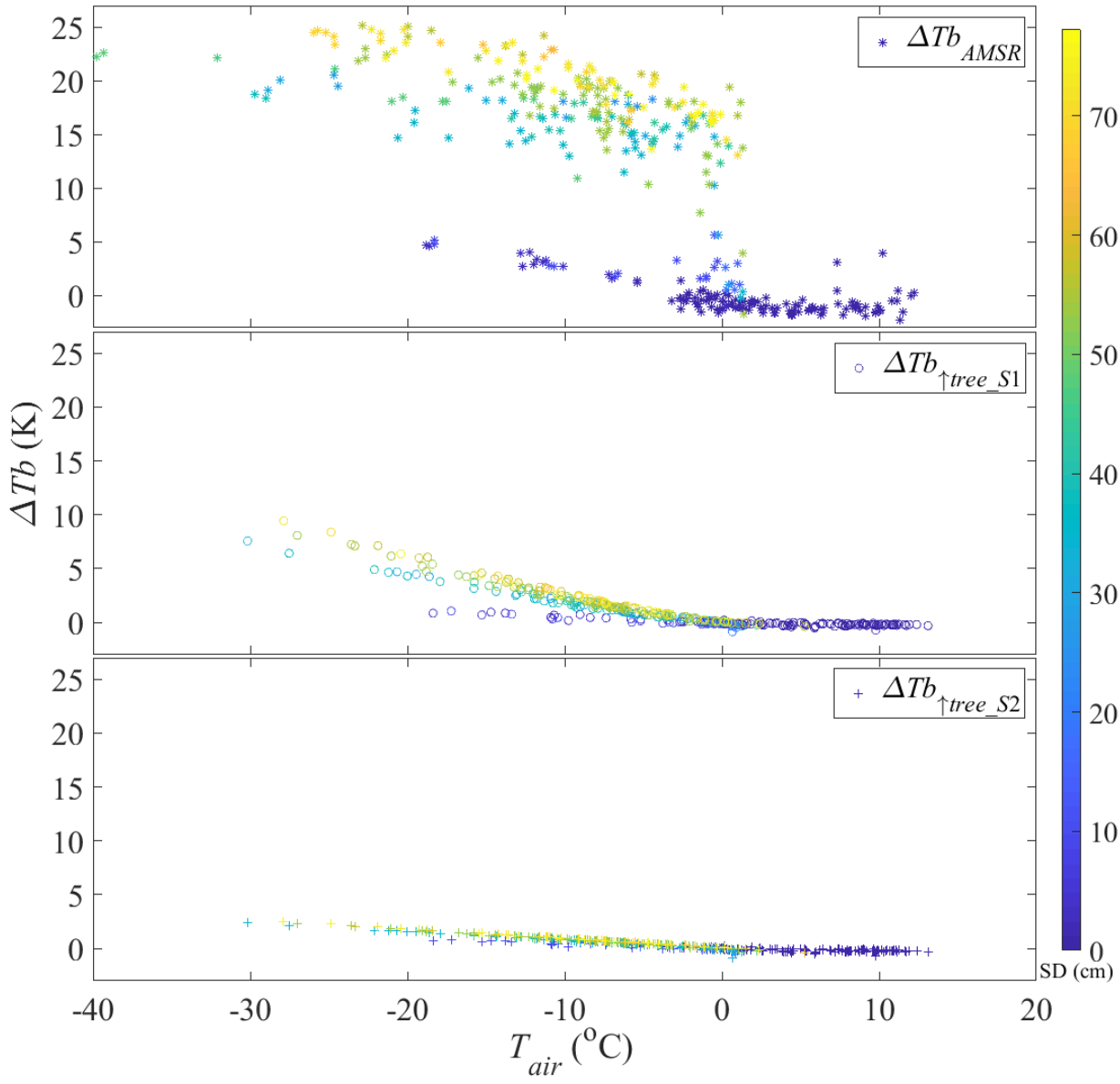

Fig. 5.8 $\Delta Tb_{\uparrow tree\_S1}$ (circle marker), $\Delta Tb_{\uparrow tree\_S2}$ (cross marker), and ΔTb_{AMSR} (star marker). Blue-green-yellow colors of the markers represent different snow depths (Blue-Green-Yellow scale) in the forest opening.

5.4. Discussion

5.4.1. The relationship between the air temperature and tree transmissivity

With a continued decrease of air temperature below freezing, the water content of the vegetation tissue gradually freezes. This effect increases the transmissivity of the tree [95], but this effect has yet to be modelled effectively. From our study driven by Fig. 5.5, air temperature can be considered one of the most important factors influencing tree transmissivity under sub-zero temperatures. According to Fig. 5.5 and Table 5.2, the model developed in this paper effectively described the temperature-transmissivity relation for a sample tree. The implications of this effect were explored further in Fig. 5.6 and Fig. 5.7, which demonstrate that this temperature-transmissivity relation significantly influences the downward and upward tree emission under sub-zero temperature. Therefore, to ignore the temperature-transmissivity relationship during the tree emission modelling could lead to a significant bias. As Fig. 5.6 shows, the difference between $Tb_{\downarrow tree\_S1}$ and $Tb_{\downarrow tree\_S2}$ is larger than 30 K in -30 °C temperatures. Hence, we suggest that this temperature-transmissivity relationship under sub-zero temperature should be accounted for in the retrievals of scene paramaters under forested landscapes.

With temperature decreasing, the freezing processing tends to slow down because less and less water content remained in the vegetation tissue could be frozen. Hence, a curve function should be introduced into the temperature-transmissivity relationship model to simulate this tendency (e.g. $\frac{1}{1-a_\gamma * T}$ in equation (5.5)). However, the biophysical processing controlling the water content of the tree under sub-zero temperature is complicated [35, 61]. In addition to the freezing and thawing, other factors, for example, drought, xylem embolism, could also influence

the water content of the tree during winter [99]. Beside, the types of tree is another factor should be considered. In this study, we found that using the rational function $\frac{1}{1-a_\gamma * T}$ as the curve function to control the curve line shape of equation (5.5) provided a better fit than other types of curve functions, for example, exponential or logarithmic functions. However, the curve line shape of temperature-transmissivity relationship maybe different in different types of trees or environmental conditions. Hence, the curve function may need to be adjusted. Besides, the value of a_γ is also influenced by the type of trees and environment conditions.

Since our experiment only focused on one target tree, the developed model about the temperature-transmissivity relationship should be tested in more situations. Besides, a comprehensive experiment evaluating tree winter biophysical dynamics concurrent with microwave observations could help us to develop a better characterization of the tree emission mechanisms.

5.4.2. The influence of the temperature-transmissivity relationship on tree emission and on the AMSR2 observation in forested regions.

The comparison between the simulated Tbs in $Scenario1$ and $Scenario2$ indicates that the temperature-transmissivity relationship influences $Tb_{\downarrow tree}$ (Fig. 5.6), $Tb_{\uparrow tree}$ (Fig. 5.7) and $\Delta Tb_{\uparrow tree}$ (Fig. 5.8). Compared AMSR2 observation with $Scenario1$ and $Scenario2$, the influence of the temperature-transmissivity relationship on spaceborne observation can be observed.

The thermal emission is the major component of $Tb_{\downarrow tree}$. A progressively cooler sub-zero temperature, the corresponding increase in tree transmissivity decreases the tree emissivity.

Because the tree emissivity has a positive correlation with air temperature, the sensitivity of $Tb_{\downarrow tree}$ to air temperature is enhanced by the influence of temperature-transmissivity relationship.

In $Tb_{\uparrow tree}$, besides tree thermal emission, the ground emission penetrated through the tree canopy is an important element. Since tree transmissivity has an opposite correlation with tree emissivity and air temperature, the sensitivity of $Tb_{\uparrow tree}$ to air temperature is decreased by the influence of temperature-transmissivity relationship on the ground emission penetrated through the tree canopy. In $Tb_{\uparrow tree}$, tree thermal emission decreases with temperature decrease, while the ground emission penetrated through the tree canopy increases, and vice versa.

Therefore, in $Tb_{\uparrow tree}$, the temperature-transmissivity relationship influences both tree thermal emission and ground emission penetrated through the tree canopy, and these two effects tend to cancel each other out. When Tb_{ground} is relatively high, the influence of temperature-transmissivity relationship on ground emission penetrated through the tree canopy dominates. In this situation, the sensitivity of $Tb_{\uparrow tree}$ to air temperature decreases (e.g. 10.65, 18.7 GHz in Fig. 5.7). While when Tb_{ground} is relatively low, the influence of temperature-transmissivity relationship on tree thermal emission dominates, so the sensitivity of $Tb_{\uparrow tree}$ to air temperature increases (e.g. 36.5 GHz in Fig. 5.7). Over snow-covered ground, Tb_{ground} in low frequency channels are higher than the Tb_{ground} in high frequency channels (Fig. 5.3). Therefore, the influence of the temperature-transmissivity relationship on $Tb_{\uparrow tree}$ is frequency dependent when the ground is covered by snow.

As Fig. 5.7 shows, the temperature-transmissivity relationship decreases the sensitivity of $Tb_{\uparrow tree}$ to air temperature in low frequencies, but slightly increases its sensitivity in high frequencies. Therefore, the $\Delta Tb_{\uparrow tree}$ is influenced by temperature-transmissivity relationship. As

Fig. 5.8 shows, comparing the simulated results in $Scenario1$ (considering the influence of temperature-transmissivity relationship) with the one in $Scenario2$ (ignoring the influence of temperature-transmissivity relationship), the sensitivity of $\Delta Tb_{\uparrow tree\_S1}$ to snow depth increases with air temperature decrease. The difference between $\Delta Tb_{\uparrow tree\_S1}$ and $\Delta Tb_{\uparrow tree\_S2}$ is about 10 K in minus 30 °C. In the frequency difference algorithm developed by Chang [100], 10 K Tb difference change means 15.9 cm SD variation.

Tb_{AMSR} and ΔTb_{AMSR} show similar behaviors as $Tb_{\uparrow tree\_S1}$ and $\Delta Tb_{\uparrow tree\_S1}$ to the air temperature variation according to Fig. 5.7 and Fig. 5.8. This result indicates that both Tb_{AMSR} and ΔTb_{AMSR} are influenced by the temperature-transmissivity correlation. Hence, the influence of temperature-transmissivity relationship cannot be ignored in spaceborne PM observations.

One of the major purposes to introduce the low frequency channel into the frequency difference algorithm is to use the low frequency channel as a reference channel to cancel the influence of the physical temperature in the PM snow retrieval [1]. The results of this paper indicated that this approach cannot reduce completely the influence of the temperature-transmissivity relationship in forest vegetation. The ΔTb_{AMSR} variation caused by temperature change has the risk to be regarded as SD and SWE variation in current frequency difference algorithms. Therefore, this temperature-transmissivity relationship should be considered into the PM snow retrieval algorithms in forested regions.

5.5. Conclusion

Tree transmissivity is strongly influenced by air temperature under sub-zero temperature. As this study shows, transmissivity changes up to 0.3 for the tree specimen at 10.65, 18.7, 21 and

36.5 GHz when the physical temperature drop from 0 to minus 30 °C. The temperature-transmissivity relationship significantly influences the tree emission, and this influence could be observed by both ground-base and spaceborne observations. The temperature-transmissivity relationship could have a further influence on the spaceborne PM snow retrieval algorithms because ΔTb_{AMSR} has a negative correlation with air temperature under sub-zero temperatures. This correlation between ΔTb_{AMSR} with the air temperature may cause the current spaceborne PM frequency difference snow observation algorithms regard air temperature variation as the SD and SWE variation by mistake. Therefore, in this study, the model to explain this temperature-transmissivity relationship has been developed. We suggest that this temperature-transmissivity relationship should be considered into future PM snow retrieval algorithms. The biophysical processes related to tree water content variation during the winter time should be considered into future active and passive microwave retrievals of geophysical parameters, which usually use the static parameters to model the RT of the forest medium.

Chapter 6

Modelling the influence of tree transmissivity variation on frequency difference passive microwave snow retrieval algorithms under sub-zero temperature conditions

Overview

Existing correction approaches to brightness temperatures of Northern boreal forest regions consider forest transmissivity constant during wintertime. However, due to biological protection mechanisms, below freezing air temperatures freeze the water content of the tree vegetation only gradually; as a consequence, the permittivity of many northern tree species decreases with the decrease of air temperature under sub-zero temperature conditions. This results in a monotonically increase of the tree vegetation transmissivity, as the permittivity contrast between the surrounding air decreases. The influence of this tree temperature-transmissivity relationship on the performance of the frequency difference passive microwave snow retrieval algorithms has not been considered. Using ground-based observations and an analytical model simulation based on Mätzler's (1994) approach, the influence of the temperature-transmissivity relationship on the frequency difference passive microwave snow retrieval algorithm is characterized. A simple approximation approach is then developed to successfully characterize this influence (the RMSE between the analytical model simulation and the approximation approach estimation is below 0.3 k). The approximation is applied to spaceborne observations, and demonstrates a strong

reduction in the influence of forests on the spaceborne or airborne passive microwave frequency difference brightness temperature.

6.1. Introduction

Spaceborne passive microwave (PM) snow retrieval methods are an important approach to estimate the snow depth (SD) and snow water equivalent (SWE) (e.g. [1-7]). Over snow-covered ground, the brightness temperatures (Tb) at lower frequencies (e.g. 10.65 and 18.70 GHz.) are less attenuated by the snow than at higher frequencies (e.g. 36.5 GHz.). Hence, the Tb difference between a lower frequency channel and a higher frequency channel (ΔTb) of the snow-covered ground is sensitive to SD and SWE (e.g. 18.70 GHz and 36.5 GHz) [1]. The frequency difference algorithms were developed to estimate global SWE and SD based on this sensitivity of ΔTb (e.g. [1], [2], [3], [11], [75], [76]). However, the sensitivity of the spaceborne or airborne observed ΔTb to the ground SWE and SD is decreased in the presence of forest cover because the ground emission is attenuated. Therefore, the frequency difference algorithms tend to underestimate the SWE and SD in forested regions [8], [9], necessitating correction for forest cover effects. Boreal forests with varying density cover large parts of snow-covered areas, and even though efforts have been made to reduce its influence on PM snow retrieval (e.g. [10-17]), it remains a major challenge in the retrieval of snow parameters [18] and other geophysical parameters, e.g. soil moisture [54].

Considering the forest vegetation as a simple, non-scattering homogeneous layer, the capacity of the forest for thermal emission and microwave attenuation can be expressed by its transmissivity. Previous studies have established relations between transmissivity and e.g. vegetation biomass and stem volume (e.g. [14], [15], [27], [32]), assuming transmissivity to

remain constant in frozen conditions. However, Li et al. [95] observed a temperature-transmissivity relationship under sub-zero temperature conditions in which the transmissivity increased with decreasing temperature. As discussed by Li et al. [95], under sub-zero temperature conditions, the overall water content in the vegetation tissue of some northern tree species only gradually freezes due to the biological protection mechanisms and the heterogeneous nature of the tree thermal state. Therefore, the overall tree permittivity is sensitive to air temperature [101]. Therefore, the tree transmissivity increases as the temperature decreases.

Upwelling emission above the tree canopy consists mainly of the combined upwelling tree thermal emission and ground emission which penetrates through the tree canopy. Under sub-zero temperatures, as shown by Li et al. [95] for a scots pine specimen, the tree transmissivity can increase with decreasing temperature. Therefore, the tree thermal emission decreases, and the proportion of ground emission which penetrates through the tree increases. For this reason, with decreasing temperature, the upwelling emission above the tree canopy is influenced more and more by the ground emission instead of the tree thermal emission. Hence, the sensitivity of spaceborne- or airborne-observed ΔTb to the ground SWE and SD increases with decreasing air temperatures in forested landscapes under sub-zero temperature conditions.

The ΔTb of the tree thermal emission in winter is typically lower than the one of the snow-covered ground as Fig 6.3 shows. With the increase of the tree transmissivity, more upwelling ground emission can penetrate through the trees. Hence, spaceborne or airborne observed ΔTb above the tree canopy tends to increase with the decrease in air temperatures below 0ºC conditions during the period in which the ground is covered by snow.

In this study, we develop a semi-empirical approximation to describe how the ΔTb of the ground emission is moderated by the forest through the temperature-transmissivity relationship found by Li et al. [101]. As a result, the influence of the forest on the performance of the frequency difference PM snow retrieval algorithms can be mitigated. This allows to reduce the errors of the forest emission on ΔTb, which is often used in SWE or SD retrievals.

6.2. Methodology

The workflow figure below gives an overview of the methodology of this study, more details are provided by the following sections.

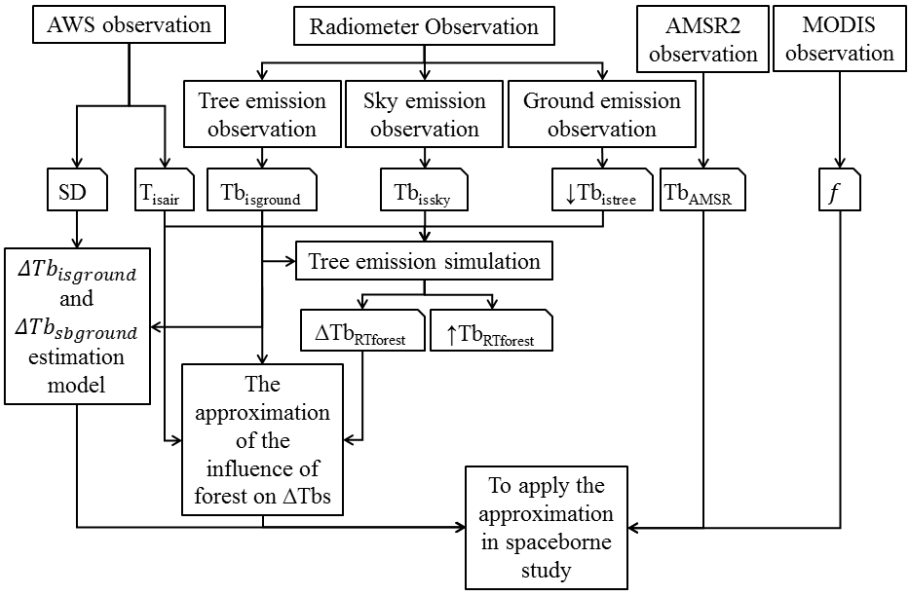

Fig. 6.1 The workflow of the methodology

As the figure shows, the instruments used in ground observation include the automatic weather stations (AWS) and radiometer, the spaceborne Tb observation was obtained by AMSR2 sensor. The air temperature (T_{isair}) and snow depth (SD) were collected by AWS. The ground Tb ($Tb_{isground}$), downwelling radiation from the trees ($\downarrow Tb_{istree}$), and the sky (Tb_{issky}) were collected

by radiometer. The satellite observed ground emission (Tb_{amar2}) was obtained by the AMSR2 sensor. The forest fraction (f) was extracted from MODIS MOD44b product. Accordingly, the model simulated up-welling tree emission ($\uparrow Tb_{RTforest}$) and the model simulated brightness temperature difference ($\Delta Tb_{RTforest}$) is calculated by the tree radiative transfer model. With the model simulated results, the approximation approach for forest Tb correction has been developed. With the spaceborne observed data, this approximation approach has been adopted into the spaceborne scale study.

6.2.1. The study site

The study site is close to the Finnish Meteorological Institute's (FMI) Arctic Research Center in Sodankylä, Finland (67.36 N, 26.63 E), located in the boreal forest belt of the northern Scandinavian Peninsula. In this region, the forest consists of pine (about 54.7%), spruce (about 14.7%), and birch (about 9.8%) [46]. Ground observations were made in an intensive observation area (IOA) which is a forest opening surrounded by sparse pine forest. The Scots pine (*Pinus sylvestris L.*) is the dominant species in this region.

6.2.2. Data collection

i. *In-situ* ground radiometer observations and satellite passive microwave observations

The SodRad (Sodankylä Radiometer) radiometer system was used for the *in-situ* ground based down and upward-looking observations of the IOA and forest. This radiometer operates at 10.65, 18.7, 21 and 36.5 GHz channels in both horizontal (H) and vertical (V) polarizations (pol). The bandwidth is 400 MHz, Half-Power Beam Width (HPBW) is 6.0°, the absolute system stability is 1.0 K, and the sidelobe level is less than -30dB [47].

The radiometer was installed on a 4.1 m high platform located at the edge of the IOA opening. A mature Scots pine about 15 m tall was selected as a specimen (target tree). The distance between the target tree and the radiometer was about 3 m. The ground and the sky were scanned in the opposite direction of the tree scan. Fig. 6.2 shows the configuration of the radiometer observation frame.

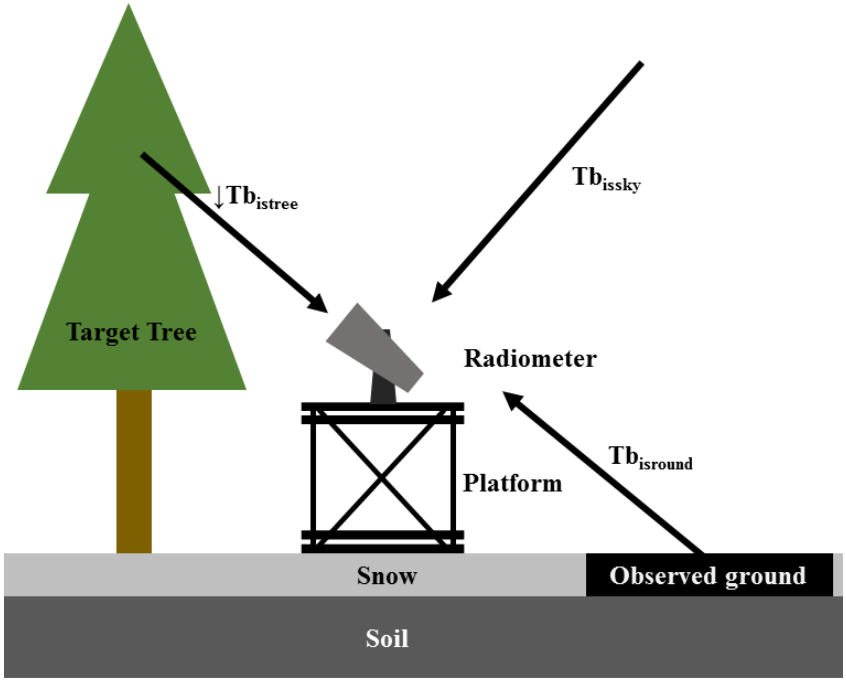

Fig. 6.2 Configuration of the *in-situ* ground radiometer observation modified from Li *et al.* [95].

In-situ radiometer measurements were made of the upwelling microwave Tb of the ground ($Tb_{isground}$), the downwelling Tb of the specimen tree ($\downarrow Tb_{istree}$), and the downwelling Tb of the sky observed at 45° elevation. Measurement were made twice per day (one during daytime and one at night) from Sep 5, 2016 to Apr 17, 2017. Because the downwelling Tb of the sky was stable during the observation period, we used the average value of the observed downwelling Tb of the sky (Tb_{issky}) to represent the sky emission in this observation period [95].

Satellite-observed ground Tbs (Tb_{AMSR}) at 10.65, 18.7, 21 and 36.5 GHz in both H and V pol were obtained by the Advanced Microwave Scanning Radiometer 2 (AMSR2) [96] from Sept 1, 2016 to Apr. 30, 2017. The descending passes were chosen. At this latitude, every night usually had one or two descending passes observing the IOA during the period of 11 pm to 2:30 am. This study used the Level 1 Resampling product (L1R) [97] with the footprints of the Tb_{AMSR} in all the frequencies resampled to 24 × 42 km ellipse (along scan × along track). The MODIS MOD44b Version 6 Vegetation Continuous Fields product [98] in 2016 was used to estimate the forest spatial fraction of the AMSR2 footprint in this study. f is forest fraction of the AMSR2 footprint in this study. According to MOD44b data, the value of f = 0.28 (f = 1 means a full forest-covered scene). Because even in a forested area is unlikely fully covered by trees, the percentage of MODIS forest fraction tends to lower than the percentage of forest cover [101].

Fig. 6.3 shows the *In-situ* radiometer observed Tbs and spaceborne AMSR2 observed Tbs. According to this figure, $Tb_{isground}$ was mainly influenced by the snow depth, while $\downarrow Tb_{istree}$ was affected by the air temperature or tree skin temperature. Because the forest and the snow-covered ground are the two main components of the land cover inside the footprint of AMSR2 observation, Tb_{AMSR} is influenced by both the temperature and the snow depth.

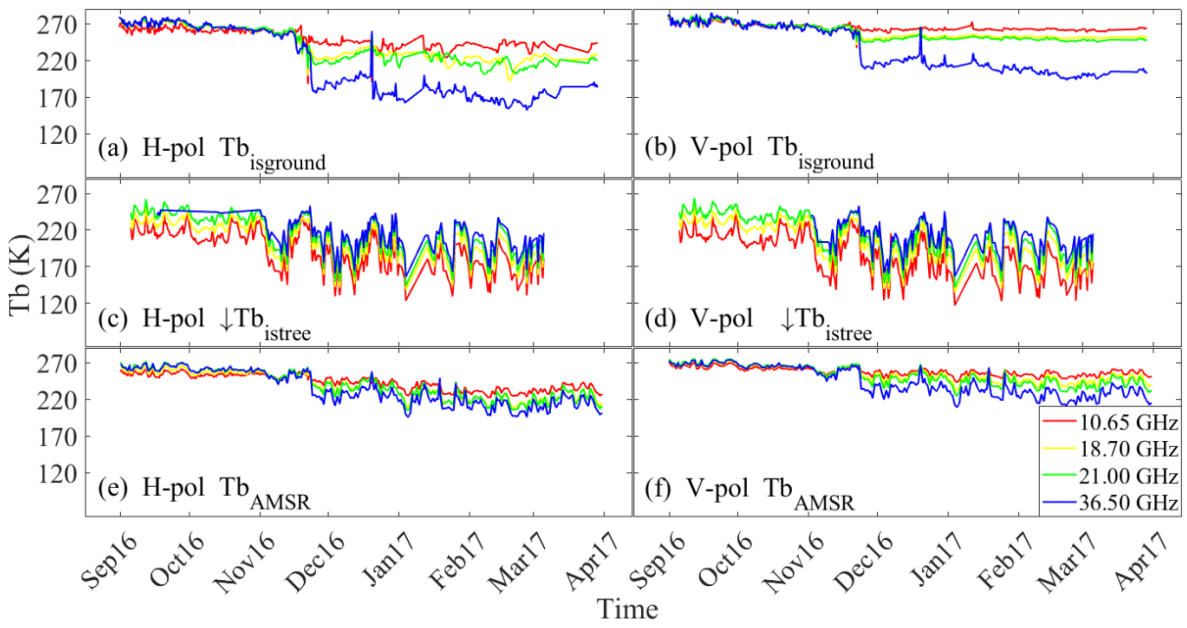

Fig. 6.3 (a) and (b) show *in-situ* radiometer-observed $Tb_{isground}$, (c) and (d) show *in-situ* radiometer-observed $\downarrow Tb_{istree}$, and (c) and (d) show AMSR2 observed Tb_{AMSR}

ii. Ancillary data

Two automatic weather stations (AWS) were installed at the study site, one is in the forest and another is in the forest opening. The air temperature, the soil temperature, and the snow depth were measured every 10 minutes by the AWS. These AWS data were matched with the ground radiometer observations and spaceborne observation data according to the time stamps. The air temperature was measured by Vaisala PT100 sensor at 2 meters above ground level, and the snow depth was measured by Campbell Scientific SR50. The AWS measured snow depth in the forest (SD_{forest}) and forest opening (SD_{open}). Because the forest and the forest opening are the two major landscape components in the AMSR2 footprint, the weighted average of SD_{forest} and SD_{open} was used to represent the *in-situ* measured snow depth of the AMSR2 footprint (SD_{is}). SD_{is} was calculated as $SD_{is} = fSD_{forest} + (1-f)SD_{open}$. As explained, f = 0.28 in this study. The average value of these two AWS measured air temperatures were used to represent the

overall air temperature of the study site (T_{isair}). The soil temperature ($T_{isground}$) was measured by Campbell Scientific 107-L at the forest opening [101].

In addition to the AWS measurements, two thermometers were installed at the bark-cambium interface of the target tree's trunk, facing to the north at a height of 2.2 m and 4.5 m. The temperature of the bark-cambium interface was measured in the interval of 10 minutes, and the averaged value of the two thermometers' measurement is used to represent the tree skin temperature (T_{istree}).

Fig. 6.4 shows the snow depth and temperature information in the IOA. The first snowfall was on Oct. 28, 2016. The snow depth in the forest is about 70% compared with the snow depth in the forest opening. During the period that the ground was snow-free, T_{isair}, $T_{isground}$ and T_{istree} were similar with variable fluctuations, while during the period that the ground was covered by snow, $T_{isground}$ became more stable, while T_{isair} and T_{istree} remained fluctuating.

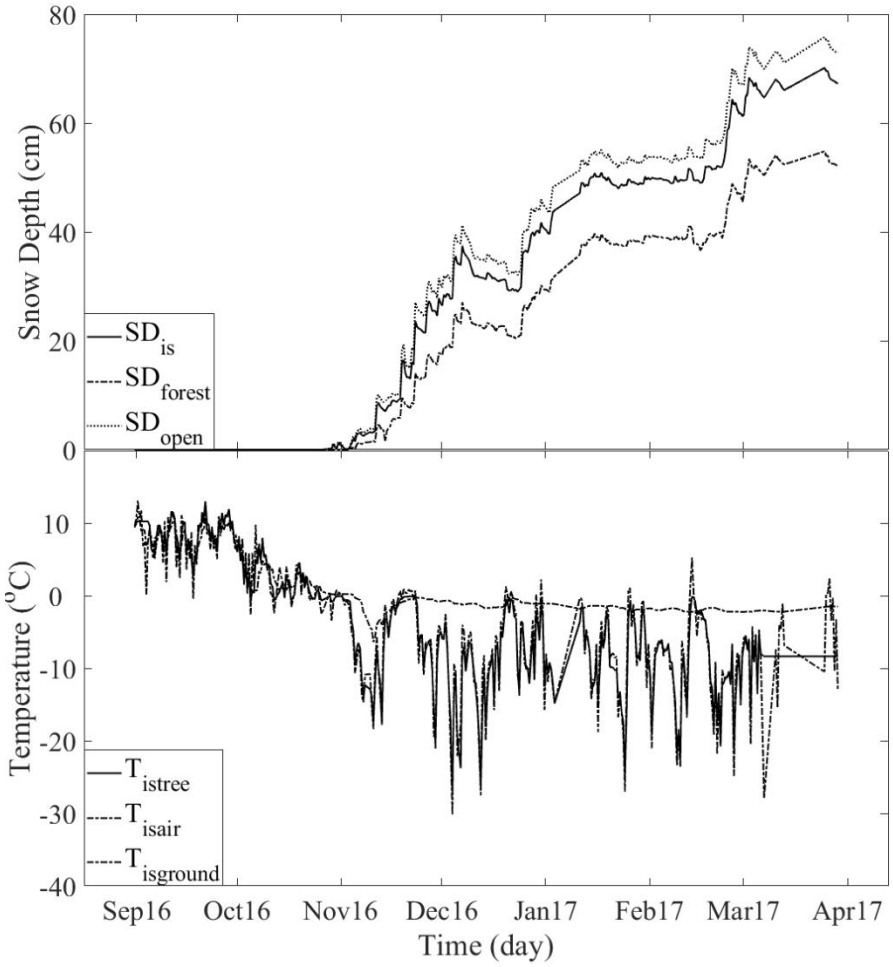

Fig. 6.4 Time series of the AWS observed snow depth (upper panel) and temperature (lower panel) in IOA

6.2.3. Forest emission modelling

Following the approach of Mätzler [21], the downwelling ($\downarrow Tb_{forest}$) and upwelling ($\uparrow Tb_{forest}$) emission observed beneath and above the forest cover can be expressed by the radiative transfer (RT) equations below:

$$\downarrow Tb_{forest} = \gamma Tb_{sky} + r_{forest} Tb_{ground} + (1 - r_{forest} - \gamma)T \tag{6.1}$$

$$\uparrow Tb_{forest} = \gamma Tb_{ground} + \left(1 - r_{forest} - \gamma\right)T + \left(1 - r_{forest} - \gamma\right)r_{ground}\gamma T$$

$$+r_{forest}Tb_{sky} + r_{ground}\gamma^2 Tb_{sky} \quad (6.2)$$

where γ and r_{forest} are the transmissivity and the reflectivity of the forest vegetation layer, r_{ground} is the reflectivity of the ground, T is air temperature, Tb_{sky} is the downwelling sky emission, and Tb_{ground} is the upwelling ground emission. In thermal equilibrium, r_{ground} can be estimated by:

$$r_{ground} \approx 1 - \frac{Tb_{ground}}{T_{ground}} \quad (6.3)$$

where T_{ground} is the ground soil temperature. Based on results by Li et al. [101], an empirical model can be applied to estimate tree transmissivity under sub-zero temperature conditions so that transmissivity γ as a function of temperature may be given by

$$\gamma = 1 - \frac{(1-\gamma_0)}{1 - a_\gamma * T} \qquad T \leq 0$$

$$\gamma = \gamma_0 \qquad T > 0 \quad (6.4)$$

where a_γ is an empirical parameter, T is the air temperature, and γ_0 is the mean transmissivity of the forest layer measured when the air temperature higher than 0 °C. The rational function $\frac{1}{1-a_\gamma * T}$ in the second term of equation (6.4) is called a curve function because this function is used to control the curve line shape of equation (6.4) by adjusting the value of $1 - \gamma_0$. For estimating the value of γ_0 and a_γ, the approach developed by Mätzler (1994) is applied to obtain the tree transmissivity as a training dataset based on the observed value of $\downarrow Tb_{istree}$, Tb_{issky}, and T_{isair}:

$$\gamma = \frac{T - \downarrow Tb_{forest}}{T - Tb_{sky}}. \quad (6.5)$$

The average value of the Mätzler's estimated transmissivity when the air temperature is greater than 0 °C is used to represent γ_0 in equation (6.4). With γ_0 obtained, a_γ in equation (6.4) was

estimated by least squares fitting with the value of T_{isair} and transmissivity estimated by Mätzler's approach. Table 6.1 below shows the estimated parameters of equation (6.4) and its R^2 and the RMSE (Root Mean Square Error) compared to the transmissivity values calculated by Mätzler's approach (equation (6.5)). More detailed discussion about how temperature could influence tree transmissivity is presented in the work of Li et al., [95], and the details of transmissivity simulation with equation (6.4) is presented in the work of Li et al. [101].

Table 6.1 Estimated parameters, R^2 and the RMSE of transmissivity model (equation (6.4)) [101]

	H10	**V10**	**H18**	**V18**	**H21**	**V21**	**H37**	**V37**
$\boldsymbol{\gamma_0}$	0.23	0.24	0.18	0.19	0.15	0.14	0.13	0.12
$\boldsymbol{a_\gamma}$	0.02	0.03	0.02	0.02	0.02	0.02	0.01	0.02
$\mathbf{R^2}$	0.84	0.83	0.89	0.85	0.90	0.87	0.87	0.81
RMSE	0.03	0.03	0.02	0.03	0.02	0.03	0.02	0.03

In the *in-situ* forest emission simulation of this study, *in-situ* measured values $Tb_{isground}$, Tb_{issky}, T_{isair}, and $T_{isground}$ are used as Tb_{ground}, Tb_{sky}, T, and T_{ground}. The RT model (equation (1) and (2)) calculated $\downarrow Tb_{forest}$ and $\uparrow Tb_{forest}$ are named as $\downarrow Tb_{RTforest}$ and $\uparrow Tb_{RTforest}$. γ is estimated by equation (5.4), and r_{ground} is estimated by equation (6.3). Because the r_{forest} is relatively small, vegetation is typically treated as an attenuating layer in the commonly simplified approximations (e.g. [28], [32], [54], [55]). Similarly, we follow this approach so r_{forest} is considered equal to 0. $\downarrow Tb_{RTforest}$ (the simulated downwelling tree Tb) was simulated by equations (6.1) and (6.4), while $\uparrow Tb_{RTforest}$ (the simulated upwelling tree Tb) was simulated by equations (6.2) and (6.4). Details of this *in-situ* forest emission simulation can be found in the work of Li et al. [101].

In Fig. 6.4, $Tb_{isground}$ (*in-situ* radiometer observed ground Tb), $\downarrow Tb_{istree}$ (*in-situ* radiometer observed downwelling tree Tb), $\downarrow Tb_{RTforest}$ (equation (6.1) simulated downwelling tree Tb), and $\uparrow Tb_{RTforest}$ (equation (6.2) simulated upwelling tree Tb) are compared. The y-axis represents the Tb, and Temperature in x-axis represents T_{isair}.

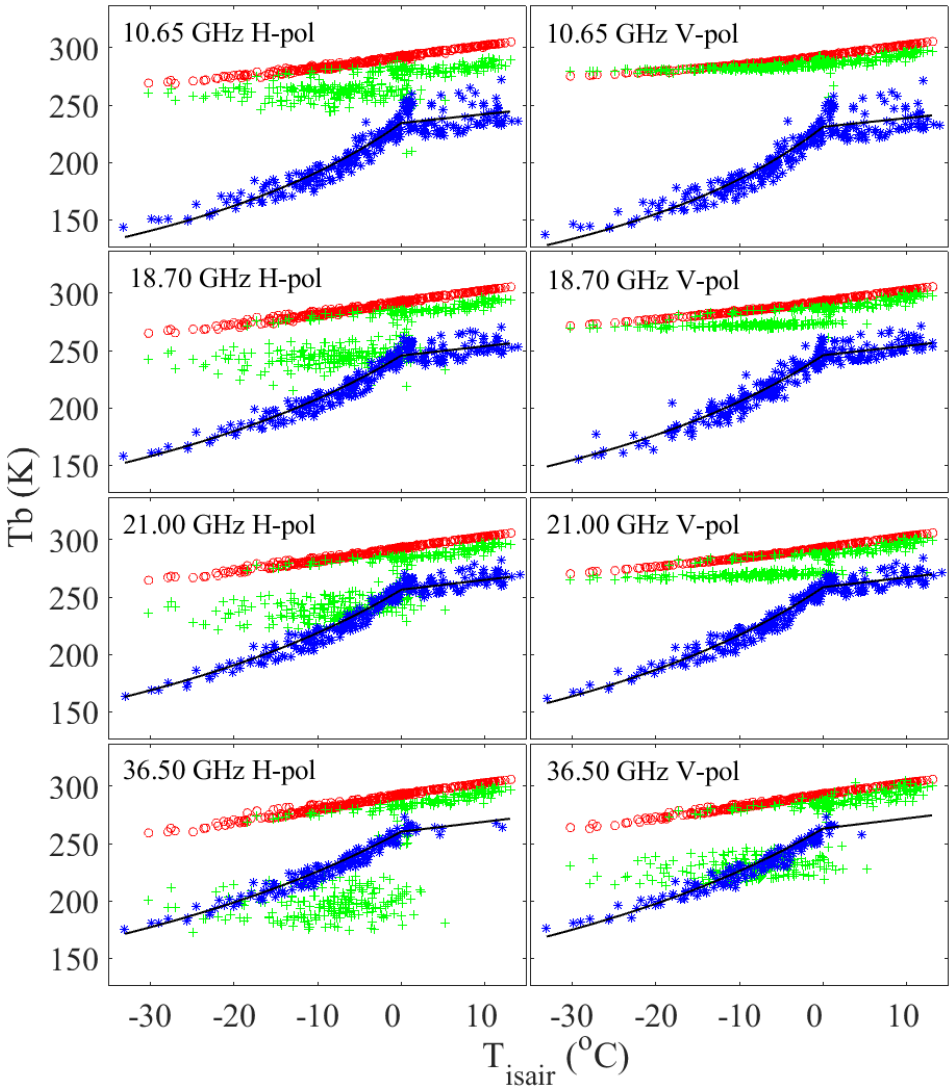

Fig. 6.5 Comparison of the $Tb_{isground}$ (green cross markers), $\uparrow Tb_{RTforest}$ (red circle markers), $\downarrow Tb_{istree}$ (blue star markers), and $\downarrow Tb_{RTtree}$ (black solid lines)

As Fig. 6.5 shows, the model simulated $\downarrow Tb_{RTforest}$ matched the radiometer observed $\downarrow Tb_{istree}$. The sensitivity of $\downarrow Tb_{istree}$ and $\downarrow Tb_{RTforest}$ to the air temperature is high under sub-zero temperature conditions because γ decreases with sub-zero air temperatures. This sensitivity gradually decreases with the decreasing air temperature.

$Tb_{isground}$ is sensitive to the snow depth because of the attenuation effect by the snowpack. For $Tb_{isground}$, the H-pol channels are attenuated by the snowpack more than the V-pol channels, and the higher frequency channels are attenuated by the snowpack more than the lower frequency channels. $T_{isground}$ is usually warmer than T_{isair}, and therefore, $Tb_{isground}$ is usually higher than $\downarrow Tb_{istree}$ on account of the thermal insulation effect of the snowpack.

In $\uparrow Tb_{RTforest}$, $Tb_{isground}$ provides a significant contribution to $\uparrow Tb_{RTforest}$ passing through the tree canopy in addition to the thermal emission of the trees. Under sub-zero temperature conditions, the thermal emission of the tree decreases with the air temperature (as $\downarrow Tb_{istree}$ shows), while the contribution of $Tb_{isground}$ which passes through the tree canopy increases because of the increasing tree transmissivity. Therefore, for $\uparrow Tb_{RTforest}$, the influence of the temperature on the tree thermal emission and the influence of the temperature on ground emission which passes through the tree canopy offset each other. Hence, $\uparrow Tb_{RTforest}$ appears as less sensitive to changes in temperature than $\downarrow Tb_{istree}$. Furthermore, the $Tb_{isground}$ emission at low frequency is greater than at high frequencies in a snow-covered ground. Therefore, the $\uparrow Tb_{RTforest}$ in a low frequency channel is less sensitive to air temperature than at higher frequencies. The difference between low frequencies and high frequencies can be easily observed in Fig. 6.7.

6.2.4. An approximation of the influence of forest emission on spaceborne ΔTbs developed based on the *in-situ* forest emission simulation.

In forested areas, under full forest covered conditions, the ΔTb of the ground emission beneath the forest ($\Delta Tb_{fground}$) is the desired value for PM snow retrievals because it is the emission from snow un-influenced by forest cover effects. However, the ΔTb of the upwelling emission observed above the canopy (ΔTb_{forest}) is that which is actually obtained by spaceborne or airborne instruments. Therefore, the key to reducing the influence of the forest cover on the frequency difference PM snow retrieval algorithms is to estimate $\Delta Tb_{fground}$ through ΔTb_{forest}. Although the $\Delta Tb_{fground}$ can be estimated from ΔTb_{forest} by the forest RT models (e.g. equation (6.1) and (6.2)), the parameters for the RT model (e.g. transmissivity) are difficult to obtain at the satellite observation scale. The influence of temperature on tree transmissivity under sub-zero temperature conditions makes this procedure even more complicated. Therefore, a more feasible simplified semi-empirical approximation is developed in this study:

$$\Delta Tb_{forest} = b_{is} * T * \Delta Tb_{fground} \tag{6.6}$$

where b_{is} is an empirical parameter in this *in-situ* study, and T is the air temperature. For calibrating equation (6.6), the brightness temperature difference estimated by the tree RT model ($\Delta Tb_{RTforest}$) is calculated based on the value of $\uparrow Tb_{RTforest}$. By using the $\Delta Tb_{RTforest}$, T_{isair}, and the radiometer observed ΔTb of $Tb_{isground}$ to represent ΔTb_{forest}, T, and $\Delta Tb_{fground}$, b_{is} is estimated by the least squares fitting method. Combinations of the Tb difference of the channels 18.7 - 36.5 GHz V pol (18-37V) and 21 - 36.5 GHz V pol (21-37V) were studied. Table 6.3 presents the value of b_{is} and the fit of the model.

The ΔTb_{forest} estimated by this approximation (equation (6.6)) is named as $\Delta Tb_{APPforest}$. In this study, based on the AWS measured T_{isair}, $\Delta Tb_{APPforest}$ was simulated with $\Delta Tb_{fground}$ values of 10, 20, 30, 40, and 50 K using equation (6.6). In Fig. 6.6, $\Delta Tb_{APPforest}$ is compared with $\Delta Tb_{RTforest}$.

To demonstrate the potential of this approximation in the spaceborne application, a simple test was made using AMSR2 observations. The scene of a snow covered AMSR2 observation footprint is simplified into two main elements: forest and forest opening. Accordingly, the ΔTb of the spaceborne observation (ΔTb_{sb}) is expressed below:

$$\Delta Tb_{sb} = f * \Delta Tb_{forest} + (1 - f) * \Delta Tb_{oground} \tag{6.7}$$

where ΔTb_{forest} is the ΔTb of the upwelling emission above the canopy in the forest region, $\Delta Tb_{oground}$ is the ΔTb of the ground emission in the forest openings, and f is the percentage of the forest fraction. As explained, f = 0.28.

For convenience, we followed the approach of Langlois [32], assuming the ground conditions in the forest region and in the forest opening are similar. Therefore, we used the variable $\Delta Tb_{sbground}$ to represent the overall ΔTb of ground emission underneath forests from the spaceborne AMSR2 observation footprint. Accordingly, $\Delta Tb_{sbground} = \Delta Tb_{oground} = \Delta Tb_{fground}$. Equation (6.7) can be re-written as:

$$\Delta Tb_{sb} = f * b_{sb} * T * \Delta Tb_{sbground} + (1 - f) * \Delta Tb_{sbground} \tag{6.8}$$

where b_{sb} is an empirical parameter of this spaceborne based study, which has a similar function as b_{is} in equation (6.6). By rearranging equation (6.8), the $\Delta Tb_{sbground}$ can be estimated through

ΔTb_{sb}. As explained, $\Delta Tb_{sbground}$ is the value theoretically not influenced by the forest cover. Therefore, using $\Delta Tb_{sbground}$ instead of ΔTb_{sb} in the spaceborne snow retrieval procedure, we can reduce the influence of forest emission on passive microwave snow retrieval in forested terrain.

For estimating the empirical parameter b_{sb} in this spaceborne study, the values of $\Delta Tb_{sbground}$, ΔTb_{sb} and T are needed for calibrating equation (6.8) as a training dataset. The values of ΔTb_{sb} and T were obtained through AMSR2 observations and AWS data. The $\Delta Tb_{sbground}$ for equation (6.8) calibration is obtained by the approach below.

Since the ground emission has been observed by the *in-situ* radiometer observation, the regression model between the ΔTb of the ground emission at the *in-situ* observation scale ($\Delta Tb_{isground}$) and the snow depth (SD) is established based on the radiometer observed ground emission:

$$\Delta Tb_{isground} = c * SD^2 + d * SD \tag{6.9}$$

where the c and d are the regression coefficients. Equation (5.9) was calibrated by the least squares fitting method based on SD_{open} (the AWS measured snow depth in the forest opening) and the ΔTb of the radiometer observed $Tb_{isground}$ in the forest opening. Fig. 5.5 compared the equation (6.9) simulated results (solid lines) with the radiometer observed ΔTb of $Tb_{isground}$ in (blue-green-red circle markers), The blue-green-red bar represents the air temperature. Table 6.2 shows the estimated parameters c and d, R^2 and the RMSE.

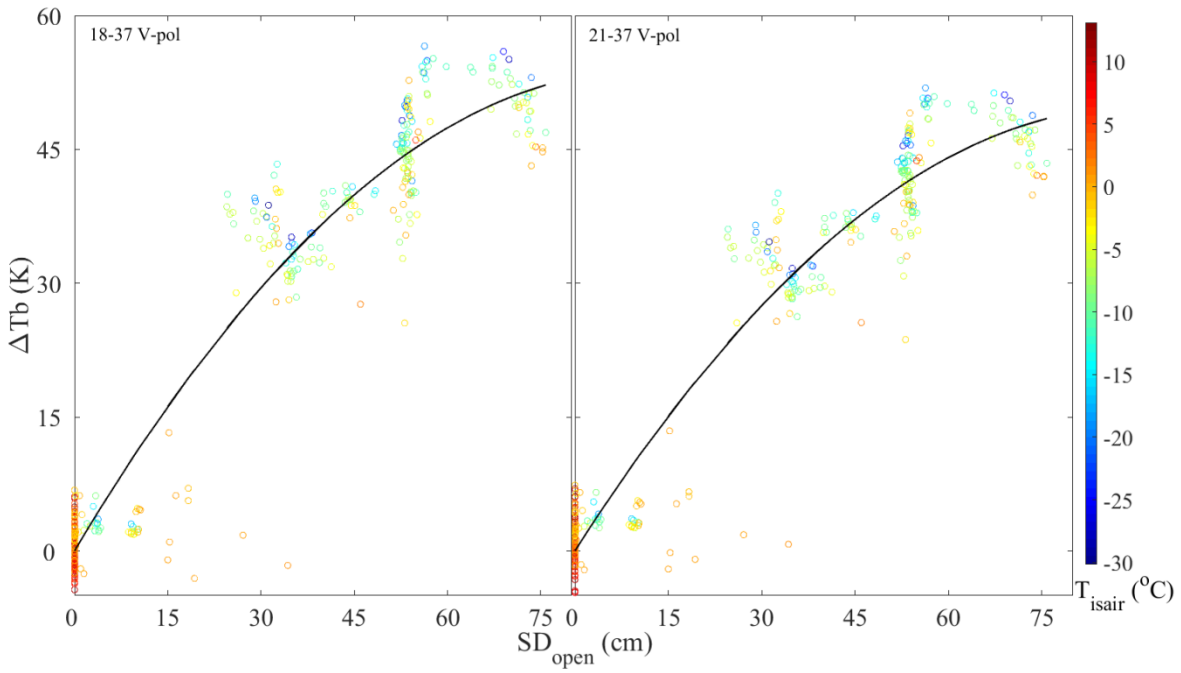

Fig. 6.6 The radiometer observed ΔTb of $Tb_{isground}$ (blue-green-red circle markers) with the equation (6.9) simulated results (black solid lines), the blue-green-red bar represents T_{isair}

Table 6.2 Estimated parameters, R^2, and RMSE of equation (5.9)

	18-37 V-pol	21-37 V-pol
c	-0.0064	-0.0061
d	1.18	1.10
R^2	0.85	0.86
RMSE	6.68	5.94

With the calibrated equation (6.9), $\Delta Tb_{isground}$ is estimated from the *in-situ* AWS-measured snow depth. However, the $\Delta Tb_{isground}$ calculated by equation (6.9) is an estimation at the *in-situ* observation scale, the heterogeneous ground conditions inside an AMSR2 footprint makes the estimated ground emission at the *in-situ* scale different from the overall spaceborne scale ground

emission in AMSR2 footprint. Therefore, $\Delta Tb_{isground}$ cannot be used to represent $\Delta Tb_{sbground}$ directly.

In general, although factors such as wind-blown snow redistribution and canopy interception cause the heterogeneous nature of ground snow distribution, precipitation and climate conditions are relatively consistent within an AMSR2 footprint. The precipitation is a dominant control on snow accumulation [103]. Therefore, an assumption is made that the overall SD and SWE of the AMSR2 footprint are statistically correlated with the *in-situ* AWS measured SD and SWE inside AMSR2 footprint. Introducing an adjustment factor to match *in-situ* snow state observations with regional scale model estimates is a common approach in modelling regional scale snow accumulation and ablation (e.g. [40], [103], [104], [105]). Since the snowpack is the major factor to influence the ground emission, we adopt this adjustment approach. Therefore, an empirical adjustment factor e, with a positive value, is introduced to represent the influence of the heterogeneous ground emission. $\Delta Tb_{sbground}$ is estimated from $\Delta Tb_{isground}$ by:

$$\Delta Tb_{sbground} = e * \Delta Tb_{isground} \tag{6.10}$$

Equation (6.10) was substituted into equation (6.8). Then, $\Delta Tb_{isground}$ was estimated by equation (6.9) with SD_{is} (the *in-situ* measured snow depth of the AMSR2 footprint). In equation (5.8), the ΔTb of Tb_{AMSR} (ΔTb_{AMSR}) is used as ΔTb_{sb}, and T_{isair} is used as T. b_{sb} and e were estimated by the least squares fitting method.

Since the equation (6.8) has been calibrated, the ΔTb_{sb} simulated by this approximation approach (equations (6.8)) is named as ΔTb_{APPsb}. ΔTb_{APPsb} was simulated by equations (6.8), (6.9), and (6.10) at the SD equels to 10, 25, 40, 55, and 70 cm respectively based on the value of T_{isair} and f.

As discussed, $\Delta Tb_{sbground}$ is the value theoretically not influenced by the forest cover. Therefore, to estimate $\Delta Tb_{sbground}$ through ΔTb_{sb} is the key to reduce the influence of forest emission on passive microwave snow retrieval in forested terrain. Since equation (6.8) has been calibrated, we applied this approximation approach to reduce the influence of forest on ΔTb_{AMSR} in this study as a simple testing. With the rearranged equation (6.8), $\Delta Tb_{sbground}$ is calculated based on the ΔTb_{AMSR} and T_{isair}. The $\Delta Tb_{sbground}$ calculated by this approximation approach is named as $\Delta Tb_{APPsbground}$. For demonstrating how the approximate approach developed in this paper could reduce the influence of the forest on the ground ΔTb, $\Delta Tb_{APPsbground}$ and ΔTb_{AMSR} are compared with the ΔTb of $Tb_{isground}$.

6.3. Results

In Fig. 6.7, the RT model-simulated $\Delta Tb_{RTforest}$ (represented by colored circles) and the approximation approach (equation (6.6)) simulated $\Delta Tb_{APPforest}$ (represented by colored lines) at the combinations of 18-36V and 21-36V are compared. $\Delta Tb_{APPforest}$ was simulated using equation (6.6), with values of $\Delta Tb_{fground}$ = 10, 20, 30, 40, and 50 K. In this figure, the y-axis represents the ΔTb value for $\Delta Tb_{APPforest}$ and $\Delta Tb_{RTforest}$, and the x-axis represents T_{isair}. Because $\Delta Tb_{RTforest}$ is calculated based on the radiometer observed ground Tb in the forest opening, the blue-green-red bar represents SD_{open}. According to Fig. 6.7, the $\Delta Tb_{RTforest}$ and $\Delta Tb_{APPforest}$ is influenced by both the air temperature and the snow depth. $\Delta Tb_{RTforest}$ with a deeper snow depth has a higher sensitivity to the air temperature. This is because with the snow depth increases, the ΔTb of the ground emission also tends to increase (as Fig. 6.7 shows). Table 6.3 presents the estimated parameters and the goodness of fit of the equation (6.6) during the model calibration with the training dataset ($\Delta Tb_{RTforest}$, T_{isair}, and the ΔTb of $Tb_{isground}$).

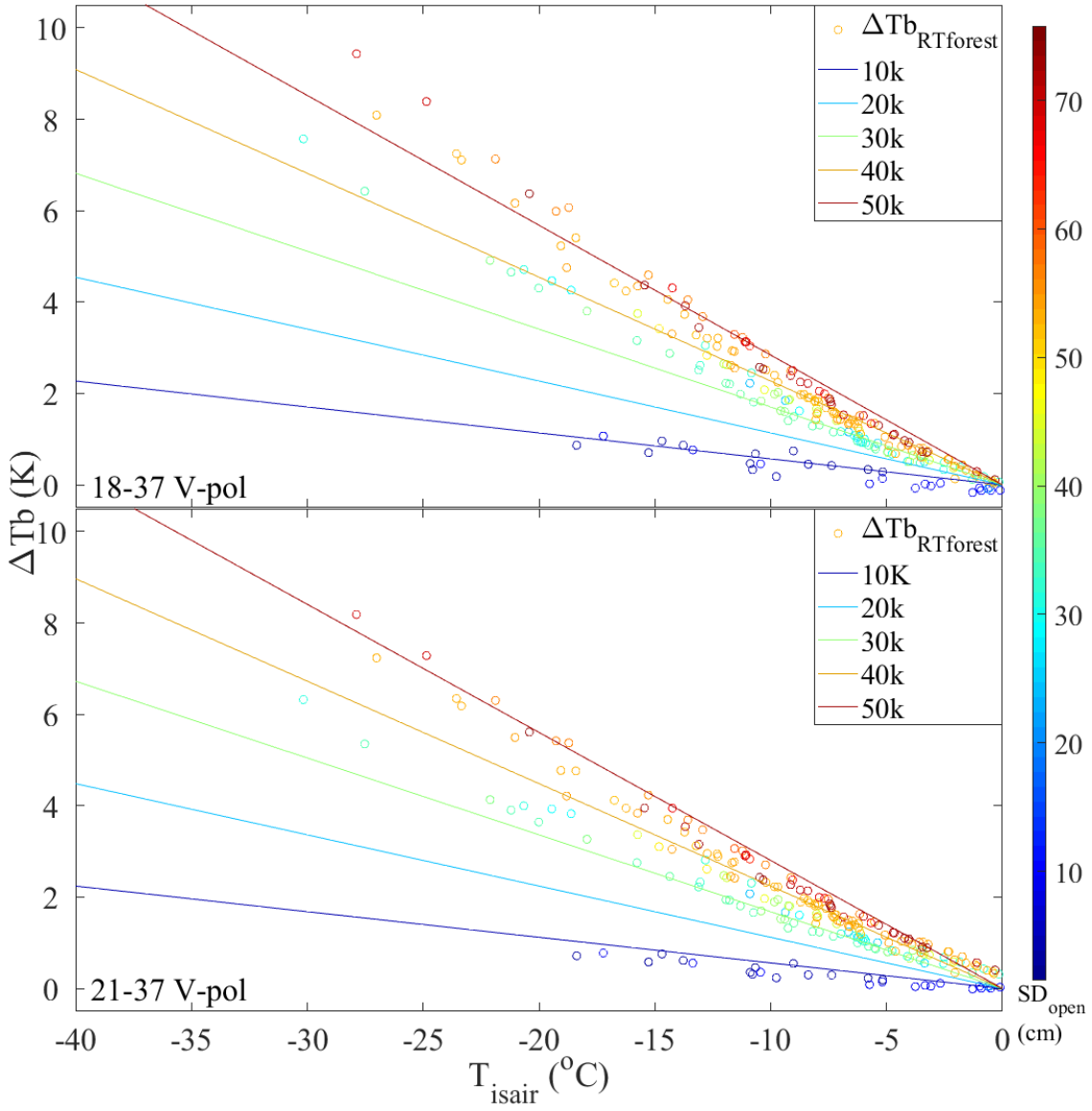

Fig. 6.7 The comparison between $\Delta Tb_{RTforest}$ (blue-green-red circle markers) and $\Delta Tb_{APPforest}$ which is simulated at $\Delta Tb_{fground}$ equals to 10, 20, 30, 40, and 50 K (colored lines), the blue-green-red bar represents SD_{open}

Table 6.3 The estimated b_{is}, R^2, and RMSE of equation (6.6) during the model calibration with training dataset

	b_{is}	R^2	RMSE
18-37 V-pol	-0.0057	0.98	0.25
21-37 V-pol	-0.0056	0.99	0.13

According to Fig. 6.7 and Table 6.3, the approximation approach (equation (6.6)) estimated $\Delta Tb_{APPforest}$ has a good agreement with the RT model simulated $\Delta Tb_{RTforest}$. This result indicates that the approximation developed in this paper can be applied as a simplified method to reduce the influence of forest emission on ground ΔTb.

In Fig 6.8, the approximation approach is applied to AMSR2 data. ΔTb_{AMSR} (the AMSR2 observed ΔTb) is represented by the colored circles, and ΔTb_{APPsb} (simulated ΔTb in AMSR2 footprint) is represented by the colored lines. ΔTb_{APPsb} was simulated by equations (6.8), (6.9), and (6.10) at the SD equals to 10, 25, 40, 55, and 70 cm. In this figure, the y-axis represents the ΔTb value of ΔTb_{AMSR} and ΔTb_{APPsb}, the x-axis represents T_{isair}. Because ΔTb_{AMSR} and ΔTb_{APPsb} are the ΔTb in AMSR footprint, the blue-green-red bar in Fig. 6.8 represents SD_{is}. Fig. 6.8 shows that ΔTb_{AMSR} and ΔTb_{APPsb} are sensitive to both air temperature and the snow depth, which is similar to $\Delta Tb_{RTforest}$ and $\Delta Tb_{APPforest}$ in Fig. 6.7. For non-forested areas exist inside AMSR2 footprints, only snow depth influences the ground ΔTb. Therefore, compared with $\Delta Tb_{RTforest}$ and $\Delta Tb_{APPforest}$ which are simulated in a full forest covered condition, ΔTb_{AMSR} and ΔTb_{APPsb} have a higher sensitivity to the snow depth, and a lower sensitivity to the air temperature. Table 6.4 shows the estimated parameters and the goodness of fit of the equations (6.8), (6.9), and (6.10) during the model calibration with training dataset (ΔTb_{AMSR}, T_{isair}, and SD_{is}).

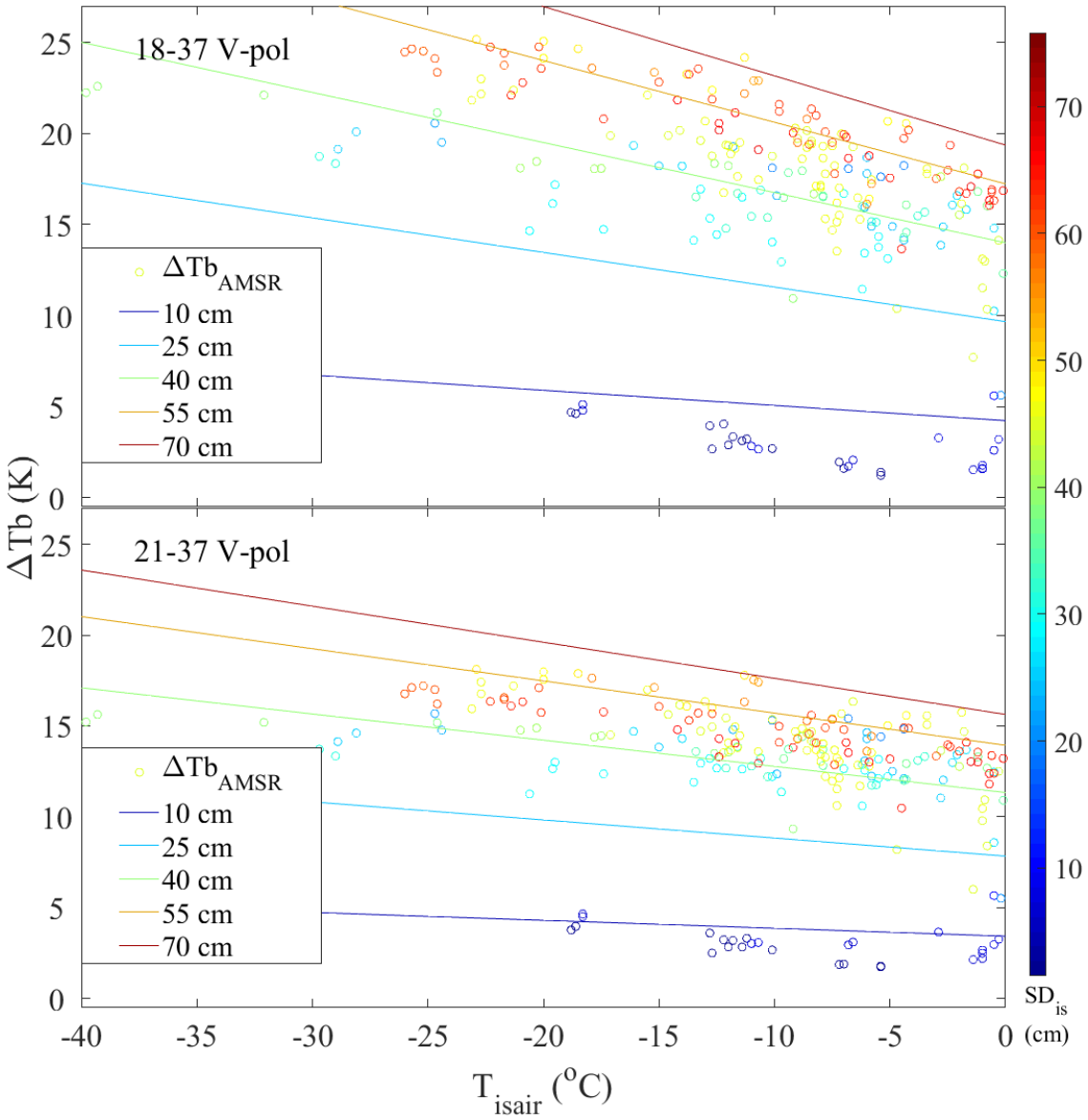

Fig. 6.8 Comparison between ΔTb_{AMSR} (blue-green-red circle markers) and ΔTb_{APPsb} which is simulated at snow depths equal to 10, 25, 40, 55, and 70 cm (colored lines), the blue-green-red bar represents SD_{is}

Table 6.4 The estimated parameters, R^2, and RMSE of the ΔTb_{sb} during the model calibration with training dataset

	b_{sb}	e	R^2	RMSE
18-37 V-pol	-0.050	0.51	0.79	2.72
21-37 V-pol	-0.032	0.44	0.63	2.42

According to Fig. 6.8 and Table 6.4, the ΔTb_{APPsb} has a good agreement with ΔTb_{AMSR}, which indicates that the approximation approach developed in this study can be used to simulate how the forest cover influences the ΔTb of the ground emission as a simplified approach in spaceborne observation. Therefore, the rearranged approximation approach (equation (6.8)) can be applied to reduce the influence of forest on spaceborne observed ΔTb.

Fig. 6.9 presents $\Delta Tb_{APPsbground}$ calculated from the rearranged approximation approach (equation (6.8)) based on ΔTb_{AMSR}, T_{isair}, and SD_{is}. As discussed, $\Delta Tb_{APPsbground}$ can be considered as the estimated ground ΔTb reduced the influence of forest by the approximation approach. As Fig. 6.9 shows, $\Delta Tb_{APPsbground}$ is not influence by T_{isair} as ΔTb_{AMSR} in Fig. 6.8. In this figure, the y-axis represents the value of $\Delta Tb_{APPsbground}$, the x-axis represents T_{isair}, and the Blue-green-red bar represents SD_{is}.

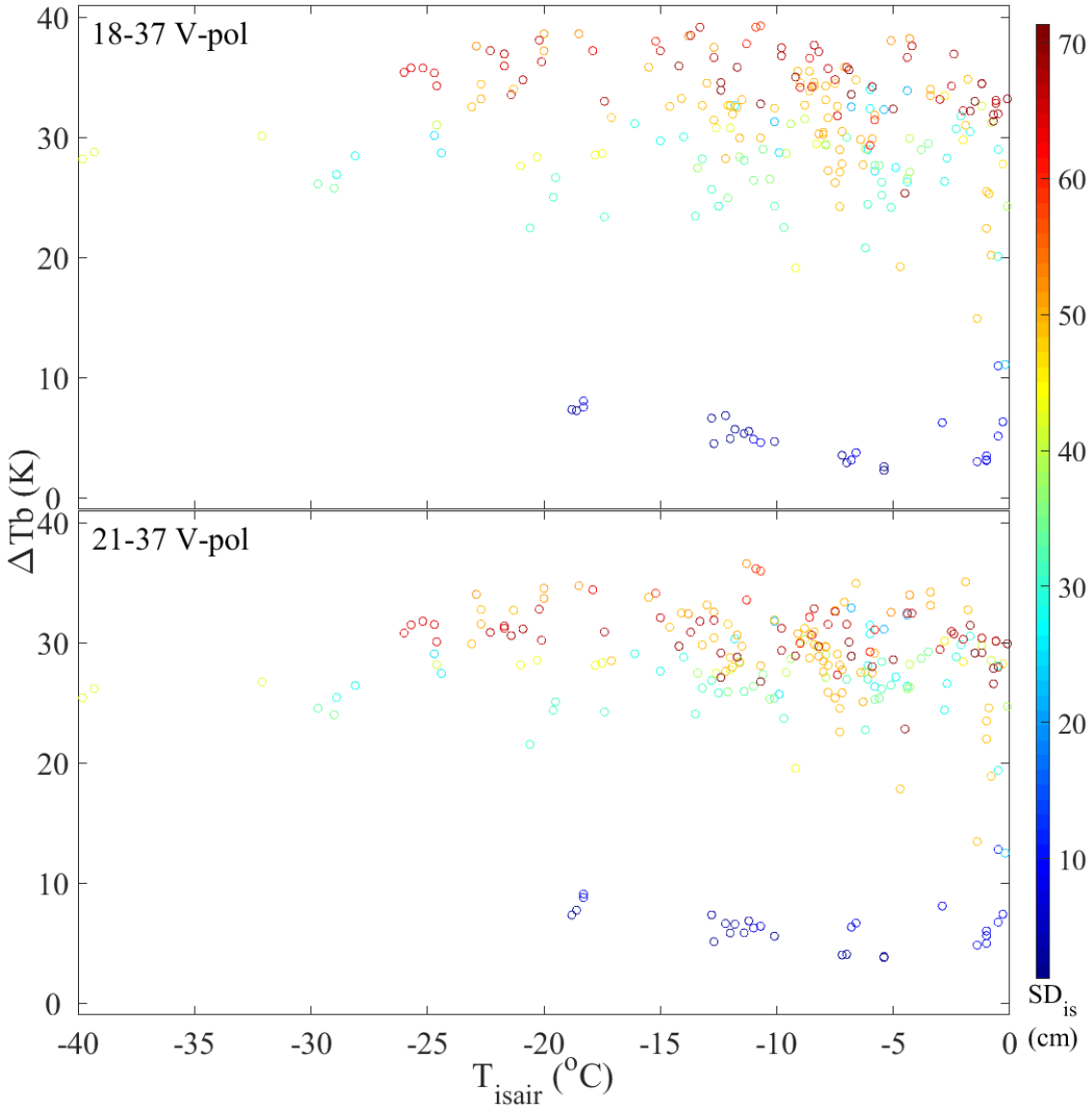

Fig. 6.9 $\Delta Tb_{APPsbground}$ (blue-green-red circle markers) against T_{isair}, the blue-green-red bar represents SD_{is}

Finally, in Fig. 6.10, we compared $\Delta Tb_{APPsbground}$ (blue-green-red circles in panels (a) and (b)) and ΔTb_{AMSR} (blue-green-red circles in panels (c) and (d)) with the radiometer observed ΔTb of $Tb_{isground}$ (black cross marker). The blue-green-red bar represents T_{air}. The x-axis represents the snow depth (cm). For the ΔTb of $Tb_{isground}$, because the radiometer ground observation made in

the forest opening, the x-axis represents SD_{open}. While for $\Delta Tb_{APPsbground}$ and ΔTb_{AMSR}, because they are the simulation and observation in AMSR2 footprint, x-axis represents SD_{is}.

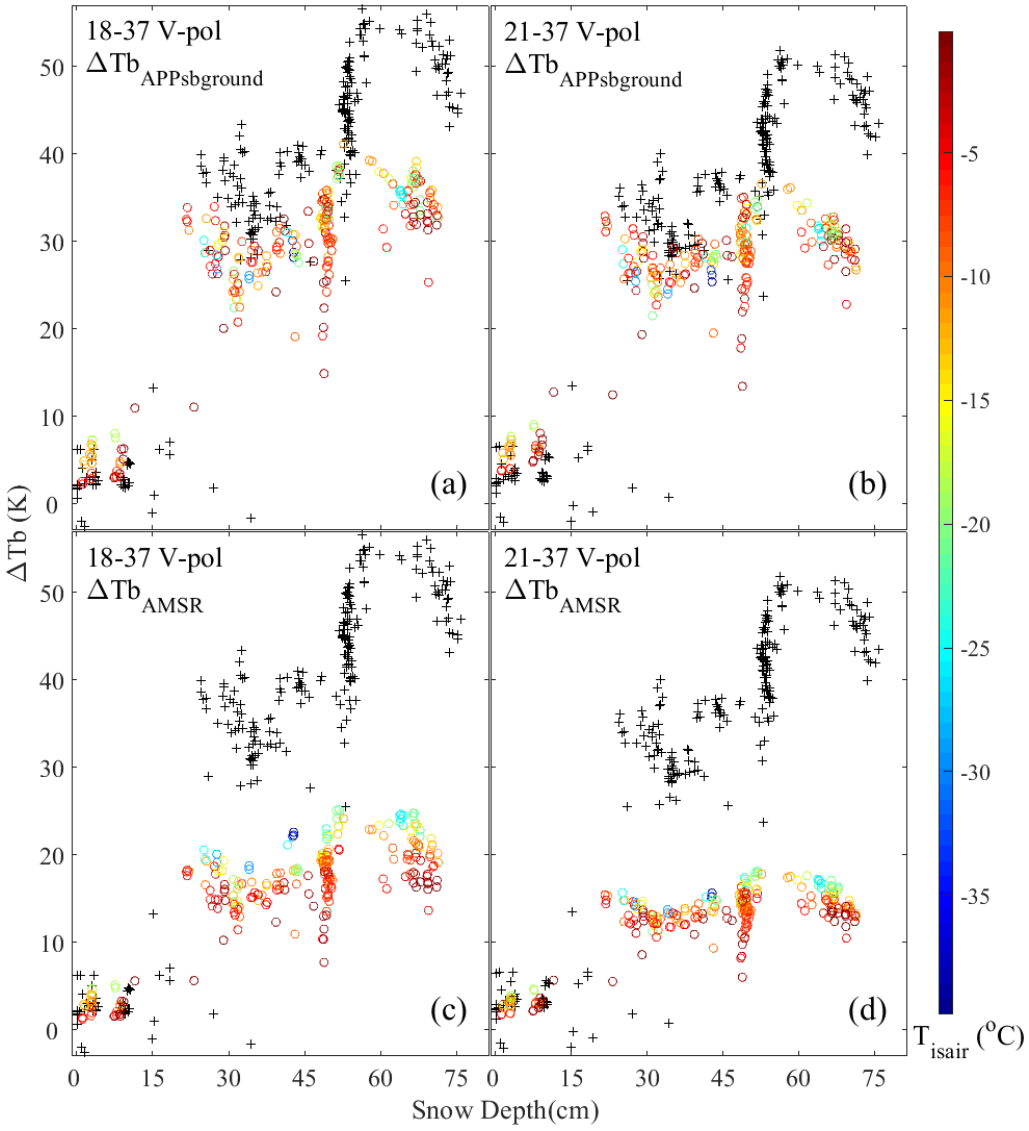

Fig. 6.10 Compared $\Delta Tb_{APPsbground}$ (blue-green-red circle markers in (a) and (b)) and ΔTb_{AMSR} (blue-green-red circle markers in (c) and (d)) with the radiometer observed ΔTb of $Tb_{isground}$ (black cross markers), the blue-green-red bar represents T_{isair}

Comparing $\Delta Tb_{APPsbground}$ with ΔTb_{AMSR}, $\Delta Tb_{APPsbground}$ is not influenced by the air temperature, and has a higher sensitivity to the snow depth. Comparing $\Delta Tb_{APPsbground}$ and ΔTb_{AMSR} with the ΔTb of $Tb_{isground}$, $\Delta Tb_{APPsbground}$ has a higher similarity with the ΔTb of $Tb_{isground}$. As discussed, the temperature-transmissivity relationship reduced the sensitivity of ΔTb_{AMSR} to snow depth, and it also causes the ΔTb_{AMSR} sensitivity to air temperature under sub-zero temperatures. According to Fig. 6.6, the ΔTb of $Tb_{isground}$ is not sensitive to air temperature. The results of this comparison indicate that the influence the temperature-transmissivity relationship of the forest vegetation on the AMSR2 observed ΔTb is reduced in $\Delta Tb_{APPsbground}$ by the approximation approach developed in this paper.

6.4. Discussion

The attenuation effect of the forest decreases the sensitivity of ΔTb observations from spaceborne or airborne instruments to the ground SD and SWE. Empirical parameters have been introduced as an adjustment coefficient for snow parameter retrievals over forested regions [10], [12]. However, a temperature-transmissivity relationship, first reported by Li et al. [95], showed that the sensitivity of ΔTb to the ground SD and SWE increases as air temperatures decreases under sub-zero temperature conditions (as Fig. 6.7 shows). When observed by aircraft or satellite radiometers, according to equation (6.6), the sensitivity of the ΔTb above the forest canopy to the ΔTb of the ground emission underneath the forest approximately has a linear relationship with the air temperature under sub-zero temperature conditions. The strong influence of the air temperature on the ΔTb shown in Fig. 6.7 and Fig. 6.8 explains the reason that a constant adjustment coefficient [10], [12] is insufficient to correct the influence of forest attenuation on PM snow retrievals.

According to Fig. 6.9 and Fig. 6.10, $\Delta Tb_{APPsbground}$ has a higher sensitivity to the snow depth than ΔTb_{AMSR}. Besides, $\Delta Tb_{APPsbground}$ is not influenced by air temperature. Compared with ΔTb_{AMSR}, the behavior of $\Delta Tb_{APPsbground}$ to the air temperature and snow depth has a higher agreement with the ΔTb of $Tb_{isground}$. This result indicates that the approximation approach developed in this paper (equation (6.8)) can effectively reduce the influence from both the forest attenuation effect [12] and the temperature-transmissivity relationship discussed in this study on the spaceborne or airborne observed ΔTb during snow retrievals.

The approximation approach is designed to only describe the relationship between the ΔTb of the ground emission beneath the forest and the ΔTb of the upwelling emission observed above the canopy. Therefore, the very localized ground ΔTb estimation approach (equation (6.9)) can be easily replaced by a more generally applicable modelling approach (e.g. HUT [28], MEMLS [73], and DMRT-ML [74]).

It is also recognized that the permittivity of the tree vegetation and the structure of the forest medium (e.g. density, stem volume, and height) might also influence the parameter b_{is} or b_{sb} of this simplified approximation approach. Since this study only operated at one study site, the influence of the forest structure variation is not discussed. However, if applying this approximation approach at a global or regional scale PM, the influence of these factors on the parameter b_{is} or b_{sb} will require further evaluation.

According to the work of Li et al. [95], the snow cover on the trees has negligible influence on tree emission in this study. However, the canopy interception changed the ground snow distribution according to Fig. 6.4 (SD_{open} and SD_{forest}). The fraction of land use type inside AMSR2 footprint (e.g. forest against opening area) can influence the pattern of sub-grid snow

distribution [106]. Therefore, the parameter *e* in equation (6.10) is also influenced by the fraction of land use type. Although a number of snow distribution models [39], [107], have been developed, and studies (see.[108]) have been made to evaluate the influence of the sub-grid heterogeneous ground snow distribution on PM observation, to effectively describe the sub-grid snow distribution inside AMSR2 footprint requires high spatial resolution snow depth measurement. Therefore, how to effectively use limited *in-situ* observations for the snow retrieval models training and validation in the daily based global scale course spatial resolution PM snow observation remains a challenge in this study.

6.5. Conclusion

In this study we found that the sensitivity of the ΔTb observed above the forest canopy to the ΔTb of the ground emission underneath the forest canopy can be approximately considered as a linear relationship with the air temperature. A simplified approximation was developed to describe this relationship. This approximation has successfully been applied to AMSR2 observations over the FMI Arctic Research Center study site, and it has shown a strong potential to reduce the influence of the forest on the performance of the PM frequency difference snow retrieval algorithms. Therefore, we recommend that this approximation should be evaluated and be adopted into the regional and global scale PM snow observations in the future.

Chapter 7

Summary, discussion and Conclusions

7.1. Summary

This study has shown that the phenological changes of coniferous trees during the wintertime can have significant influences on tree emission. Based on an extensive season-long experiment, the change of biomass water content and freeze-thaw state has a significant influence on the RT of trees. At low temperatures, the vegetation water content can be frozen. As the consequence, the water content of vegetation decreases due to the phase change of the water, resulting in the decrease in vegetation permittivity. Hence, the vegetation transmissivity increases. Although the decreasing of the vegetation permittivity with the temperature decrease has been observed during a previous experiment on a small amount of chopped vegetation tissues [20], the influence of the sub-zero temperature on trees or forests emission under a natural condition is unknown.

The influence of the temperature on forest transmissivity caused by the phase change of the water in vegetation has a significant influence on the RT of forest cover. However, the relationship between physical temperature and forest transmissivity is ignored by most spaceborne microwave studies. Previously, how this phenomenon could influence the tree emission modelling and the spaceborne observation was unclear. Therefore, this study focused on the tree emission variations during the wintertime and more specifically, explored the relationship between tree transmissivity and physical temperature during the wintertime to evaluate how this relationship could influence spaceborne PM observations. For this purpose, an

experiment to study the tree microwave emission variation during fall-winter-spring was made at the FMI Arctic Research Centre, Sodankylä, Finland located 120 km north of the Arctic Circle (67° 22' N, 26° 38' E). This location is representative of the northern boreal forest belt with forest cover being the dominant land cover type. Observations of the microwave emission of a single coniferous tree specimen (a scots pine) were made from Sep 5, 2016 to Mar 24, 2017 by a ground-based upward-pointing multi-frequency radiometer. Observations were supported by both spaceborne Tb observation and the *in-situ* geophysical property measurements. The *in-situ* geophysical property measurements included: snow depth and air temperature measured by automatic weather station, tree skin temperatures measured by thermometers, and the daily photo image of the specimen tree collected by the web camera. The ground-based Tb observations were compared with the spaceborne radiometer observations (AMSR2) to evaluate if the phenomena observed by ground-based observation could be also observed by the spaceborne observation.

In Chapter 4, based on the experiment, we verified that the tree transmissivity is sensitive to physical temperature in a natural environment under sub-zero temperatures. The transmissivity tends to increase with the decrease of physical temperature when the physical temperature is lower than 0º C, but when the physical temperature greater than 0º C, the tree transmissivity is insensitive to physical temperature. As a result of this finding, a model to describe the temperature-transmissivity relationship was developed.

In Chapter 5, the influences of the temperature-transmissivity relationship on tree emission, spaceborne PM observation, and spaceborne PM snow retrievals are evaluated based on the ground-based observations, spaceborne observations, and model simulations. The results of the study show that the temperature-transmissivity relationship observed in this study has a

significant influence on the tree emission. It could influence both ground-based radiometer observations and spaceborne AMSR2 observations.

Since the influence of the temperature on upwelling tree emission is frequency dependent, the frequency difference approaches for PM SD and SWE retrievals are also influenced by the physical temperature variations below freezing. When air temperatures are below 0º C, the sensitivity of the ΔTb observed above the forest canopy to the ΔTb of the ground emission underneath the forest canopy can be approximately considered as a linear relationship with the air temperature. Therefore, in Chapter 6, a feasible solution to reduce the influence of this temperature-transmissivity relationship on PM snow retrieval was developed and tested.

7.2. Discussion: contributions and implications of this study

This study explores how air temperature influences the radiative transfer processes of the tree under sub-zero temperatures and has its important implications. The relationship between the temperature, vegetation water content, and vegetation permittivity has been explored in previous studies. However, few studies have connected the biological processes of the tree with the microwave radiative transfer in the tree microwave emission observation and modelling. The tree mass is the living tissue; hence its physical properties are controlled by the its biological activities. Accordingly, the biological processes of the tree play an important role in the tree radiative transfer. This study demonstrates how the knowledge of tree biology could help us to develop a better understanding about the tree radiative transfer. It also shows the possibility for introducing biology state knowledge into current tree microwave emission models during the microwave geophysical parameter retrieval in forested environments. Evaluation of the temperature-transmissivity relationship elucidated in this paper indicates that this temperature-

transmissivity relationship phenomenon has a strong influence on tree emission. Therefore, to ignore this phenomenon will introduce a significant bias in tree emission modelling under sub-zero temperatures. Therefore, the finding and quantification of this temperature-transmissivity relationship suggests a future research direction to improve the accuracy of the tree radiative transfer modelling and ultimately, corrections to retrieval of ground surface features (eg. Snow, soil moisture) that are covered by forest canopy.

The temperature-transmissivity relationship characterized in this paper is an element in current tree radiative transfer study that is not well defined and so this work has a significant potential influence on airborne or spaceborne radiometry observations of forested landscapes. Based on ground-based radiometer observation, the temperature-transmissivity relationship model developed in this study provides a quantitative description about how air temperature influences tree transmissivity. This is a very important contribution because this model not only revealed an important source of uncertainty in current tree radiative transfer modelling, but also provided a numerical solution to reduce its influence. According to this thesis, by introducing the temperature-transmissivity relationship model developed in this paper, the influence of the temperature-transmissivity relationship on tree emission modelling could be largely reduced. Since many geophysical parameter retrieval procedures involved with the tree radiative transfer, the model developed in this paper can be applied to many airborne or spaceborne passive microwave geophysical parameter retrieval algorithms to reduce the influence of temperature-transmissivity relationship on spaceborne or airborne retrievals of snow, soil moisture, and atmosphere parameters. Therefore, the temperature-transmissivity relationship model is a unique contribution in the tree emission modelling and the microwave geophysical parameter retrievals.

This thesis also indicates that the influence of the temperature-transmissivity relationship on upwelling tree emission is frequency dependent. This is another important finding because the frequency difference algorithms are widely used in PM snow retrievals. The model simulation and the discussion about this phenomenon in this paper explained the mechanism of how the temperature-transmissivity relationship could influence the frequency difference algorithms in PM snow retrievals. Hence, an important source of uncertainties that relate to the temperature and the ΔTb in the current airborne or spaceborne passive microwave snow retrievals under freezing conditions has been revealed by this thesis.

The approximation model developed in this study to describe the influence of tree transmissivity variation on frequency difference passive microwave snow brightness temperatures under sub-zero temperatures is an important contribution of this paper which directly relates to passive microwave retrievals of SD and SWE. As discussed, the difficulty of global forest structure parameter estimation limits the application of complex forest RT models within PM snow retrievals. For this reason, a straightforward solution is required to be developed. The approximation model developed in Chapter 6 quantitatively described the relationship between air temperature and ΔTb of the upwelling tree emission. Although it is a semi-empirical approximation approach, its simplification allows this approach to be conveniently adopted in regional to global scale studies. The application of this approximation model in AMSR2 observation at Chapter 6 demonstrated a strong potential for application at both regional and global scales for PM snow observation applications. Therefore, this approximation model is very useful in the passive microwave SD and SWE retrievals.

Finally, another contribution of this thesis is the elucidation of the impact of snow accumulation in a tree canopy on the microwave Tb reponse. Although a large amount of snow

precipitation is intercepted by the forest canopy, few studies have characterized how the snow on canopy can influence the tree microwave emission. The field experiment in this research that includes radiometer and snow microstructure observations of tree canopy snow, shows that canopy snow accumulation has a relatively weak signal and is unlikely to be a major uncertainty in geophysical parameter retrievals of snow accumulation. Although ground-based observations are different from spaceborne or airborne PM observations, the analysis in this study is consistent between satellite and ground-based observations. However, despite this outcome, a decisive conclusion cannot be fully made without further canopy snow accumulation studies of different snow and forest types. Several studies are underway that could be leveraged for this experimentation including the Sodankylä ARC field site and the ECCC BERMS field site. These experiments could fully confirm this outcome.

7.3. Limitations and Future works

Through ground-based and spaceborne observations, and model simulation, the impact of the freezing of vegetation water content on tree microwave emission has been studied in this thesis. The study also shows that the biological processes of the tree cannot be ignored during the tree emission observation and modelling. However, due to the limitation of the experiment design, the quantitative analysis about the vegetation water content freezing needs further evaluation. Specifically, the tree vegetation water content freezing is a gradual process in a natural condition that has been confirmed. This freezing process is different compared with previous studies of El-Rayes, and Ulaby [20] that significantly modified the vegetation tissues. It is unclear what causes the difference in freezing observed in this study compared with the one by El-Rayes, and T. Ulaby. One possible explanation is that the biological protection mechanisms of many northern

tree species mitigates the freezing process, suggesting that the ice and the liquid water can coexist in the vegetation tissue, and the proportion of ice and water is influenced by the external air temperature. Another possible explanation is that the heterogeneous thermal characteristics of the tree make it unlikely that the entire tree freezes at the same time. Rather, it is a progressive freezing process as air temperatures decrease, causing more and more parts of the tree to freeze form the outside in. Despite the new knowledge created in this thesis, our understanding of the tree freezing process in a natural condition needs further development. Therefore, future work should focus on the design of a comprehensive experiment evaluating tree winter biophysical dynamics concurrent with microwave observations. Such an experiment could help to develop a better characterization of the tree emission mechanisms. It could also help to quantify the difference between the leaves, twigs, and trunk during the freezing process; the freezing process is likely to vary between woody biomass such as the trunk, and canopy leaves and small stalks. And the freezing process will vary depending on the temperature profile through the tree canopy and above. From a more comprehensive experiment evaluating the tree vegetation water content variability, a more complete numerical biophysical model about the vegetation water content freezing could be developed and incorporated into the tree microwave emission modelling. This work will also be of relevance to retrieval approaches used for the GlobSnow product and the JAXA AMSR2 product which adopt very simplistic tree correction procedures that are typically parameterized by simple spatial forest cover parameters.

The experiment needs describe above should also adopt a different radiometer observation approach. The experiment in this study only observed the downwelling tree emission. However, the upwelling tree emission is more important for spaceborne and airborne observations. Although the upwelling tree emission is simulated by the RT model in this study, the verification

from a physical downward-pointing radiometer observation is necessary. Having an upward pointing multi-frequency radiometer (observing downwelling emission through the trees from beneath the canopy) and downward pointingmulti-frequency radiometer (observing upwelling emission from sub-canopy snow from a tower-based system above the canopy) would be ideal. In this new experiment, two radiometers would be required along with supporting measurements from permittivity and temperature sensors installed in the tree trunk at different depths in the tree to obtain the tree vegetation permittivity and skin temperature gradients from the bark to the interior. Such an experiment could help us improve our understanding about how the vegetation water content freezing influences the airborne and spaceborne PM observations. In addition to an improved characterization of relative permittivity and tree temperature, this new radiometer observation configuration will enable the evaluation of canopy intercepted snow on tree emission from above. Although this evaluation was conducted in the thesis, the evaluation was made from below canopy based on the down welling tree emission which has a very different viewing angle compared with airborne and spaceborne observations made from above the canopy. A web camera could also be used to obtain the snow cover condition of the tree canopy in this new radiometer experimental configuration. Thus, the influence of the canopy intercepted snow on spaceborne or airborne tree emission observation can be better evaluated in. This new experiment setup is currently being operated by FMI at the Sodankylä ARC field site.

Another limitation of this study is that the experiment only has been made at one study site on a single conifer tree. Considering the complexity of tree geometry and structure, more observations of different types of tree under different kinds of natural environments should be conducted. It will be important to verify whether the temperature-transmissivity relationship found in this thesis can be replicated in different tree species, especially the deciduous trees. Due

to the defoliation during the fall-winter, deciduous trees only have woody biomass (trunks and the branches) during the snow season. Since the contributions from trunks, leaves, and branches to the temperature-transmissivity relationship are still unknown, a profitable experiment that evaluates how the transmissivity of the deciduous tree responsds to air temperature during the wintertime would be beneficial. Equation (5.5) is developed to describe the temperature-transmissivity relationship with the parameters γ_0 and a_γ. Further work is needed to test this equation for different types of tree to evaluate how these two parameters could be used to characterize the temperature-transmissivity relationship for trees. More specifically, the different combinations of γ_0 and a_γ values, which are obtained from the radiometer observations and model simulations, can be used to test if the approximation model developed in Chapter 6 can be applied to different forest types. This would produce a more generally applicable temperature-transmissivity relationship model that in turn can be used to develop a more robust approximation model to correct forest attenuation. As the first step, the tree radiometer observation data collected by the Boreal Ecosystem Research and Monitoring Sites (BERMS) in Canada could be used for this effort and be used to compare with the results found in Sodankylä site from this study.

Overall, this thesis indicates that further effort should be made to adopt the ground-based temperature-transmissivity relationship model and the approximation model developed in the relevant chapters of this thesis paper to correct spaceborne passive microwave observations from forest environments. In the spaceborne study, the ground snowpack properties measured by the meteorological stations could be used as the ground truth for model training and validation. The temperature-transmissivity relationship model could be introduced into existing spaceborne snow retrieval approaches (e.g. GlobSnow and AMSR2), and a test should be made to evaluate if the

accuracy of the snow retrieval algorithms could be improved by introducing this temperature-transmissivity relationship model. This evaluation should be done for different forest types: evergreen needleleaf, evergreen broadleaf, deciduous broadleaf, and mixed forest.

In conclusion, the temperature-transmissivity relationship has been observed in a robust albeit limited way at 10.65, 18.7, 21 and 36.5 GHz in this thesis. How the physical temperature influences tree transmissivity at other frequencies now needs to be evaluated further and more comprehensively. In addition, the use of available and concurrent L band radiometer observations could also be used to test the forest correction approach for soil moisture estimates and for soil freeze-thaw state detection. The influence of the temperature-transmissivity relationship is shown to be important for snow retrievals in forested landscapes but has a potentially wider implication for other retrieval applications.

Reference

[1] R. Kelly, A. Chang, L. Tsang, and J. Foster, "A prototype AMSR-E global snow area and snow depth algorithm," *IEEE Transactions on Geoscience and Remote Sensing*, vol. 41, no. 2, pp. 230-242, 2003.

[2] R. Kelly, "The AMSR-E snow depth algorithm: Description and initial results," *Journal of the Remote Sensing Society of Japan*, pp. 307-317, 2009.

[3] M. Takala, K. Luojus, J. Pulliainen, C. Derksen, J. Lemmetyinen, J. Kärnä, J. Koskinen, and B. Bojkov, "Estimating northern hemisphere snow water equivalent for climate research through assimilation of space-borne radiometer data and ground-based measurements," *Remote Sensing of Environment*, vol. 115, no. 12, pp. 3517-3529, 2011.

[4] G. Picard, L. Brucker, A. Roy, F. Dupont, M. Fily, and A. Royer, "Simulation of the microwave emission of multi-layered snowpacks using the dense media radiative transfer theory: the DMRT-ML model," *Geoscientific Model Development Discussions*, vol. 5, no. 4, pp. 3647-3694, 2012.

[5] M. Tedesco, and J. Jeyaratnam, "A new operational snow retrieval algorithm applied to historical AMSR-E brightness temperatures," *Remote Sensing*, vol. 8, no. 12, p. 1037, 2016.

[6] J. Pan, M. Durand, M. Sandells, J. Lemmetyinen, E. Kim, J. Pulliainen, A. Kontu, and C. Derksen, "Differences between the HUT snow emission model and MEMLS and their effects on brightness temperature simulation," *IEEE Transactions on Geoscience and Remote Sensing*, vol. 54, no. 4, pp. 2001-2019, 2016.

[7] N. Saberi, R. Kelly, P. Toose, A. Roy, and C. Derksen, "Modeling the observed microwave emission from shallow multi-Layer tundra snow using DMRT-ML," *Remote Sensing*, vol. 9, no. 12, p. 1327, 2017.

[8] J. Foster, A. Chang, D. Hall, and A. Rango, "Derivation of snow water equivalent in boreal forests using microwave radiometry," *ARCTIC*, vol. 44, no. 5, pp. 147-152, 1991.

[9] B. Vander Jagt, M. Durand, S. Margulis, E. Kim, and N. Molotch, "The effect of spatial variability on the sensitivity of passive microwave measurements to snow water equivalent," *Remote Sensing of Environment*, vol. 136, pp. 163-179, 2013.

[10] A. Chang, J. Foster, and D. Hall, "Effects of forest on the snow parameters derived from microwave measurements during the BOREAS winter field campaign," *Hydrological Processes*, vol. 10, no. 12, pp. 1565-1574, 1996.

[11] J. Pulliainen, and J. Grandel. "HUT snow emission model and its applicability to snow water equivalent retrieval," *IEEE Transactions on Geoscience and Remote Sensing*, vol. 37, no. 3, pp. 1378-1390, 1999.

[12] J. Foster, C. Sun, J. Walker, R. Kelly, A. Chang, J. Dong, and H. Powell, "Quantifying the uncertainty in passive microwave snow water equivalent observations," *Remote Sensing of Environment*, vol. 94, no. 2, pp. 187-203, 2005.

[13] C. Derksen, "The contribution of AMSR-E 18.7 and 10.7 GHz measurements to improved boreal forest snow water equivalent retrievals," *Remote Sensing of Environment*, vol. 112, no. 5, pp. 2701-2710, 2008.

[14] A. Roy, A. Royer, J. Wigneron, A. Langlois, J. Bergeron, and P. Cliche, "A simple parameterization for a boreal forest radiative transfer model at microwave frequencies," *Remote Sensing of Environment*, vol. 124, pp. 371-383, 2012.

[15] J. Cohen, J. Lemmetyinen, J. Pulliainen, K. Heinila, F. Montomoli, J. Seppanen, and M. Hallikainen, "The effect of boreal forest canopy in satellite snow mapping—a multisensor analysis," *IEEE Transactions on Geoscience and Remote Sensing*, vol. 53, no. 12, pp. 6593-6607, 2015.

[16] B. Forman, and Y. Xue, "Machine learning predictions of passive microwave brightness temperature over snow-covered land using the special sensor microwave imager (SSM/I)," *Physical Geography*, vol. 38, no. 2, pp. 176-196, 2016.

[17] Q. Li, and R. Kelly, "Correcting satellite passive microwave brightness temperatures in forested landscapes using satellite visible reflectance estimates of forest transmissivity," *IEEE Journal of Selected Topics in Applied Earth Observations and Remote Sensing*, vol. 10, no. 9, pp. 3874-3883, 2017.

[18] F. Larue, A. Royer, D. De Sève, A. Langlois, A. Roy, and L. Brucker, "Validation of GlobSnow-2 snow water equivalent over eastern Canada," *Remote Sensing of Environment*, vol. 194, pp. 264-277, 2017.

[19] F. Ulaby, and R. Jedlicka, "Microwave dielectric properties of plant materials," *IEEE Transactions on Geoscience and Remote Sensing*, vol. 22, no. 4, pp. 406-415, 1984.

[20] M. El-Rayes, and T. Ulaby, "Microwave dielectric spectrum of vegetation-part I: experimental observations," *IEEE Transactions on Geoscience and Remote Sensing*, vol. GE-25, no. 5, pp. 541-549, 1987.

[21] C. Mätzler, "Microwave transmissivity of a forest canopy: Experiments made with a beech," *Remote Sensing of Environment*, vol. 48, no. 2, pp. 172-180, 1994.

[22] M. Parde, K. Goita, A. Royer, and F. Vachon, "Boreal forest transmissivity in the microwave domain using ground-based measurements," *IEEE Geoscience and Remote Sensing Letters*, vol. 2, no. 2, pp. 169-171, 2005.

[23] F. Ulaby, K. Sarabandi, K. Mcdonald, M. Whitt, and M. Dobson, "Michigan microwave canopy scattering model," *International Journal of Remote Sensing*, vol. 11, no. 7, pp. 1223-1253, 1990.

[24] P. Ferrazzoli, and L. Guerriero, "Passive microwave remote sensing of forests: a model investigation," *IEEE Transactions on Geoscience and Remote Sensing*, vol. 34, no. 2, pp. 433-443, 1996.

[25] A. Della Vecchia, P. Ferrazzoli, L. Guerriero, R. Rahmoune, S. Paloscia, S. Pettinato, and E. Santi, "Modeling the multifrequency emission of broadleaf forests and their components," *IEEE Transactions on Geoscience and Remote Sensing*, vol. 48, no. 1, pp. 260-272, 2010.

[26] T. Mo, B. Choudhury, T. Schmugge, J. Wang, and T. Jackson, "A model for microwave emission from vegetation-covered fields," *Journal of Geophysical Research*, vol. 87, no. 13, pp. 11229, 1982.

[27] N. Kruopis. "Passive microwave measurements of snow-covered forest areas in EMAC'95," *IEEE Transactions on Geoscience and Remote Sensing*, vol. 37, no. 6, pp. 2699-2705, 1999.

[28] J. Pulliainen, and J. Grandel. "HUT snow emission model and its applicability to snow water equivalent retrieval," *IEEE Transactions on Geoscience and Remote Sensing*, vol. 37, no. 3, pp. 1378-1390, 1999.

[29] P. Ferrazzoli, L. Guerriero, and J. Wigneron, "Simulating L-band emission of forests in view of future satellite applications," *IEEE Transactions on Geoscience and Remote Sensing*, vol. 40, no. 12, pp. 2700-2708, 2002.

[30] J. Grant, K. Saleh-Contell, J. Wigneron, M. Guglielmetti, Y. Kerr, M. Schwank, N. Skou, and A. Van de Griend, "Calibration of the L-MEB model over a coniferous and a deciduous forest," *IEEE Transactions on Geoscience and Remote Sensing*, vol. 46, no. 3, pp. 808-818, 2008.

[31] M. Butt, and R. Kelly, "Estimation of snow depth in the UK using the HUT snow emission model," *International Journal of Remote Sensing*, vol. 29, no. 14, pp. 4249-4267, 2008.

[32] A. Langlois, A. Royer, F. Dupont, A. Roy, K. Goita, and G. Picard, "Improved corrections of forest effects on passive microwave satellite remote sensing of snow over boreal and subarctic regions," *IEEE Transactions on Geoscience and Remote Sensing*, vol. 49, no. 10, pp. 3824-3837, 2011.

[33] M. Guglielmetti, M. Schwank, C. Mätzler, C. Oberdorster, J. Vanderborght, and H. Fluhler, "FOSMEX: Forest soil moisture experiments with microwave radiometry," *IEEE Transactions on Geoscience and Remote Sensing*, vol. 46, no. 3, pp. 727-735, 2008.

[34] W. Havranek, and W. Tranquillini, "Physiological processes during winter dormancy and their ecological significance," in *Ecophysiology of Coniferous Forests*, W. Smith and T. Hinckley ed. San Diego, CA, USA: Academic Press, 1995, pp. 95-117.

[35] A. Sakai, "Comparative study on freezing resistance of conifers with special reference to cold adaptation and its evolutive aspects," *Canadian Journal of Botany*, vol. 61, no. 9, pp. 2323-2332, 1983.

[36] I. Leinonen, "Changing environmental effects on frost hardiness of scots pine during dehardening," *Annals of Botany*, vol. 79, no. 2, pp. 133-137, 1997.

[37] M. Sturm, T. Grenfell, and D. Perovich, "Passive microwave measurements of tundra and taiga snow covers in Alaska, U.S.A," *Annals of Glaciology*, vol. 17, pp. 125-130, 1993.

[38] M. Sturm, J. Holmgren, and G. Liston, "A seasonal snow cover classification system for local to global applications," *Journal of Climate*, vol. 8, no. 5, pp. 1261-1283, 1995.

[39] J. Pomeroy, J. Parviainen, N. Hedstrom, and D. Gray, "Coupled modelling of forest snow interception and sublimation," *Hydrological Processes*, vol. 12, no. 15, pp. 2317-2337, 1998.

[40] G. Liston, and M. Sturm, "Winter precipitation patterns in arctic Alaska determined from a blowing-snow model and snow-depth observations," *Journal of Hydrometeorology*, vol. 3, no. 6, pp. 646-659, 2002.

[41] R. Essery, and J. Pomeroy, "Vegetation and topographic control of wind-blown snow distributions in distributed and aggregated simulations for an arctic tundra basin," *Journal of Hydrometeorology*, vol. 5, no. 5, pp. 735-744, 2004.

[42] N. Hedstrom, and J. Pomeroy, "Measurements and modelling of snow interception in the boreal forest," *Hydrological Processes*, vol. 12, no. 10-11, pp. 1611-1625, 1998.

[43] A. Gelfan, J. Pomeroy, and L. Kuchment, "Modeling forest cover influences on snow accumulation, sublimation, and melt," *Journal of Hydrometeorology*, vol. 5, no. 5, pp. 785-803, 2004.

[44] K. Andreadis, P. Storck, and D. Lettenmaier, "Modeling snow accumulation and ablation processes in forested environments," *Water Resources Research*, vol. 45, no. 5, 2009.

[45] V. Mahat, and D. Tarboton, "Representation of canopy snow interception, unloading and melt in a parsimonious snowmelt model," *Hydrological Processes*, vol. 28, no. 26, pp. 6320-6336, 2014.

[46] E. Tomppo, M. Katila, K. Mäkisara, and J. Peräsaari, "The Multi-source national forest inventory of Finland — methods and results 2011," Finnish Forest Res. Inst., Vantaa, Finland, Tech. Rep., 2011. [Online]. Available: http://www.metla.fi/julkaisut/workingpapers/2014/mwp319.htm

[47] J. Lemmetyinen, A. Kontu, J. Pulliainen, J. Vehviläinen, K. Rautiainen, A. Wiesmann, C. Mätzler, C. Werner, H. Rott, T. Nagler, M. Schneebeli, M. Proksch, D. Schüttemeyer, M. Kern, and M. Davidson, "Nordic snow radar experiment," *Geoscientific Instrumentation, Methods and Data Systems Discussions*, pp. 1-23, 2016.

[48] N. Zuanon. "IceCube, a portable and reliable instrument for snow specific surface area measurement in the field," in *Proc. Int. Snow Sci. Workshop Grenoble*, Oct. 2013, pp. 1020-1023.

[49] L. Leppänen, A. Kontu, H. Hannula, H. Sjöblom, and J. Pulliainen, "Sodankylä manual snow survey program," *Geoscientific Instrumentation, Methods and Data Systems*, vol. 5, no. 1, pp. 163-179, 2016.

[50] T. Pellarin, Y. Kerr, and J. Wigneron, "Global simulation of brightness temperatures at 6.6 and 10.7 GHz over land based on SMMR data set analysis," *IEEE Transactions on Geoscience and Remote Sensing*, vol. 44, no. 9, pp. 2492-2505, 2006.

[51] C. Fierz, R. Armstrong, Y. Durand, P. Etchevers, E. Greene, D. McClung, K. Nishimura, P. Satyawali, and S. Sokratov, "The International Classification for Seasonal Snow on the Ground," UNESCO-IHP, Paris, France, Tech. Rep., 2009.

[52] R. Essery, J. Pomeroy, C. Ellis, and T. Link, "Modelling longwave radiation to snow beneath forest canopies using hemispherical photography or linear regression," *Hydrological Processes*, vol. 22, no. 15, pp. 2788-2800, 2008.

[53] A. Mavrovic, A. Roy, A. Royer, B. Filali, F. Boone, C. Pappas, and O. Sonnentag. "Vegetation dielectric characterization in L-band using an open-ended coaxial probe",

Geoscientific Instrumentation," *Methods and Data Systems Discussions*, vol. 7, pp. 195-208, 2018.

[54] T. J. Jackson, and T. J. Schmugge. "Vegetation effect on the microwave emission of soils," *Remote Sensing of Environment*, vol. 36, no. 3, pp. 203-212, 1991.

[55] E. Njoku, D. Entekhabi, Passive microwave remote sensing of soil moisture," *Journal of Hydrology*, vol. 184, pp. 101-129, 1996.

[56] A. Roy, P. Toose, and A. Royer, "A passive microwave L-Band boreal forest freeze/thaw experiment," in *Proc. IGARSS*, Valencia, Spain, 2018.

[57] E. Santi, S. Paloscia, P. Pampaloni, and S. Pettinato. "Ground-based microwave investigations of forest plots in Italy," *IEEE Transactions on Geoscience and Remote Sensing*, vol.47, no. 9, pp. 3016-3025, 2009.

[58] R. D. De Roo, A. R. Chang, and A. W. England, "Radiobrightness at 6.7-, 19-, and 37-GHz downwelling from mature evergreen trees observed during the Cold Lands Processes Experiment in Colorado," *IEEE Transactions on Geoscience and Remote Sensing*, vol. 45, no.10, pp. 3224-3229, 2007.

[59] H. Huang, L. Tsang, E. Njoku, A. Colliander, T. Liao, and K. Ding, "Propagation and scattering by a layer of randomly distributed dielectric cylinders using Monte Carlo simulations of 3D Maxwell equations with applications in microwave interactions with vegetation," *IEEE Access*, vol. 5, pp. 11985-12003, 2017.

[60] J. Levitt, "An overview of freezing injury and survival, and its interrelationships to other stresses," in *Plant cold hardiness and freezing stress*, New York, USA: academic press, pp.3-16, 1987

[61] S. Mayr, G. Wieser, and H. Bauer, "Xylem temperatures during winter in conifers at the alpine timberline," *Agricultural and Forest Meteorology*, vol. 137, no. 1-2, pp. 81-88, 2006.

[62] T. Karl, and K. Trenberth, "Modern global climate change," *Science*, vol. 302, no. 5651, pp. 1719-1723, 2003.

[63] R. Garcia-Herrera, and D. Barriopedro, "Northern hemisphere snow cover and atmospheric blocking variability," *J. Geophys. Res.-Atmos.*, vol. 111, no. D21, pp. 1–16, 2006.

[64] A. Mazurkiewicz, D. Callery, and J. McDonnell, "Assessing the controls of the snow energy balance and water available for runoff in a rain-on-snow environment," J. *Hydrol.*, vol. 354, pp. 1–14, 2008.

[65] R. Sommerfeld, A. Musselman, and R. Mosier, "CO_2, CH_4 and N_2O flux through a Wyoming snowpack and implications for global budgets", *Nature*, vol. 361, no. 6408, pp. 140–142, 1993.

[66] T. Barnett, L. Dumenil, U. Schlese, E. Roeckner, and M. Latif, "The effect of Eurasian snow cover on regional and global climate variations," *J. Atmos. Sci.*, vol. 46, no. 5, pp. 661–686, 1989.

[67] P. Groffman, C. Driscoll, T. Fahey, J. Hardy, R. Fitzhugh, and G. Tierney, "Colder soils in a warmer world: a snow manipulation study in a northern hardwood forest ecosystem," *Biogeochemistry*, vol. 56, no. 2, pp.135-150, 2001.

[68] J. Pomeroy, D. Gray, K. Shook, B. Toth, R. Essery, A. Pietroniro, and N. Hedstrom, "An evaluation of snow accumulation and ablation processes for land surface modelling," *Hydrological Processes*, vol. 12, no. 15, pp. 2339-2367, 1998.

[69] M. Sturm, J. Holmgren, G. Liston, "A seasonal snow cover classification system for local to global applications," *Journal of Climate*, vol. 8, no. 5, pp. 1261-1283, 1995.

[70] M. Sturm, T. Grenfell, D. Perovich, "Passive microwave measurements of tundra and taiga snow covers in Alaska, USA," *Annals of Glaciology*, vol. 17, no. 1, pp. 125-130, 1993.

[71] J. Dietz, C. Kuenzer, U. Gessner, S. Dech, "Remote sensing of snow - a review of available methods," *International Journal of Remote Sensing*, vol. 33, no. 13, pp. 4094-4134, 2012.

[72] T. Maeda, Y. Taniguchi, K. Imaoka, "GCOM-W1 AMSR2 Level 1R Product: Dataset of Brightness Temperature Modified Using the Antenna Pattern Matching Technique," *IEEE Transactions on Geoscience and Remote Sensing*, vol. 54, no. 2, pp. 770-782, 2016.

[73] A. Wiesmann, C. Mätzler, "Microwave emission model of layered snowpacks," *Remote Sensing of Environment*, vol. 70, pp. 307-316, 1999.

[74] G. Picard, L. Brucker, A. Roy, F. Dupont, M. Fily, A. Royer, C. Harlow, "Simulation of the microwave emission of multi-layered snowpacks using the Dense Media Radiative transfer theory: the DMRT-ML model," *Geoscientific Model Development*, vol. 6, pp. 1061-1078, 2013.

[75] K. Luojus, J. Pulliainen, M. Takala, et al., "GlobSnow-2 Product User Guide Version 1.0," European space agency, Tech. Rep., 2013, [Online]. Available : http://www.globsnow.info/se/GlobSnow2_SE_SWE_Product_User_Guide_v1_r1.pdf

[76] R. Kelly, N. Saberi, Q. Li, "The AMSR2 Satellite-based Microwave Snow Algorithm (SMSA) to estimate regional to global snow depth and snow water equivalent," in *Proc. AGU Fall Meeting*, New Orleans, USA, Dec. 2017.

[77] C. Mätzler, "Applications of the interaction of microwaves with the natural snow cover," *Remote Sensing Reviews*, vol. 2, pp. 259-387, 1987.

[78] D. Polder, J. Van Santeen, "The effective permeability of mixtures of solids", *Physica*, vol. 12, no. 5, pp. 257-271, 1946.

[79] W. Tinga, W. Voss, D. Blossey, "Generalized approach to multiphase dielectric mixture theory", *Journal of Applied Physics*, vol. 44, pp. 3897, 1973.

[80] T. Ulaby, and M. El-Rayes, "Microwave dielectric spectrum of vegetation-Part II: Dual-dispersion model. IEEE Transactions on Geoscience and Remote Sensing," *IEEE Transactions on Geoscience and Remote Sensing*, vol. GE-25, no. 5, pp.550-557, 1987.

[81] U. Nakaya, *Snow crystals: natural and artificial*," Cambridge, UK: Harvard University Press, 1954.

[82] W. Wiscombe, and S. Warren, "A model for the spectral albedo of snow. I: pure snow," *Journal of the Atmospheric Sciences*, vol. 37, pp. 2712-2733, 1980.

[83] C. Mätzler, "Relation between grain-size and correlation length of snow," *Journal of Glaciology*, vol. 48, pp. 461-466, 2002.

[84] L. Arnaud, G. Picard, N. Champollion, F. Domine, J. Gallet, E. Lefebvre, M. Fily, and J. Barnola, "Instruments and methods: Measurement of vertical profiles of snow specific surface area with a 1 cm resolution Using infrared reflectance: Instrument description and validation," *Journal of Glaciology*, vol. 57, pp. 17-29, 2011.

[85] L. Legagneux, A. Cabanes, and F. Dominé, "Measurement of the specific surface area of 176 snow samples using methane adsorption at 77 K," *Journal of Geophysical Research: Atmospheres*, vol. 107, no. D17, 2002.

[86] M. Sturm, B. Taras, G. Liston, C. Derksen, T. Jonas, and J. Lea, "estimating snow water equivalent using snow depth data and climate classes," *J. hydrometeorol*, vol. 11, pp.1380-1394, 2010.

[87] E. Schulz, W. Schulze, H. Koch, A. Arneth, G. Bauer, F. M. Kelliher, D. Y. Hollinger, N. Vygodskaya, W. Kusnetsova, A. Sogatchev, W. Ziegler, K. Kobak, and A. Issajev, "Aboveground biomass and nitrogen nutrition in a chronosequence of pristine dahurian larix stands in eastern Siberia," *Canadian Journal of Forest Research*, pp. 95-103, 1995.

[88] T. Kolchugina, and T. Vinson, "Role of Russian forests in the global carbon balance," *Ambio*, pp. 258-264, 1995. Tech. Rep.,

[89] J. Parviainen, "Cultural heritage and biodiversity in the present forest management of the boreal zone in Scandinavia," *Journal of forest research*, vol. 20, no. 5, pp. 445-452, 2015.

[90] D. Halliwell, M. Aps, "BOReal Ecosystem-Atmosphere Study (BOREAS) biometry and auxiliary sites: locations and descriptions," Northern Forestry Centre, Edmonton, Canada, Tech. Rep., 1997.

[91] M. Karam, A. Fung, "Electromagnetic scattering from a layer of finite length, randomly oriented, dielectric, circular-cylinders over a rough interface with application to vegetation", *International Journal of Remote Sensing*, vol. 9, pp. 1109-1134, 1988.

[92] R. Wait, *Electromagnetic radiation from cylindrical structures*, London, UK: Peregrinus, 1988.

[93] A. Chang, J. Foster, and D. Hall, "Effects of forest on the snow parameters derived from microwave measurements during the BOREAS Winter Field Campaign," *Hydrological Processes*, pp. 1565-1574, 1996.

[94] J. Wigneron, Y. Kerr, P. Waldteufel, et al., "L-band Microwave Emission of the Biosphere (L-MEB) Model: Description and calibration against experimental data sets over crop fields", *Remote Sensing of Environment*, vol. 107, no. 4, pp. 639-655, 2007.

[95] Q. Li, R. Kelly, L. Leppänen, J. Vehviläinen, A. Kontu, J. Lemmetyinen, J. Pulliainen, "The influence of thermal properties and canopy-intercepted snow on passive microwave transmissivity of a scots pine," *IEEE Transactions on Geoscience and Remote Sensing*, 2019.

[96] A. Okuyama, K. Imaoka, “Intercalibration of advanced microwave scanning radiometer-2 (AMSR2) brightness temperature,” *IEEE Transactions on Geoscience and Remote Sensing*, vol. 53, no. 8, pp. 4568-4577, 2015.

[97] T. Maeda, Y. Taniguchi, and K. Imaoka, “GCOM-W1 AMSR2 Level 1R Product: Dataset of Brightness Temperature Modified Using the Antenna Pattern Matching Technique,” *IEEE Transactions on Geoscience and Remote Sensing*, vol. 54, no. 2, pp. 770-782, 2016.

[98] C. Dimiceli, M. Carroll, R. Sohlberg, R. Kim, D. Kelly, M. Townshend, and J. R. G, "MOD44B MODIS/Terra Vegetation Continuous Fields Yearly L3 Global 250m SIN Grid V006 [Data set]," NASA EOSDIS Land Processes DAAC, South Dakota, USA, Tech. Rep., 2015. [Online]. Available: https://lpdaac.usgs.gov/dataset_discovery/modis/modis_products_table/mod44b_v006

[99] S. Mayr, M. Wolfschwenger, and H. Bauer, “Winter-drought induced embolism in Norway spruce (Picea abies) at the Alpine timberline,” *Physiologia Plantarum*, vol. 115, pp. 74-80, 2002.

[100] A. Chang, J. Foster, D. Hall, “Nimbus-7 SMMR derived global snow cover parameters”, *Annals of glaciology*, vol. 9, pp. 39-44, 1987.

[101] Q. Li, R. Kelly, J. Lemmetyinen, and J. Pan, " Simulating the influence of temperature on microwave transmissivity of trees during winter observed by spaceborne microwave radiometery", *IEEE Transactions on Geoscience and Remote Sensing*, submitted in 2019.

[102] A. Roy, P. Toose, and A. Royer, “A passive microwave L-band boreal forest freeze/thaw experiment,” *in Proc. IGARSS*, Valencia, Spain, 2018.

[103] G. Liston, C. Hiemstra. "A simple data assimilation system for complex snow distributions (SnowAssim)", *Journal of Hydrometeorology*, vol. 9, no. 8, pp. 989-1004, 2008.

[104] M. Woo, K. Young, "Modeling arctic snow distribution and melt at the 1 km grid scale," *Hydrology Research*, vol. 35 no. 4-5, pp. 295-307, 2004

[105] J. Cherry, L. Tremblay, S. Déry, and M. Stieglitz, “Reconstructing solid precipitation from snow depth measurements and a land surface model,” *Water resources research*, vol. 41, no. 9, pp. 1-15, 2005.

[106] G. Liston, "Representing subgrid snow cover heterogeneities in regional and global models," *Journal of climate*, vol. 17, no. 6, pp. 1381-1397, 2004.

[107] G. Liston, M. Sturm, “snow-transport model for complex terrain,” *Journal of Glaciology*, vol. 44, no. 148, pp .498-516, 1998.

[108] C. Derksen, A. Walker, B. Goodison, J. Strapp, “Integrating in situ and multiscale passive microwave data for estimation of subgrid scale snow water equivalent distribution and variability”, *IEEE Transactions on Geoscience and Remote Sensing*, vol. 43, no. 5, pp. 960-972, 2005.